Development of Analytical Solutions for Quasistationary Electromagnetic Fields for Conducting Spheroids in the Proximity of Current-Carrying Turns

by

Nandaka Jayasekara

A Thesis submitted to the Faculty of Graduate Studies of

The University of Manitoba

in partial fulfillment of the requirements for the degree of

Doctor of Philosophy

Department of Electrical and Computer Engineering

University of Manitoba

Winnipeg, Manitoba, Canada

To my parents.

Acknowledgements

I would like to express my deep appreciation and gratitude to Prof. I.R. Ciric for his continuous advice, guidance and encouragement throughout the research work. I would like to thank all my colleagues and the staff of the Department of Electrical and Computer Engineering for their continuous encouragement, stimulating discussions related to the research work and for making my years at the University of Manitoba a pleasant one.

Conducting this research work would not have been possible without the financial assistance from the University of Manitoba Graduate Fellowship and from National Science and Engineering Research Council of Canada.

I extend my heartfelt gratitude to my parents for their support and encouragement throughout my academic career to pursue graduate studies. A special thank for my elder sister for all the support given to me over the years.

I extend my heartfelt gratitude to my wife for her understanding and encouraging me during my hard times, my little son for keeping me happy all the time and my in-laws for their love and caring of my son.

Nandaka Jayasekara

Winnipeg, Manitoba

December, 2012.

Abstract

Exact analytical solutions for the quasistationary electromagnetic fields in the presence of conducting objects require the field solutions both internal and external to the conductors. Such solutions are limited for certain canonically shaped objects but are useful in testing the accuracy of various approximate models and numerical methods developed to solve complex problems related to real world conducting objects and in calibrating instruments designed to measure various field quantities. Theoretical investigations of quasistationary electromagnetic fields also aid in improving the understanding of the physical phenomena of electromagnetic induction.

This thesis presents rigorous analytical expressions derived as benchmark solutions for the quasistationary field quantities both inside and outside, Joule losses and the electromagnetic forces acting upon a conducting spheroid placed in the proximity of a non-uniform field produced by current-carrying turns. These expressions are used to generate numerous numerical results of specified accuracy and selected results are presented in a normalized form for extended ranges of the spheroid axial ratio, the ratio of the depth of penetration to the semi-minor axis and the position of the inducing turns relative to the spheroids. They are intended to constitute reference data to be employed for comprehensive comparisons of results from approximate numerical methods or from boundary impedance models used for real world conductors.

Approximate boundary conditions such as the simpler perfect electric conductor model or the Leontovich surface impedance boundary condition model can be used to obtain approximate solutions by only analyzing the field external to the conducting object. The range of validity of these impedance boundary condition models for the analysis of axisymmetric eddy-current problems is thoroughly investigated. While the simpler PEC model can be employed only when the electromagnetic depth of penetra-

tion is much smaller than the smallest local radius of curvature, the results obtained using the surface impedance boundary condition model for conducting prolate and oblate spheroids of various axial ratios are in good agreement with the exact results for skin depths of about 1/5 of the semi-minor axis when calculating electromagnetic forces and for skin depths less than 1/20 of the semi-minor axis when calculating Joule losses.

List of Principal Symbols

t	time [s]
ω	angular frequency [rad/s]
i	imaginary unit in a complex number $a + ib$, where $i^2 = -1$,
(x, y, z)	rectangular cartesian coordinate system
(η, ξ, φ)	prolate or oblate spheroidal coordinate systems
a_0, b_0	semi minor and semi major axes of a prolate spheroid and vice versa for an oblate spheroid (for example, see figures 2.1 and 2.2)
c	semi-focal distance of a spheroid, where $c = \sqrt{a_0^2 - b_0^2}$ for prolate spheroids and $c = \sqrt{b_0^2 - a_0^2}$ for oblate spheroids
$(h_\eta, h_\xi, h_\varphi)$	scale factors in prolate or oblate spheroidal coordinate systems
$\boldsymbol{r}$	position vector
$(\boldsymbol{u}_x, \boldsymbol{u}_y, \boldsymbol{u}_z)$	the unit vectors in the rectangular cartesian coordinate system
$(\boldsymbol{u}_\eta, \boldsymbol{u}_\xi, \boldsymbol{u}_\varphi)$	the unit vectors in the spheroidal coordinate system
μ	permeability of a material
μ_0	permeability of free space
ϵ	permittivity of a material
σ	conductivity of a conducting material
$\lambda_{m,n}$	spheroidal eigenvalues, where m and n are integers
d_r^{mn}	spheroidal expansion coefficients
$S_{mn}^{(p)}$	spheroidal angle function of the p^{th} kind
$R_{mn}^{(p)}$	spheroidal radial function of the p^{th} kind
$\delta_{nn'}$	Kroneckr delta
$j_n(Z)$	spherical Bessel functions
$y_n(Z)$	spherical Neumann functions
$h_n^{(p)}$	Hankel functions of the p^{th} kind
P_n^m, Q_n^m	associated Legendre functions of the first and second kinds, respectively
δ	depth of penetration of electromagnetic fields (also known as skin depth)
$\boldsymbol{A}$	magnetic vector potential
P	power loss
F	force acting on spheroids
I_s	current in the filamentary turn
Z_s	surface impedance
R_s	surface resistance
$\boldsymbol{n}$	outwardly directed unit vector normal to the surface

List of Acronyms

SIBC	Leontovich Surface Impedance Boundary Condition
PEC	Perfect Electric Conductor

Table of Contents

List of Figures

List of Tables

Chapter 1

Introduction

Exact analytical solution for the quasistationary electromagnetic field in the presence of induced conducting bodies can only be derived for certain geometric shapes. In three dimensions, such a solution was first obtained for spheres in a uniform field and in the field of a coaxial circular current-carrying turn (see, for example, [1], [2]). In [3] analytical solutions are presented for the quasistationary fields produced by spheroidal, spherical and cylindrical bodies in the presence of magnetic dipole. To overcome the complexity of the problem, the spheroid is taken to be perfectly conducting. A complete analysis of the fields produced by circular turns carrying current varying sinusoidally with time and by arbitrarily oriented magnetic dipoles in the presence of conducting spherical shells has been presented in [4] and [5]. General expressions of the vector potential for axisymmetric quasistationary time-harmonic magnetic fields outside and inside conducting bodies have been derived in [6], [7] by using the method of separation of variables in spherical coordinates (including conical conducting regions, in terms of conical functions), in prolate and oblate spheroidal coordinates (including regions bounded by hyperboloids of revolution) and, also, in toroidal coordinates and in bispherical coordinates. In the later two cases the vector potential equation is separable only outside the conductors. The constants of

integration in the general potential expressions can be determined by imposing the boundary conditions on the conductor surfaces. In [8] second order vector potential formulation for conducting sphere excited by an arbitrary shaped filamentary element is presented. The solution to the vector field equations are derived from the solution of two scalar wave equations which are separable in a number of coordinate systems.

Due to the recent developments of advanced techniques for the detection and discrimination of subsurface objects, the demand for analytical solutions for canonical shaped objects needed for testing numerical codes, calibration of instruments and development of model-based inversion methods has increased [9]. An analytical solution has been used to determine the equivalent induced magnetic dipole moment and the magnetic field of conducting spheroids immersed in uniform magnetic fields [10],[11],[12], with applications in geophysics and in detecting subsurface metallic targets. Numerical results were presented for the induced magnetic dipole moment and for the field response at points outside the spheroid located on one of the axes of the spheroid with a uniform external field oriented either along the axis of revolution or transverse with respect to it. To reduce the necessary amount of numerical computation, the field outside solid conductors in the presence of general field sources can be expressed in terms of magnetic scalar potentials [12], [6]. An analytical formulation for the field produced by a highly conductive and permeable objects is formulated in ellipsoidal coordinate system [13] which allows more freedom in modeling three dimensional geometries when compared to other coordinate systems involving bodies of revolutions. In [12] and [13] a hybrid approach, combining the solution of the Laplace equation exterior to the object and a high frequency approximation based on small penetration depth for the field internal to the object is considered in generating numerical results. This significantly reduces the complexity of the problem involving the solution of the wave equation inside the object in terms of spheroidal wave func-

tions for spheroidal objects or ellipsoidal wave functions for ellipsoidal objects and results a considerable reduction in the computational time.

An accurate study of the induced currents in a conducting object requires the field solution both inside and outside of the conductor. The exact analytical solutions are possible only for a limited number of cases. On the other hand numerical solutions require a great deal of computations since the interior of the conducting object has to be discretized using a sufficiently large grid. In order to simplify the complexity of the problem, approximate boundary conditions can be used to obtain approximate solutions to various field problems by only analyzing the field outside the object. The accuracy of the results computed under approximate conditions can be evaluated by comparing them with the numerical values found from the exact solution available for certain canonical shapes (see for example - [14]). The range of applicability of the simpler boundary condition models depends on the type of excitation, material properties and the geometric shape of the objects under consideration. For solid conducting bodies in the presence of time-varying magnetic fields, the simplest model is the perfect electric conductor (PEC) which is particularly useful for a quick, approximate solution at higher frequencies. A more accurate and often used model is the Leontovich surface impedance boundary condition (SIBC) model [15], [16], [17] which can also be applied at lower frequencies when the electromagnetic skin depth is still small compared to the smallest radius of curvature of the conducting body [18]. A simple derivation is presented in [19] for the classical skin effect approximation in a good conductor of general shape. The requirement for the validity of the approximations are illustrated for few simple examples of conducting half-space with incident plane wave, infinitely long current-carrying wire and a line current over a conducting half-space. The concept of surface impedance in analyzing radio wave propagation over a inhomogeneous and irregular earth surface is studied in [20]. The advantages

and limitations of the surface impedance concept were shown in connection with an integral equation for the field strength. Practical conclusions were drawn with regard to the existence and the measurement of the effective earth electrical parameters and to some aspects of geological prospecting by radio wave propagation over real earth surface.

The validity of the SIBC model in solving electromagnetic wave scattering problems involving lossy dielectric bodies was investigated in [21] for objects of cylindrical, spherical and spheroidal shapes. For cylindrical and spherical objects, a comparison was presented between numerical results for the scattering cross section using the SIBC model and the analytical expressions derived by imposing the exact boundary conditions, whereas, for spheroidal shapes, the comparison was made with the numerical results generated by employing the method of moments for both the SIBC and the exact formulations. An analytic solution is presented in [22] for plane electromagnetic wave scattering by a coated prolate spheroidal object with axial incidence by using the impedance boundary conditions.

In [23], impedance boundary conditions are used with the boundary integral equations to analyze the eddy currents in conducting magnetic cylinders with circular and rectangular cross sections when subjected to transverse-magnetic time-harmonic fields. A variety of numerical techniques based on finite volume and boundary element formulations have been developped using the SIBC model (see, for example, [24],[25]). Modified expressions for the surface impedance which are applicable near edges and corners of two- and three- dimensional conducting structures have been proposed in [26],[27]. In [28] surface impedance concept is used to calculate the energy related quantities of conductors, such as energy stored in the electromagnetic field in the skin layer and power losses as well as the per unit length inductance and

resistance. This method is applicable to the 2-D problem of calculating high frequency per unit length parameters of lossy, uniform and quasi TEM multiconductor transmission lines. An application of the SIBC to calculate the electric field intensity at the earth surface during geomagnetic disturbances are presented in [29],[30]. The real time magnetic field measurements from magnetic observatories together with earth conductivity models helps to compute in real-time the electric field intensity which causes an induced currents in power transmission systems, natural gas pipelines and railway lines. Geomagnetically induced currents in electric power transmission lines will saturate the power transformers causing increased reactive power demand, overheating of transformers and false triggering of protective relays due to high level of harmonics.

Higher order surface impedance boundary conditions take into account the body curvature [18], [16],[31], with a first order correction in the Rytov-Mitzner model, where the penetration of the field is assumed only in the normal direction, whereas in the Rytov model a second order correction is also incorporated by considering both the normal and the tangential diffusion of the field into the conducting bodies. While the latter two models yield, in general, an increased accuracy of the results, their implementation is more difficult since it involves the local principal curvature radii which have to be determined numerically for arbitrarily shaped bodies, when their surfaces are described by a discretized grid in the absence of analytical equations.

An analytical formulation to study the accuracy of the impedance boundary conditions for the analysis of eddy currents in spherical solid conductors is presented in [32]. It is found that the maximum percentage error for Joule losses and for electromagnetic forces calculated using the SIBC model is bellow 1 % for skin depths less than one tenth of the radius of the sphere, while to obtain an error less than 4% with

the PEC model the skin depth should be less than 1/35 of the radius. In the special case of a sphere, the Rytov-Mitzner boundary condition is identical to that in the SIBC model and, thus, there is no first order curvature correction. A comprehensive analysis of the power losses in and the forces acting upon induced perfectly conducting spheroids is presented in [33], with applications to electromagnetic levitation, where the validity of the PEC model for spheroids with different axial ratios is investigated by comparing analytical results with experimental data. A comparison between the performance of surface integral equations based on the PEC and the SIBC models for quasi-stationary field analysis is investigated in [34] considering induced conducting spheres and spheroids. The benchmark accurate numerical results published based on a complete rigorous analytical solution for the fields outside and inside conducting prolate and oblate spheroids in the presence of current-carrying circular turns [14] are very well be used to evaluate the performance of various numerical methods developed for practical systems containing induced solid conductors. These numerical results can also be used, to determine the applicability and the range of validity of various approximate boundary conditions used in the analysis of eddy-current related problems.

1.1 Motivation Behind the Selection of the Research Topic

Exact analytical solution for the quasistationary fields produced by conducting spheroid in the presence of non-uniform field due to coaxial circular turn carrying current is not solved in literature. This is mainly due to the complicated mathematical treatment and the electromagnetic field modeling techniques required to solve such a problem. It also requires an advanced knowledge of special functions such as spheroidal wave functions involved in the solution. This problem has a practical significance as the spheroidal geometry can be used to approximate many real world objects which can

be found in a wide range of engineering applications such as detection and discrimination of subsurface objects, induction heating applications, electromagnetic levitation and levitation of molten metals and non-destructive testing. The existing analytical solutions presented in [10],[11] and [12] determine the equivalent induced magnetic dipole moment to approximate the secondary magnetic field due to induced currents in the conducting spheroid assumed to be immersed in an uniform magnetic field, with applications to geophysics and to detecting subsurface metallic targets. The electromagnetic sensor used to detect these metallic objects mainly comprises of circular current carrying turns. The assumption of an uniform inducing field as the primary field, with the secondary field due to induced currents in the conducting spheroid as the field produced by an induced magnetic dipole, are valid only if the relative dimensions of the conducting spheroid are small compared to the radius of the inducing turn and if the relative distance between the spheroid and the turn is sufficiently large.

In this thesis, the problem of the non-uniform quasistationary fields produced by a coaxial circular turn carrying current in the presence of conducting spheroids is solved on the basis of exact field equations and imposing the actual boundary conditions, without adopting the above approximations. Numerical results generated based on exact analytical solutions are also important in testing the efficiency of numerical methods and simpler impedance boundary condition models used in solving real world electromagnetic induction related problems.

1.2 Thesis Objectives

The main objective of this thesis research work are:

1. to derive exact analytical expressions for quasistationary field quantities, both

inside and outside of conducting spheroids, power losses and forces exerted upon them, when placed in an non-uniform field produced by a current carrying circular turn.

2. to generate benchmark accurate numerical results for a large range of values for the characteristic parameters such as axial ratio, the ratio of the skin depth to the spheroid semi-minor axis, the ratio of the distance between the spheroid origin and the circular turn to the spheroid semi-minor axis and the ratio of the spheroid semi-minor axis to the diameter of the current carrying circular turn.

3. to use the benchmark numerical data to investigate the range of applicability (in terms of frequency and field non-uniformity) of simpler surface impedance models for the analysis of eddy-current problems.

1.3 Thesis Overview

Chapter-2 of this thesis gives a brief introduction to the spheroidal coordinate system and the derivation of the solution of the scalar wave equation in spheroidal coordinates. It also describes in brief the methods used in determining the spheroidal eigenvalues and expansion coefficients required for the numerical computations of the angle and the radial spheroidal wave functions.

In chapter-3, exact analytical expressions were derived for the quasistationary field quantities both inside and outside of conducting prolate and oblate spheroids immersed in a nonuniform field produced by coaxial current-carrying circular turns. In the quasistationary fields regime, the displacement currents are negligible when compared to the conduction currents [35],[36]. Exact expressions were also derived for the power losses in spheroids and for the forces exerted upon them. The main goal of this study is to use these expressions to generate accurate numerical results

for a large range of values for the characteristic parameters, namely, the axial ratio, the relative distance between the spheroids and the inducing turns, and the ratio of the penetration depth to the linear dimension of the spheroids. The calculation of the current density distribution inside the spheroid and the evaluation of losses are necessary for the determination of the heat and temperature distributions, as in eddy-current and skin effect problems related to induction heating, melting and surface treatment ([37], [38],[39],[40],[40]), eddy current shielding ([41],[42]), while the calculation of forces is important in electromagnetic levitation or propulsion problems.

Chapter-4 begins with a brief description of the computational methods used in the numerical computation of special functions in the exact analytical expressions derived for various field quantities in chapter-3. These expressions are used to generate numerical results of specified accuracy for the field quantities, Joule losses and forces acting upon conducting spheroids. Selected results are presented in a normalized form for determined, extended ranges of the spheroid axial ratio, the ratio of the depth of penetration to the semi-minor axis, and the relative position of the inducing turn with respect to the spheroids. The accurate numerical results presented here are needed for testing the efficiency of various approximate numerical methods developed to analyze real world situations − see, for instance, [43],[44],[45] and for determining the range of applicability of simple surface impedance models [32].

In chapter-5 the range of validity of the simplest and most used PEC and SIBC models was investigated considering conducting spheroids immersed in a nonuniform field produced by a circular turn carrying current varying sinusoidally with time [46]. First, analytical expressions for the magnetic vector potential and for the field components outside the spheroids were derived by imposing these approximate boundary condition at the conductor surface. Analytical expressions were also derived for the

power losses due to induced currents in the spheroids and the electromagnetic forces acting upon them. The numerical results generated on the basis of these approximate models were compared with the numerical results generated from the exact analytical expressions derived in chapter-3. Accurate computations of Joule losses due to induced currents in conducting objects are important in various areas of applied electromagnetics such as induction heating, melting and surface treatment, while an accurate computation of electromagnetic forces is necessary in the design of various electromagnetic devices, and of levitation and propulsion systems. The study performed employing prolate and oblate spheroids of various axial ratios is indicative of the order of magnitude of the errors introduced when using the PEC and the SIBC models for real world conductors in the presence of nonuniform inducing magnetic fields.

Finally, in Chapter 6, conclusions are drawn and some suggestions are given to extend this research work to solve quasistationary field problems associated with a conducting spheroid in the presence of arbitrarily oriented inducing turns, as well as problems relative to systems of arbitrarily oriented spheroids placed in an external field.

Some of the findings of this research were already published in two regular papers in the *IEEE Transactions on Magnetics* [14],[46] and in two international conference papers [47],[48].

Chapter 2

Solution of the Wave Equation in Spheroidal Coordinates

2.1 The Prolate and Oblate Spheroidal Coordinate Systems

Spheroidal harmonics appear in the solution of wave equation in either prolate or oblate spheroidal coordinates which belong to the eleven orthogonal coordinate systems where the wave equation is separable. Spheroidal wave functions have found many practical applications in different physical applications due to the flexibility in modeling real world objects. The use of spheroidal wave functions spread over diverse areas in physics and engineering, namely in electromagnetic field modeling, acoustics, light scattering, nuclear physics, signal processing and communication theory.

The prolate and oblate spheroidal coordinate systems usually denoted by (η, ξ, φ) are three dimensional orthogonal coordinate systems which can be formed by rotating two-dimensional elliptic coordinate system, consisting of confocal ellipses and hyperbolas, about the major and minor axes of the ellipses, respectively [49]. In each case, the coordinates η, ξ, φ form a right-handed system. It is customary to chose the $z-$

axis as the axis of revolution.

The prolate spheroidal coordinates η, ξ, φ are related to the rectangular cartesian coordinates x, y, z by [49].

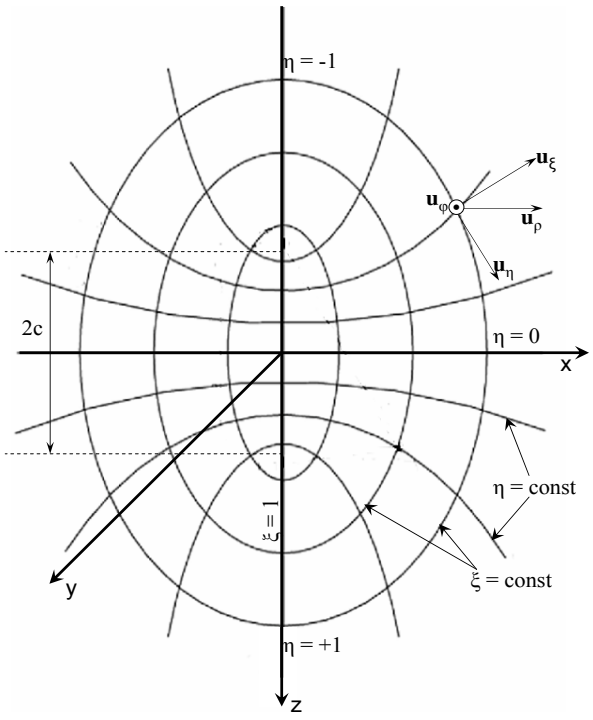

Figure 2.1: Prolate spheroidal coordinate system: η, ξ, φ ($-1 \leq \eta \leq +1$, $1 \leq \xi \leq \infty$, and $0 \leq \varphi \leq 2\pi$).

$$\begin{aligned} x &= c[(1-\eta^2)(\xi^2-1)]^{1/2} cos\varphi \\ y &= c[(1-\eta^2)(\xi^2-1)]^{1/2} sin\varphi \\ z &= c\eta\xi. \end{aligned} \tag{2.1}$$

The metric coefficients (also known as scale factors) h_η, h_ξ and h_φ are

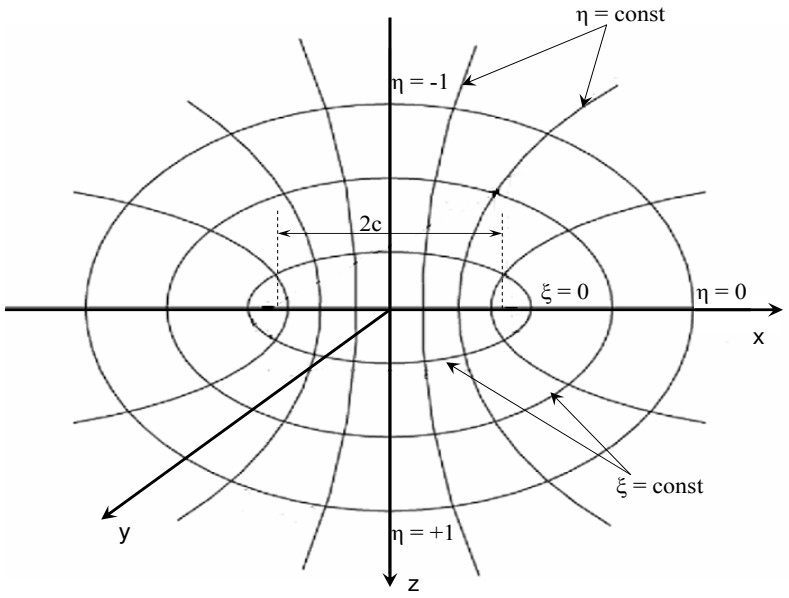

Figure 2.2: Oblate spheroidal coordinate system: η, ξ, φ ($-1 \leq \eta \leq +1$, $0 \leq \xi \leq \infty$, and $0 \leq \varphi \leq 2\pi$).

$$
\begin{aligned}
h_\eta &= c\left[\frac{\xi^2-\eta^2}{1-\eta^2}\right]^{1/2} \\
h_\xi &= c\left[\frac{\xi^2-\eta^2}{\xi^2-1}\right]^{1/2} \\
h_\varphi &= c[(1-\eta^2)(\xi^2-1)]^{1/2}.
\end{aligned}
\tag{2.2}
$$

The oblate spheroidal coordinates η, ξ, φ ($-1 \leq \eta \leq +1$, $0 \leq \xi \leq \infty$, $0 \leq \varphi \leq 2\pi$) are related to the rectangular coordinates x, y, z by the following relations.

$$
\begin{aligned}
x &= c[(1-\eta^2)(\xi^2+1)]^{1/2} cos\varphi \\
y &= c[(1-\eta^2)(\xi^2+1)]^{1/2} sin\varphi \\
z &= c\eta\xi
\end{aligned}
\tag{2.3}
$$

where $c = \sqrt{a_0^2 - b_0^2}$ is the semi-focal distance of the spheroids with $\xi = constant$, a_0

and b_0 are the semi-major and semi-minor axes of the prolate spheroid respectively. The corresponding scale factors are

$$\begin{aligned} h_\eta &= c\left[\frac{\xi^2+\eta^2}{1-\eta^2}\right]^{1/2} \\ h_\xi &= c\left[\frac{\xi^2+\eta^2}{\xi^2+1}\right]^{1/2} \\ h_\varphi &= c[(1-\eta^2)(\xi^2+1)]^{1/2} \end{aligned} \tag{2.4}$$

and the semi-focal distance is given by $c = \sqrt{b_0^2 - a_0^2}$. It is important to notice that the transformations $\xi \to i\xi$ and $c \to -ic$ in the expressions obtained for the field quantities in prolate spheroidal coordinates give the corresponding expressions in oblate spheroidal coordinates [49]. The unit vectors $\boldsymbol{u}_\eta$, $\boldsymbol{u}_\xi$ and $\boldsymbol{u}_\varphi$ are given by

$$\begin{aligned} \boldsymbol{u}_\eta &= \frac{1}{h_\eta}\frac{\partial \boldsymbol{r}}{\partial \eta} \\ \boldsymbol{u}_\xi &= \frac{1}{h_\xi}\frac{\partial \boldsymbol{r}}{\partial \xi} \\ \boldsymbol{u}_\varphi &= \frac{1}{h_\varphi}\frac{\partial \boldsymbol{r}}{\partial \varphi} \end{aligned} \tag{2.5}$$

where the position vector $\boldsymbol{r} = x\boldsymbol{u}_x + y\boldsymbol{u}_y + z\boldsymbol{u}_z$, in which x, y, z are expressed as in (2.1) and the scale factors h_η, h_ξ and h_φ are as given in (2.4) and(2.4) in case of prolate and oblate spheroids, respectively. In the limit when the semi-focal distance $c \to 0$, both prolate and oblate systems reduces to the spherical coordinate systems. For a finite c, the surface defined by $\xi = constant$ in each case becomes spherical as $\xi \to \infty$.

2.2 The Scalar Wave Equation and its Solution in Spheroidal Coordinates

The prolate and oblate spheroidal coordinate systems are two of coordinate systems where the scalar Helmholtz equation $(\nabla^2 + k^2)\Psi = 0$ is separable out of eleven coordinate systems. In general curvilinear orthogonal coordinate system (u_1, u_2, u_3) the scalar Helmholtz equation can be written as [50]

$$\frac{\partial}{\partial u_1}\left(\frac{h_2 h_3}{h_1}\frac{\partial \Psi}{\partial u_1}\right) + \frac{\partial}{\partial u_2}\left(\frac{h_3 h_1}{h_2}\frac{\partial \Psi}{\partial u_2}\right) + \frac{\partial}{\partial u_3}\left(\frac{h_1 h_2}{h_3}\frac{\partial \Psi}{\partial u_3}\right) + k^2 h_1 h_2 h_3 \Psi = 0. \quad (2.6)$$

The scale factors h_i are given by

$$h_i = \left|\frac{\partial r}{\partial u_i}\right|. \quad (2.7)$$

Substituting for scale factors either from (2.3) or from (2.4) for prolate or oblate spheroidal coordinates, respectively, to the wave equation in (2.6) we obtain [49]

$$\frac{\partial}{\partial \eta}\left[(1-\eta^2)\frac{\partial \Psi}{\partial \eta}\right] + \frac{\partial}{\partial \xi}\left[(\xi^2-1)\frac{\partial \Psi}{\partial \xi}\right] + \frac{\xi^2-\eta^2}{(1-\eta^2)(\xi^2-1)}\frac{\partial^2 \Psi}{\partial \varphi^2} + c_1^2(\xi^2-\eta^2)\Psi = 0 \quad (2.8)$$

for prolate spheroids, and

$$\frac{\partial}{\partial \eta}\left[(1-\eta^2)\frac{\partial \Psi}{\partial \eta}\right] + \frac{\partial}{\partial \xi}\left[(\xi^2+1)\frac{\partial \Psi}{\partial \xi}\right] + \frac{\xi^2+\eta^2}{(1-\eta^2)(\xi^2+1)}\frac{\partial^2 \Psi}{\partial \varphi^2} + c_1^2(\xi^2+\eta^2)\Psi = 0 \quad (2.9)$$

for oblate spheroids, where $c_1^2 = kc$. Equations (2.8) and (2.9) can be solved using the method of separation of variables. As an example, in case of a prolate spheroid, the solution for (2.8) can be expressed in the form $\Psi(c_1, \eta, \xi, \varphi) = R(c_1, \xi)S(c_1, \eta)\Phi(\varphi)$,

which yields three ordinary differential equations as follows.

$$\frac{d}{d\eta}\left[(1-\eta^2)\frac{dS(c_1,\eta)}{d\eta}\right]+\left[\lambda-c_1^2\eta^2-\frac{\gamma^2}{(1-\eta^2)}\right]S(c_1,\eta)=0 \tag{2.10}$$

$$\frac{d}{d\xi}\left[(\xi^2-1)\frac{dR(c_1,\xi)}{d\xi}\right]+\left[\lambda-c_1^2\xi^2-\frac{\gamma^2}{(\xi^2-1)}\right]R(c_1,\xi)=0 \tag{2.11}$$

$$\frac{d^2\Phi(\varphi)}{d\varphi^2}+\gamma^2\Phi(\varphi)=0 \tag{2.12}$$

where λ and γ are the separation constants. The corresponding equations in oblate spheroidal coordinates can be obtained by the transformations $\xi \to i\xi$ and $c_1 \to -ic_1$ in the equations derived in prolate spheroidal coordinates. The solution for (2.12) can be expressed as

$$\Phi(\varphi)=e^{\pm i\gamma\varphi}. \tag{2.13}$$

In general, equations (2.10) and (2.11) as well as the corresponding equations in oblate spheroidal coordinates can be written in the form

$$\frac{d}{dZ}\left[(1-Z^2)\frac{dU(Z)}{\partial Z}\right]+\left[\lambda-c_1^2Z^2-\frac{\gamma^2}{(1-Z^2)}\right]U(Z)=0. \tag{2.14}$$

The differential equation (2.14) has three singularities, two regular ones at $Z=\pm1$, with exponents $\pm\gamma/2$ and an irregular one at $Z=\infty$, corresponding to the three geometric singular points of the spheroidal coordinate system [49]. Meixner and Schäfke have shown that [49] for $1<Z<\infty$ there exist a fundamental system of

solutions for (2.14) in the form

$$U_1(Ze^{i\pi}) = e^{i\nu\pi}U_1(Z) \tag{2.15}$$

$$U_2(Ze^{i\pi}) = e^{-i(\nu+1)\pi}U_2(Z) \tag{2.16}$$

for distinct values of a parameter ν.

The limiting case when $c_1 \to 0$ will reduce (2.14) into the associated Legendre equation

$$\frac{d}{dZ}\left[(1-Z^2)\frac{dU(Z)}{\partial z}\right] + \left[\lambda - \frac{\gamma^2}{(1-Z^2)}\right]U(Z) = 0. \tag{2.17}$$

The solution of (2.17) are expressed in terms of associated Legendre functions of the first kind $P_\nu^\gamma(Z)$ and the second kind $Q_\nu^\gamma(Z)$, respectively and $\lambda = \nu(\nu+1)$ [see Appendix-C].

Changing the variable $\zeta = c_1 Z$ and letting $c_1 \to 0$, (2.14) will be reduced to the spherical Bessel equation [51]

$$\zeta^2\frac{d^2U(\zeta)}{\partial\zeta^2} + 2\zeta\frac{dU(\zeta)}{\partial\zeta}\left[\zeta^2 - \lambda\right]U(\zeta) = 0 \tag{2.18}$$

where the solution is expressed in terms of spherical Bessel functions $j_\nu(\zeta)$ and Neumann functions $y_\nu(\zeta)$, respectively. In this case $\lambda = \nu(\nu+1)$.

As a special case of $\gamma = 1/2$ and after an elementary transformations $\theta = cos^{-1}(Z)$ and $U(Z) = f(\theta)/[sin^2(\theta)]^{1/4}$, (2.14) reduces to the Mathieu equation [51], [52], with $q = c_1^2/4$ and $a = \lambda - c_1^2/2 + 1/4$.

$$\frac{d^2f(\theta)}{\partial z^2} + \left[(a - 2q\cos(2\theta)\right]f(\theta) = 0. \tag{2.19}$$

Mathieu functions are thus a special case of the spheroidal wave functions.

In the present study we are not interested in the general solution of equation (2.14) for completely arbitrary parameters. In most of the electromagnetic field solutions related to spheroidal geometries we restrict to the solutions which can be used as the constituents of wave function which satisfies the scalar wave equation inside or outside of spheroidal shaped objects. Thus the physical requirements of single-valuedness and finiteness of the wave functions at the poles of the spheroid then dictate that the parameters γ and ν be integers, namely m and n and the function belongs to eigenvalues $\lambda_{m,n}$ be designated spheroidal wave functions [49]. Thus for the future reference we only consider the spheroidal wave functions belongs to integer values of m and n. Thus the solution for the wave equation (2.8) can be express in the form

$$\Psi_{mn}(c_1, \xi, \eta, \varphi) = R_{mn}(c_1, \xi) S_{mn}(c_1, \eta) \begin{matrix} cos \\ sin \end{matrix} m\varphi. \tag{2.20}$$

2.3 Spheroidal Angle Functions

The differential equation satisfy by the spheroidal angle functions can be expressed as

$$\frac{d}{d\eta}\left[(1-\eta^2)\frac{dS_{mn}(\eta)}{d\eta}\right] + \left[\lambda \pm {c_1}^2\eta^2 - \frac{m^2}{(1-\eta^2)}\right] S_{mn}(\eta) = 0. \tag{2.21}$$

Where m be an integer and $m \geq 0$. The spheroidal angle functions are the associated eigenfunctions $S_{mn}(c_1, \eta)$ corresponding to the eigenvalues $\lambda_{mn}(c_1)$ of (2.21). There are two kind of angle functions $S^{(1)}_{mn}(c_1, \eta)$, angle functions of first kind and $S^{(2)}_{mn}(c_1, \eta)$, angle functions of second kind [49]. $S^{(1)}_{mn}(c_1, \eta)$ and $S^{(2)}_{mn}(c_1, \eta)$ can be expressed in the form of an infinite series of associated Legendre functions of the first and second

kinds, respectively as given bellow.

$$S_{mn}^{(1)}(c_1,\eta) = \sum_{r=0,1}^{\infty}{}' d_r^{mn}(c_1) P_{r+m}^m(\eta) \tag{2.22}$$

$$S_{mn}^{(2)}(c_1,\eta) = \sum_{r=-\infty}^{\infty}{}' d_{c_1}^{mn}(c_1) Q_{r+m}^m(\eta). \tag{2.23}$$

The expansion coefficients $d_{c_1}^{mn}$ are to be determined and $P_{r+m}^m(\eta)$ and $Q_{r+m}^m(\eta)$ are the associated Legendre functions of the first kind and second kind, respectively. The prime over the summation sign indicates that the summation is over only the even values of r when $n-m$ is even, and over only odd values of r when $n-m$ is odd. $S_{mn}^{(1)}(c_1,\eta)$ is regular throughout the interval $-1 \geq \eta \leq +1$ and used frequently in physical problems and we simply denoted as $S_{mn}(c_1,\eta)$ in all the analytical expressions derived in chapter 3. From the general theory of Sturm-Liouville differential equations, that the spheroidal angle functions have the orthogonality property in the interval $-1 \geq \eta \leq +1$ [49],

$$\int_{-1}^{+1} S_{mn}(c_1,\eta) S_{mn'}(c_1,\eta) d\eta = \delta_{nn'} N_{mn} \tag{2.24}$$

and $\delta_{nn'}$ is the Kroneckr delta

$$\delta_{nl} = \begin{cases} 0 & \text{if } l \neq n, \\ 1 & \text{if } l = n. \end{cases} \tag{2.25}$$

The normalization constant N_{mn} is given by

$$N_{mn} = 2 \sum_{r=0,1}^{\infty}{}' \frac{(r+2m)![d_r^{mn}(c_1)])^2}{(2r+2m+1)r!}. \tag{2.26}$$

The power series expansion of $S_{mn}(c,\eta)$ in terms of $(1-\eta^2)$ is [49]

$$S_{mn}(c_1,\eta) = (1-\eta^2)^{m/2} \sum_{k=0}^{\infty} c_{2k}^{mn}(c_1)(1-\eta^2)^k,\ (n-m)\ even \tag{2.27}$$

$$S_{mn}(c_1,\eta) = \eta(1-\eta^2)^{m/2} \sum_{k=0}^{\infty} c_{2k}^{mn}(c_1)(1-\eta^2)^k,\ (n-m)\ odd \tag{2.28}$$

and c_{2k}^{mn} are the expansion coefficients to be determined.

2.4 Spheroidal Radial Functions

The spheroidal radial functions are the solution for the differential equation (2.10). Most of the physical problems require both spheroidal radial functions of the first kind $R_{mn}^1(h,\xi)$ and the second kind $R_{mn}^2(h,\xi)$, which are independent solutions of (2.10). In general the solution for the differential equation (2.10) in prolate spheroidal coordinate system can be expressed as

$$\begin{aligned} R_{mn}^{(p)}(c_1,\xi) \ = \ & \left[\sum_{r=0,1}^{\infty}{}' d_r^{mn}(c_1)\frac{(2m+r)!}{r!}\right]^{-1} \left(\frac{\xi^2-1}{\xi^2}\right)^{m/2} \\ & \cdot \sum_{r=0,1}^{\infty}{}' i^{r+m-n} d_r^{mn}(c_1)\frac{(r+2m)!}{r!} Z_{r+m}^{(p)}(c_1\xi). \end{aligned} \tag{2.29}$$

It can be shown that the expansion coefficients $d_r^{mn}(c_1)$ are the same as appeared in the spheroidal angle functions in (2.21) and (2.22) [49]. $Z_{r+m}^{(p)}(c_1\xi)$ represents spherical Bessel, Neumann and Hankel functions [50] as given bellow.

$$Z_n^{(1)}(c_1\xi) = \sqrt{\frac{\pi}{2c_1\xi}} J_{n+1/2}(c_1\xi) = j_n(c_1\xi) \tag{2.30}$$

$$Z_n^{(2)}(c_1\xi) = \sqrt{\frac{\pi}{2c_1\xi}} Y_{n+1/2}(c_1\xi) = y_n(c_1\xi) \tag{2.31}$$

$$Z_n^{(3)}(c_1\xi) = j_n(c_1\xi) + y_n(c_1\xi) = h_n^{(1)}(c_1\xi) \tag{2.32}$$

$$Z_n^{(4)}(c_1\xi) = j_n(c_1\xi) - y_n(c_1\xi) = h_n^{(2)}(c_1\xi), \tag{2.33}$$

where $j_n(c_1\xi), y_n(c_1\xi), h_n^{(1)}(c_1\xi)$, and $h_n^{(2)}(c_1\xi)$ are the spherical Bessel functions, Neumann functions, Hankel functions of the first and second kinds, respectively. The third and the fourth kind of functions $R_{mn}^{(3)}(c_1,\xi)$ and $R_{mn}^{(3)}(c_1,\xi)$ can also be defined as a linear combination of $R_{mn}^{1}(c_1,\xi)$ and $R_{mn}^{1}(c_1,\xi)$ [49] such that

$$R_{mn}^{(3)}(c_1,\xi) = R_{mn}^{(1)}(c_1,\xi) + iR_{mn}^{(2)}(c_1,\xi) \tag{2.34}$$

$$R_{mn}^{(4)}(c_1,\xi) = R_{mn}^{(1)}(c_1,\xi) - iR_{mn}^{(2)}(c_1,\xi). \tag{2.35}$$

The Wronskian provides a useful check on the accuracy of the numerical values of the radial functions. The Wronskian relationship in prolate spheroidal wave functions is

$$R_{mn}^{(1)}(c_1,\xi)\frac{d}{d\xi}R_{mn}^{(2)}(c_1,\xi) - R_{mn}^{(2)}(c_1,\xi)\frac{d}{d\xi}R_{mn}^{(1)}(c_1,\xi) = \frac{1}{c_1(\xi^2-1)}. \tag{2.36}$$

2.5 Relationship between Radial and Angle Spheroidal Functions

Both $S_{mn}^{(1)}(c_1,Z)$ and $R_{mn}^{(1)}(c_1,Z)$ as well as $S_{mn}^{(2)}(c_1,Z)$ and $R_{mn}^{(2)}(c_1,Z)$ satisfy the same differential equation. Therefore spheroidal angle functions and radial functions are

proportional to each other [49],[53], [54] and we can write

$$S_{mn}^{(1)}(c_1, Z) = K_{mn}^{(1)} R_{mn}^{(1)}(c_1, Z) \tag{2.37}$$

$$S_{mn}^{(2)}(c_1, Z) = K_{mn}^{(2)} R_{mn}^{(2)}(c_1, Z). \tag{2.38}$$

Useful expressions for the joining factors $K_{mn}^{(1)}$ and$K_{mn}^{(2)}$ are given in [49],[50].

$$k_{mn}^{(1)} = \begin{cases} \dfrac{(2m+1)(n+m)! \sum\limits_{k=0}^{\infty} d_r^{mn}(c_1)(2m+r)!/r!}{2^{n+m} d_0^{mn}(c_1) {c_1}^m m! \left(\frac{n-m}{2}\right)! \left(\frac{n+m}{2}\right)!}, & (n-m = even) \\ \dfrac{(2m+3)(n+m+1)! \sum\limits_{r=1}^{\infty} d_r^{mn}(c_1)(2m+r)!/r!}{2^{n+m} d_1^{mn}(c_1) {c_1}^{m+1} m! \left(\frac{n-m-1}{2}\right)! \left(\frac{n+m+1}{2}\right)!}, & (n-m = odd) \end{cases} \tag{2.39}$$

$$k_{mn}^{(2)} = \begin{cases} \dfrac{2^{n-m}(2m)! \left(\frac{n-m}{2}\right)! \left(\frac{n+m}{2}\right)! d_{-2m}^{mn}(c_1)}{(2m-1)m!(n+m)! {c_1}^{m-1}} \sum\limits_{k=0}^{\infty} d_k^{mn}(c_1) \dfrac{(2m+k)!}{k!}, & (n-m = even) \\ \dfrac{2^{n-m}(2m)! \left(\frac{n-m-1}{2}\right)! \left(\frac{n+m+1}{2}\right)! d_{-2m+1}^{mn}(c_1)}{(2m-3)(2m-1)m!(n+m+1)! {c_1}^{m-2}} \sum\limits_{k=1}^{\infty} d_k^{mn}(c_1) \dfrac{(2m+k)!}{k!}, & (n-m = odd). \end{cases} \tag{2.40}$$

2.6 Determination of Eigenvalues and Expansion Coefficients

2.6.1 Determination of Spheroidal Expansion Coefficients

Substituting $S_{mn}^{(1)}(c_1, \eta)$ into equation (2.21), and with the use of the recurrence relationship of Associated Legendre functions (see Appenix C.5) and setting the coefficient of $P_{m+k}^{(m)}(\eta)$ equal to zero the following recursion formula is obtained for the

coefficients [49],[50].

$$\alpha_r d_{r+2}^{mn}(c_1) + [\beta_r - \lambda_{mn}(c_1)]\, d_r^{mn}(c_1) + \gamma_r d_{r-2}^{mn}(c_1) = 0,\ r \geq 2 \tag{2.41}$$

$$\alpha_0 d_2^{mn}(c_1) + [\beta_0 - \lambda_{mn}(c_1)]\, d_0^{mn}(c_1) = 0 \tag{2.42}$$

$$\alpha_1 d_3^{mn}(c_1) + [\beta_1 - \lambda_{mn}(c_1)]\, d_1^{mn}(c_1) = 0. \tag{2.43}$$

Here we denote,

$$\alpha_r = \frac{(2m+r+1)(2m+r+1)}{(2m+2r+5)(2m+2r+3)} {c_1}^2 \tag{2.44}$$

$$\beta_r = (m+r)(m+r+1) + \frac{2(m+r)(m+r+1) - m^2 - 1}{(2m+2r-1)(2m+2r+3)} {c_1}^2 \tag{2.45}$$

$$\gamma_r = \frac{r(r-1)}{(2m+2r-3)(2m+2r-1)} {c_1}^2. \tag{2.46}$$

Equation (2.40) gives a set of homogeneous equations. In order to determine $d_r^{mn}(c_1)$ uniquely, we use the fact that when $c_1 \to 0$, the angular wave functions $S_{mn}^{(1)}(c_1, \eta)$ reduce to the corresponding associated Legendre functions. Thus, $d_r^{mn}(c_1)$ satisfy the normalization relation at $\eta = 0$ [49],[50]

$$S_{mn}^{(1)}(c_1, 0) = P_n^m(0) = \frac{(-1)^{(n-m)/2}(n+m)!}{2^n \left(\frac{n-m}{2}\right)! \left(\frac{n+m}{2}\right)!},\ (n-m = even) \tag{2.47}$$

$$S_{mn}'^{(1)}(c_1, 0) = P_n'^m(0) = \frac{(-1)^{(n-m-1)/2}(n+m+1)!}{2^n \left(\frac{n-m-1}{2}\right)! \left(\frac{n+m+1}{2}\right)!},\ (n-m = odd). \tag{2.48}$$

This will lead to normalization relations (2.49) and (2.50) which can be used to

uniquely determine the spheroidal expansion coefficients.

$$\sum_{r=0}^{\infty} \frac{(-1)^{r/2}(2m+r)!}{2^r \left(\frac{r}{2}\right)! \left(\frac{2m+r}{2}\right)!} d_r^{mn}(c_1) = \frac{(-1)^{(n-m)/2}(n+m)!}{2^{n-m} \left(\frac{n-m}{2}\right)! \left(\frac{n+m}{2}\right)!}, \quad (n-m = even) \tag{2.49}$$

$$\sum_{r=0}^{\infty} \frac{(-1)^{(r-1)/2}(2m+r+1)!}{2^r \left(\frac{r-1}{2}\right)! \left(\frac{2m+r+1}{2}\right)!} d_r^{mn}(c_1) = \frac{(-1)^{(n-m-1)/2}(n+m+1)!}{2^{n-m} \left(\frac{n-m-1}{2}\right)! \left(\frac{n+m+1}{2}\right)!} \quad (n-m = odd). \tag{2.50}$$

2.6.2 Determination of Spheroidal Eigenvalues

The two conventional methods of computing spheroidal eigenvalues are given in [49],[55]. One method is to formulate a transcendental equation in terms of continued fractions which contains $\lambda_{mn}(c_1)$ and by aid of a numerical method we can compute the roots of the equation which are the corresponding eigenvalues. In actual computations this method required a truncation of infinite continued fractions to form an equation with finite continued fractions. The other method uses the power series development of eigenvalues for small values of the argument. Both these method are cumbersome and computationally intense. In this thesis we used the method introduced by [56] where the problem of computing eigenvalues is casted into a tridiagonal matrix form and standard matrix eigenvalue computation procedures can be used to

determined the eigenvalues. Consider equation (2.40) and let us denote

$$\begin{aligned} D_q &= \gamma_{2q+s} \\ E_q &= \beta_{2q+s} \\ F_q &= \alpha_{2q+s} \\ a_q &= d_{2q+s} \end{aligned} \tag{2.51}$$

where,

$$\begin{aligned} s = 0, (n-m = even) \\ s = 1, (n-m = odd). \end{aligned} \tag{2.52}$$

For simplicity superscripts m and n and the argument c_1 are suppressed. Then (2.40) becomes

$$D_q a_{q-1} + [E_q - \lambda_{mn}]\, a_q + F_q a_{q+1} = 0,\ q \geq 0. \tag{2.53}$$

A change in variable $a_q = (D_1 D_2 D_3 .....D_q / F_1 F_2 F_3 .....F_q)^{1/2} b_q = 0, q \geq 0$ and then multiplying the resulting equation by $(F_1 F_2 F_3 .....F_q / D_1 D_2 D_3 .....D_q)$, the following form of the recursion relationship is obtained.

$$(D_q F_{q-1})^{1/2} b_{q-1} + [E_q - \lambda_{mn}]\, b_q + (D_{q+1} F_q)^{1/2} b_{q+1} = 0,\ q \geq 0. \tag{2.54}$$

The set of equations represented in (2.54) can be expressed in matrix form

$$\begin{bmatrix} (E_0-\lambda) & (D_1F_0)^{1/2} & 0 & 0 & . & . & . \\ (D_1F_0)^{1/2} & (E_1-\lambda) & (D_2F_1)^{1/2} & 0 & . & . & . \\ 0 & (D_2F_1)^{1/2} & (E_2-\lambda) & (D_3F_2)^{1/2} & . & . & . \\ 0 & 0 & (D_3F_2)^{1/2} & (E_3-\lambda) & . & . & . \\ . & . & . & . & . & . & . \\ . & . & . & . & . & . & . \\ . & . & . & . & . & . & . \end{bmatrix} \begin{bmatrix} b_0 \\ b_1 \\ b_2 \\ b_3 \\ . \\ . \\ . \end{bmatrix} = \begin{bmatrix} 0 \\ 0 \\ 0 \\ 0 \\ . \\ . \\ . \end{bmatrix} . \quad (2.55)$$

Thus, the spheroidal eigenvalue problem has been reduced to that of determining the eigenvalues of a tridiogonal, symmetric matrix. It is necessary to truncate this matrix to form an $N \times N$ matrix. Since the eigenvalues of tridiogonal matrices can be evaluated efficiently with the use of modern mathematical computational tools, this method allows us to calculate eigenvalues with sufficient accuracy for the range of problems considered in this thesis. On the other hand one can use the eigenvalues generated by this method as the good starting estimates for the continued fraction method (for example see pages 553-555 in [50]), first introduced by Bouwkamp [55] and Blanch [57] which uses three term recurrences and infinitely continued fractions. This method requires an approximation of finite continued fractions and a significantly higher intermediate working precision than the precision required in the final numerical results for the eigenvalues [52],[51].

2.7 Concluding Remarks

A brief introduction to the prolate and the oblate spheroidal coordinate systems was presented. The relationships between spheroidal and the rectangular cartesian coordinate systems, metric coefficients, the transformations from prolate to oblate spheroidal systems and the unit vectors are important in deriving the analytical expressions given in chapter-3 and in appendices A and B. A general solution to the scalar wave equation in spheroidal coordinates is given in terms of angle and radial spheroidal wave functions particularly for the field solutions inside and outside of spheroidal objects by considering the physical requirements of single-valuedness and finite solutions at the poles of the spheroids. The methods used for the numerical computation of spheroidal eigenvalues and spheroidal expansion coefficients were also discussed.

Chapter 3

Formulation of the Exact Analytical Solution for Axisymmetric Eddy-Current Fields

3.1 Exact Analytical Solution for Magnetic Vector Potential

Consider a conducting object in the form of a prolate spheroid placed in an external magnetic field produced by a coaxial circular turn carrying a quasistationary time-harmonic current of angular frequency ω, as shown in Fig. 2.1. The time dependency $e^{-i\omega t}$ is adopted and this factor is suppressed in the subsequent expressions derived for the field quantities in this thesis. The prolate spheroidal coordinates η, ξ, φ are used to derive expressions for various field quantities [49]. Since the system is axially symmetric, a simple analytical formulation and an efficient numerical computation are obtained by using a magnetic vector potential which has only a φ-component depending on η and ξ. Outside the conducting spheroid the magnetic vector potential is of the form

$$\boldsymbol{A}_{out} = \boldsymbol{A}'_{out} + \boldsymbol{A}''_{out} \tag{3.1}$$

where $\boldsymbol{A}'_{out} = \boldsymbol{u}_\varphi A'_{out}$ is the magnetic vector potential produced by the induced currents in the conducting spheroid and $\boldsymbol{A}''_{out} = \boldsymbol{u}_\varphi A''_{out}$ is produced by the circular turn alone. Imposing the Coulomb gauge, $\boldsymbol{A}'_{out}$ satisfies the vector Laplace equation

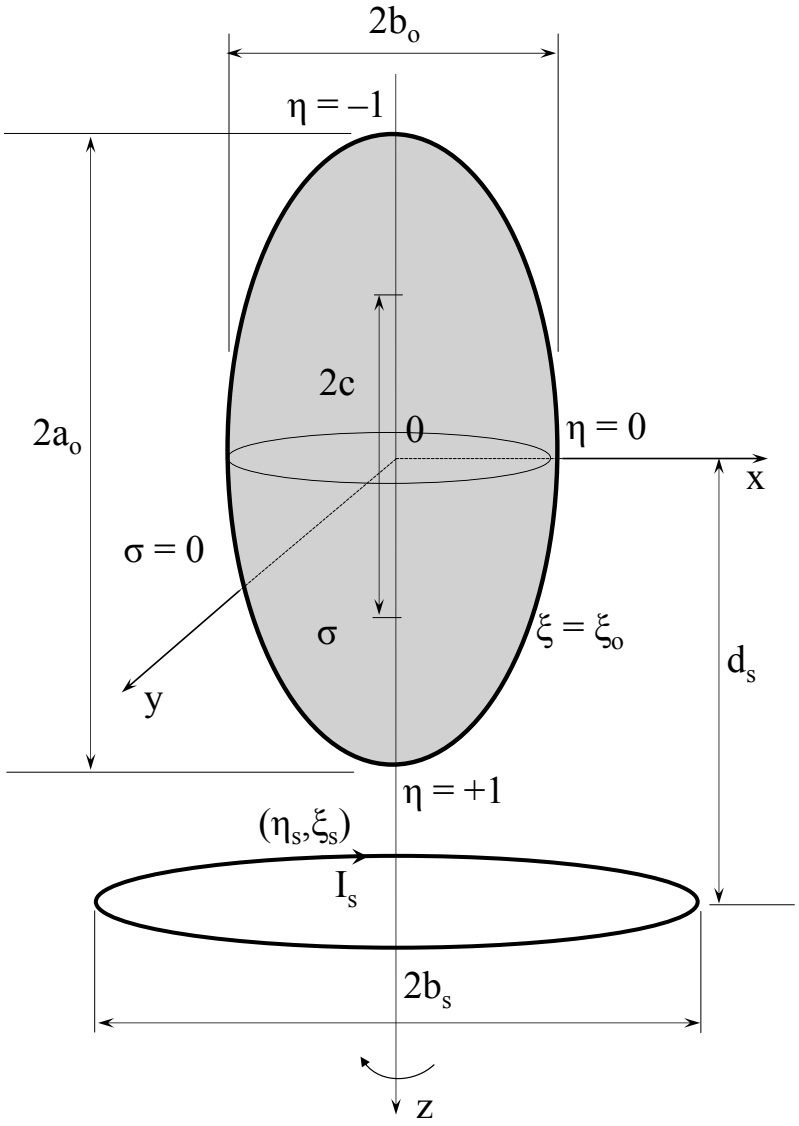

Figure 3.1: Conducting prolate spheroid in the presence of a coaxial current-carrying circular turn.

$$\nabla^2 \boldsymbol{A}'_{out} = 0 \tag{3.2}$$

while $\boldsymbol{A}''_{out}$ is a particular solution of the equation

$$\nabla^2 \boldsymbol{A}''_{out} = -\mu_0 \boldsymbol{J}_s \tag{3.3}$$

with μ_0 the permeability of the region outside the spheroid and $\boldsymbol{J}_s$ the current density in the filamentary turn carrying the current I_s. J_s can be expressed as

$$J_s = \frac{I_s[(1-\eta_s^2)(\xi_s^2-1)]^{1/2}\delta(\eta-\eta_s)\delta(\xi-\xi_s)}{c^2(\xi_s^2-\eta_s^2)} \tag{3.4}$$

where η_s, ξ_s are the coordinates of the circular turn and $\delta(\xi-\xi_s)$ and $\delta(\eta-\eta_s)$ are Dirac delta functions. Equation (3.2) can be simplified into the form (see Appendix A for the complete derivation)

$$\begin{aligned}\frac{1}{c^2(\xi^2-\eta^2)}\{&(1-\eta^2)^{1/2}\frac{\partial^2}{\partial\eta^2}[(1-\eta^2)^{1/2}A'_{out}]\\ &+(\xi^2-1)^{1/2}\frac{\partial^2}{\partial\xi^2}[(\xi^2-1)^{1/2}A'_{out}]\} = 0.\end{aligned} \tag{3.5}$$

The solution of (3.5) is given by the method of separation of variables in the form

$$A'_{out} = \sum_{n=1}^{\infty} C_n Q_n^1(\xi) P_n^1(\eta) \tag{3.6}$$

where P_n^1 and Q_n^1 are the associated Legendre functions of the first and second kinds, respectively, and the C_n are constants of integration. A particular solution of (3.3) can be obtained from the volume integral

$$\boldsymbol{A}''_{out}(\boldsymbol{r}) = \frac{\mu_0}{4\pi}\int_v \frac{\boldsymbol{J}_s(\boldsymbol{r}')}{|\boldsymbol{r}-\boldsymbol{r}'|}dv', \tag{3.7}$$

$\boldsymbol{r}$ and $\boldsymbol{r}'$ being the position vectors of the observation point and the source point, respectively. Substituting (3.4) into (3.7) and expanding the inverse of $|\boldsymbol{r} - \boldsymbol{r}'|$ in terms of prolate spheroidal harmonics [2], [7] yields

$$A''_{out} = -\frac{\mu_0 I_s}{2}[(1-\eta_s^2)(\xi_s^2-1)]^{1/2} \sum_{n=1}^{\infty} \frac{2n+1}{[n(n+1)]^2} \cdot P_n^1(\xi_<) Q_n^1(\xi_>) P_n^1(\eta_s) P_n^1(\eta) \tag{3.8}$$

where $\xi_<$ and $\xi_>$ are the smallest and the largest of ξ and ξ_s, respectively. Thus, the total magnetic vector potential outside the conducting spheroid can be expressed as

$$A_{out} = \sum_{n=1}^{\infty} C_n Q_n^1(\xi) P_n^1(\eta) - \frac{\mu_0 I_s}{2}[(1-\eta_s^2)(\xi_s^2-1)]^{1/2} \cdot \sum_{n=1}^{\infty} \frac{2n+1}{[n(n+1)]^2} P_n^1(\xi_<) Q_n^1(\xi_>) P_n^1(\eta_s) P_n^1(\eta). \tag{3.9}$$

The magnetic vector potential inside the conducting spheroid satisfies the vector Helmholtz equation

$$\nabla^2 \boldsymbol{A}_{in} + k^2 \boldsymbol{A}_{in} = 0 \tag{3.10}$$

with $\boldsymbol{A}_{in} = \boldsymbol{u}_\varphi A_{in}$. For good conductors $k^2 = -i\omega\mu(\sigma + i\omega\epsilon) \approx -i\omega\mu\sigma$, where μ, ϵ and σ being the permeability, permitivity and the conductivity of the spheroid, respectively, and $i \equiv \sqrt{-1}$. A_{in} is expressed in terms of spheroidal wave functions [49] in the form

$$A_{in} = \sum_{n=1}^{\infty} D_n R_{1n}^{(1)}(c_1, \xi) S_{1n}(c_1, \eta) \tag{3.11}$$

where the spheroidal wave-number parameter $c_1 = kc$, D_n are constants of integration, S_{1n} and $R_{1n}^{(1)}$ are angular prolate spheroidal wave functions of the first kind and radial prolate spheroidal wave functions of the first kind, respectively, given by

$$S_{1n}(c_1,\eta) = \sum_{r=0,1}^{\infty}{}' d_r^{1n}(c_1) P_{r+1}^1(\eta) \tag{3.12}$$

$$\begin{aligned} R_{1n}^{(1)}(c_1,\xi) \;=\; & \left[\sum_{r=0,1}^{\infty}{}' d_r^{1n}(c_1)\frac{(r+2)!}{r!}\right]^{-1}\left(\frac{\xi^2-1}{\xi^2}\right)^{1/2} \\ & \cdot \sum_{r=0,1}^{\infty}{}' i^{r-n+1} d_r^{1n}(c_1)\frac{(r+2)!}{r!} j_{r+1}(c_1\xi) \end{aligned} \tag{3.13}$$

d_r^{1n} are spheroidal expansion coefficients and j_{r+1} are spherical Bessel functions of the first kind. The prime over the summation symbol indicates that the summation is performed only over even values of r when $n-1$ is even and only over odd values of r when $n-1$ is odd.

The components of the electric field intensity and the magnetic flux density are derived from the corresponding vector potentials,

$$E_\varphi = -i\omega A \tag{3.14}$$

$$B_\eta = \frac{1}{c(\xi^2-\eta^2)^{1/2}}\frac{\partial}{\partial\xi}\left[(\xi^2-1)^{1/2}A\right] \tag{3.15}$$

$$B_\xi = -\frac{1}{c(\xi^2-\eta^2)^{1/2}}\frac{\partial}{\partial\eta}\left[(1-\eta^2)^{1/2}A\right]. \tag{3.16}$$

The components of the magnetic field intensity H_{in_η} and H_{in_ξ} inside the conducting spheroid are given in the form

$$H_{in_\eta} = \frac{1}{\mu c(\xi^2-\eta^2)^{1/2}}\sum_{n=1}^{\infty} D_n T_{1n}(c_1,\xi) S_{1n}(c_1,\eta) \tag{3.17}$$

$$H_{in_\xi} = -\frac{1}{\mu c(\xi^2-\eta^2)^{1/2}}\sum_{n=1}^{\infty} D_n R_{1n}^{(1)}(c_1,\xi) X_{1n}(c_1,\eta) \tag{3.18}$$

where μ is the permeability of the conductor material and $T_{1n}(c_1,\xi)$ and $X_{1n}(c_1,\eta)$

are given by

$$T_{1n}(c_1,\xi) = \frac{\partial}{\partial \xi}[(\xi^2-1)^{1/2} R_{1n}^{(1)}(c_1,\xi)] \tag{3.19}$$

$$X_{1n}(c_1,\eta) = \frac{\partial}{\partial \eta}[(1-\eta^2)^{1/2} S_{1n}(c_1,\eta)]. \tag{3.20}$$

Outside the spheroid, for $\xi_0 \leq \xi \leq \xi_s$, we have

$$\begin{aligned} H_{out_\eta} &= \frac{1}{\mu_0 c(\xi^2-\eta^2)^{1/2}} \sum_{n=1}^{\infty} \{C_n n(n+1) Q_n(\xi) \\ &\quad -\frac{\mu_0 I_s}{2}\left[(1-\eta_s^2)(\xi_s^2-1)\right]^{1/2} \frac{(2n+1)}{n(n+1)} \\ &\quad \cdot P_n(\xi) Q_n^1(\xi_s) P_n^1(\eta_s)\} P_n^1(\eta) \end{aligned} \tag{3.21}$$

$$\begin{aligned} H_{out_\xi} &= -\frac{1}{\mu_0 c(\xi^2-\eta^2)^{1/2}} \sum_{n=1}^{\infty} \{C_n n(n+1) Q_n^1(\xi) \\ &\quad -\frac{\mu_0 I_s}{2}\left[(1-\eta_s^2)(\xi_s^2-1)\right]^{1/2} \frac{(2n+1)}{n(n+1)} \\ &\quad \cdot P_n^1(\xi) Q_n^1(\xi_s) P_n^1(\eta_s)\} P_n(\eta). \end{aligned} \tag{3.22}$$

The constants of integration C_n and D_n are determined by imposing the continuity of the tangential components of the electric and the magnetic field intensities at the conductor surface $\xi = \xi_0$. From (3.9), (3.11) and (3.14) and equating the tangential components of the electric field intensity at the conductor surface, we get

$$\begin{aligned} &\sum_{n=1}^{\infty} \left[D_n R_{1n}^{(1)}(c_1,\xi_0) S_{1n}(c_1,\eta) - C_n Q_n^1(\xi_0) P_n^1(\eta)\right] \\ &= -\frac{\mu_0 I_s}{2}\left[(1-\eta_s^2)(\xi_s^2-1)\right]^{1/2} \sum_{n=1}^{\infty} \frac{2n+1}{[n(n+1)]^2} P_n^1(\xi_0) \\ &\cdot Q_n^1(\xi_s) P_n^1(\eta_s) P_n^1(\eta) \end{aligned} \tag{3.23}$$

and from (3.17) and (3.21), equating the tangential components of the magnetic field intensity at the conductor surface gives

$$\sum_{n=1}^{\infty}\left[D_n T_{1n}(c_1,\xi_0)S_{1n}(c_1,\eta)-\frac{\mu}{\mu_0}C_n n(n+1)Q_n(\xi_0)P_n^1(\eta)\right]$$
$$=-\frac{\mu I_s}{2}\left[(1-\eta_s^2)(\xi_s^2-1)\right]^{1/2}\sum_{n=1}^{\infty}\frac{2n+1}{n(n+1)}P_n(\xi_0)$$
$$\cdot Q_n^1(\xi_s)P_n^1(\eta_s)P_n^1(\eta). \tag{3.24}$$

Substituting $S_{1n}(c_1,\eta)$ from (3.12) into (3.23), then multiplying both sides by $P_{2q-1}^1(\eta)$, where $q=1,2,...$, and integrating with respect to η, $-1\leq\eta\leq+1$, and, finally, applying the orthogonality property of the associated Legendre functions [58] yields

$$\sum_{p=1}^{\infty}D_{2p-1}R_{1,2p-1}^{(1)}(c_1,\xi_0)d_{2q-2}^{1,2p-1}(c_1)-C_{2q-1}Q_{2q-1}^1(\xi_0)$$
$$=-\frac{\mu_0 I_s}{2}\left[(1-\eta_s^2)(\xi_s^2-1)\right]^{1/2}\frac{4q-1}{[2q(2q-1)]^2}P_{2q-1}^1(\xi_0)$$
$$\cdot Q_{2q-1}^1(\xi_s)P_{2q-1}^1(\eta_s). \tag{3.25}$$

Multiplying both sides of (3.23) by $P_{2q}^1(\eta)$ and integrating with respect to η, we get

$$\sum_{p=1}^{\infty}D_{2p}R_{1,2p}^{(1)}(c_1,\xi_0)d_{2q-1}^{1,2p}(c_1)-C_{2q}Q_{2q}^1(\xi_0)$$
$$=-\frac{\mu_0 I_s}{2}\left[(1-\eta_s^2)(\xi_s^2-1)\right]^{1/2}\frac{4q+1}{[2q(2q+1)]^2}P_{2q}^1(\xi_0)$$
$$\cdot Q_{2q}^1(\xi_s)P_{2q}^1(\eta_s). \tag{3.26}$$

Similarly, from (3.24) we get

$$\sum_{p=1}^{\infty} D_{2p-1} T_{1,2p-1}(c_1,\xi_0) d_{2q-2}^{1,2p-1} - \frac{\mu}{\mu_0} C_{2q-1} 2q(2q-1) Q_{2q-1}(\xi_0)$$
$$= -\frac{\mu I_s}{2} \left[(1-\eta_s^2)(\xi_s^2-1)\right]^{1/2} \frac{4q-1}{2q(2q-1)} P_{2q-1}(\xi_0)$$
$$\cdot Q_{2q-1}^1(\xi_s) P_{2q-1}^1(\eta_s) \tag{3.27}$$

and

$$\sum_{p=1}^{\infty} D_{2p} T_{1,2p}(c_1,\xi_0) d_{2q-1}^{1,2p}(c_1) - \frac{\mu}{\mu_0} C_{2q} 2q(2q+1) Q_{2q}(\xi_0)$$
$$= -\frac{\mu I_s}{2} \left[(1-\eta_s^2)(\xi_s^2-1)\right]^{1/2} \frac{4q+1}{2q(2q+1)} P_{2q}(\xi_0)$$
$$\cdot Q_{2q}^1(\xi_s) P_{2q}^1(\eta_s). \tag{3.28}$$

Eliminating C_{2q-1} from (3.25) and (3.27), we get an infinite system of linear equations for the unknowns D_{2p-1}

$$\sum_{p=1}^{\infty} D_{2p-1} \{2q(2q-1) R_{1,2p-1}^{(1)}(c_1,\xi_0) Q_{2q-1}(\xi_0) - \frac{\mu_0}{\mu} T_{1,2p-1}(c_1,\xi_0) Q_{2q-1}^1(\xi_0)\} d_{2q-2}^{1,2p-1}(c_1)$$
$$= \frac{\mu_0 I_s}{2} \left[(1-\eta_s^2)(\xi_s^2-1)\right]^{1/2} \frac{4q-1}{2q(2q-1)} \{P_{2q-1}(\xi_0) Q_{2q-1}^1(\xi_0) - P_{2q-1}^1(\xi_0) Q_{2q-1}(\xi_0)\}$$
$$\cdot Q_{2q-1}^1(\xi_s) P_{2q-1}^1(\eta_s), \qquad q = 1,2,... \tag{3.29}$$

and eliminating C_{2q} from (3.26) and (3.28), we get an infinite system in the unknowns D_{2p}

$$\sum_{p=1}^{\infty} D_{2p} \{2q(2q+1) R_{1,2p}^{(1)}(c_1,\xi_0) Q_{2q}(\xi_0) - \frac{\mu_0}{\mu} T_{1,2p}(c_1,\xi_0) Q_{2q}^1(\xi_0)\} d_{2q-1}^{1,2p}(c_1)$$
$$= \frac{\mu_0 I_s}{2} \left[(1-\eta_s^2)(\xi_s^2-1)\right]^{1/2} \frac{4q+1}{2q(2q+1)} \{P_{2q}(\xi_0) Q_{2q}^1(\xi_0) - P_{2q}^1(\xi_0) Q_{2q}(\xi_0)\}$$
$$\cdot Q_{2q}^1(\xi_s) P_{2q}^1(\eta_s), \qquad q = 1,2,... \tag{3.30}$$

The infinite systems of linear equations in (3.29) and (3.30) are appropriately truncated to solve for D_{2p-1} and D_{2p}. The numerical values for the required spheroidal expansion coefficients are computed based on the method described in chapter 2.6.1. Once D_{2p-1} and D_{2p} are determined, C_{2q-1} and C_{2q} can be computed from (3.25) and (3.26), respectively.

3.2 Power Losses and Forces due to Induced Currents

The power loss inside the conducting spheroid is calculated by integrating the complex Poynting vector over the conductor surface and taking its real part,

$$P = \frac{1}{2}\mathrm{Re}\int_s \left(\boldsymbol{E}_\varphi \times \boldsymbol{H}_\eta^*\right)_{\xi=\xi_0} \cdot d\mathbf{s} \tag{3.31}$$

where $d\mathbf{s} = h_\eta h_\varphi d\eta d\varphi \boldsymbol{u}_\xi$, with h_η and h_φ being the corresponding scale factors in spheroidal coordinates [49]. The tangential components of the electric field intensity E_φ and the magnetic field intensity H_η at the conductor surface are determined from (3.14), with the magnetic vector potential A_{out} as given in (3.9), and (3.21), respectively.

The force acting on the spheroid is equal in magnitude and opposite in direction to the force acting on the inducing turn. The resultant time-averaged force can be expressed as [7]

$$F = \pi b_s \mathrm{Re}(I_s^* B_{\rho s}^{ind}) \tag{3.32}$$

being oriented along the z-axis. $B_{\rho s}^{ind}$ is the projection of the magnetic flux density due to the induced currents along a direction perpendicular to the z-axis ($\boldsymbol{u}_\rho$), taken at the points on the inducing turn, and can be expressed as

$$B_{\rho s}^{ind} = B_{\eta s}^{ind}\boldsymbol{u}_\eta \cdot \boldsymbol{u}_\rho + B_{\xi s}^{ind}\boldsymbol{u}_\xi \cdot \boldsymbol{u}_\rho \tag{3.33}$$

B_η^{ind} and B_ξ^{ind} are determined from (3.15) and (3.16), respectively, with the magnetic vector potential A'_{out} as given in (3.6). The unit vectors $\boldsymbol{u}_\eta$ and $\boldsymbol{u}_\xi$ are given in (2.5). Due to the axisymmetry of the problem, we can chose $\boldsymbol{u}_\rho = \boldsymbol{u}_x$ (i.e. at $\varphi = 0$), thus,

$$\begin{aligned} \boldsymbol{u}_\eta \cdot \boldsymbol{u}_\rho &= \frac{-\eta(\xi^2-1)^{1/2}}{(\xi^2-\eta^2)^{1/2}} \\ \boldsymbol{u}_\xi \cdot \boldsymbol{u}_\rho &= \frac{\xi(1-\eta^2)^{1/2}}{(\xi^2-\eta^2)^{1/2}}. \end{aligned} \tag{3.34}$$

The resultant force acting on the spheroid is given by (3.32) in the form

$$\begin{aligned} F = 2\pi \mathrm{Re}\{ I_s^2 \frac{[(1-\eta_s^2)(\xi_s^2-1)]^{1/2}}{(\xi_s^2-\eta_s^2)} \\ \cdot \sum_{n=1}^{\infty} C_n (n+1) \mathcal{K}_n(\eta_s, \xi_s) \} \end{aligned} \tag{3.35}$$

where

$$\mathcal{K}_n(\eta_s, \xi_s) \equiv \eta_s Q_{n-1}^1(\xi_s) P_n^1(\eta_s) - \xi_s Q_n^1(\xi_s) P_{n-1}^1(\eta_s). \tag{3.36}$$

It should be noted that the expressions for the field quantities for oblate spheroids can be determined by performing the transformations $\xi \to i\xi$ and $c \to -ic$ in the corresponding expressions obtained in prolate spheroidal coordinates. For an inducing system consists of more than one circular current carrying turn, the resultant magnetic vector potential (thus the electric and magnetic fields) can be determined by the superposition of the magnetic vector potentials produced by individual turn acting separately.

3.3 Concluding Remarks

In this chapter, rigorous analytical expressions were derived for the magnetic vector potential and the field quantities both inside and outside of conducting prolate and

oblate spheroids immersed in a nonuniform field produced by current-carrying circular turns. Exact expressions were also derived for the power losses in spheroids and the forces exerted upon them. These exact analytical expressions can be used to generate numerical results for a large range of values for the characteristic parameters, namely, the axial ratio, the relative distance between the spheroids and the inducing turns, and the ratio of the penetration depth to the linear dimension of the spheroids.

Chapter 4

Numerical Computations of Fields, Losses and Forces

4.1 Numerical Computation of Special Functions

Numerical values of P_n^1 have been computed using the recurrence formula for the associated Legendre functions [58]. For Q_n^1 with a real argument greater than one, the algorithm in [59] has been used, and, for complex arguments, the subroutine in [60]. Spherical Bessel functions with complex arguments in (3.14) have been calculated using a Matlab built-in subroutine. The complex spheroidal eigenvalues required for the computation of the spheroidal expansion coefficients $d_{2q-1}^{1,2p}(c_1)$ and $d_{2q-2}^{1,2p-1}(c_1)$ are determined using the method presented in [56], where the problem was reduced to determining the eigenvalues of a complex tridiagonal symmetric matrix (see section 2.6.2 for the detail derivation). The resulting infinite matrix is truncated to obtain a matrix of about 200-by-200 in size and the eigenvalues of this matrix are determined by using a Matlab built-in subroutine. Then, the spheroidal expansion coefficients are obtained by using the Matlab routine given in [60] for real arguments, but with slight modifications for complex arguments.

Computation of S_{1n} and X_{1n} in (2.13) and (2.21), respectively, and of $R_{1n}^{(1)}$ and T_{1n} in (2.14) and (2.20), respectively, requires a truncation of the respective infinite series and this has been done by retaining a number of terms determined empirically as in [50], i.e. $25 + [n - 1 + |c_1|]$ terms, where [ ] indicates the integer part. As noted in [11], [12], [61], it is observed that the computation of the spheroidal wave functions becomes unstable when the spheroidal wave-number parameter increases to $|c_1| \cong 30$. Numerical values generated for S_{1n} and $R_{1n}^{(1)}$ with complex arguments, as well as their first derivatives were compared with those obtained from a software package [52],[51] developed to compute highly accurately spheroidal wave functions with complex arguments, which was achieved by testing the Wronskian, by checking the respective differential equation and by generating function values using two different levels of computational precision. The numerical values for the spheroidal wave functions used in this paper have at least 10−digit accuracy.

Finally, the infinite systems in (2.30) and (2.31) have been truncated by retaining the first 25 coefficients D_{2p-1} and D_{2p}, respectively, i.e. 50 coefficients D_n in (2.12), which is found to be sufficient in order to obtain at least a 4−digit accuracy for the numerical results presented in Figs. 3.1,3.2, a 6−digit accuracy for the results in Figs. 3.3,3.4 and an 8−digit accuracy for the results in Figs. 3.5,3.6. The inversion of the resulting near singular square matrices in (2.29) and (2.30) is performed by using the Matlab subroutine for Moore-Penrose pseudoinverse. Numerical results generated based on the formulation presented are in good agreement with the results for the special case of a conducting sphere [32].

It should be noted that the normalized magnetic vector potential, power losses and forces in Figs. 3.1−3.6 depend only on the dimensionless geometric parameters $a_0/b_0, b_0/b_s, d_s/b_s$ (see Fig. 2.1), on the relative permeability of the spheroid material

and on the ratio of the penetration depth δ to the semi-minor axis of the spheroid ($\delta = (2/(\omega\mu\sigma))^{1/2}$). Where μ is the permeability of the conducting material. The latter dimensionless parameter is especially useful in eddy-current and skin-effect problems. ξ_0, η_s, ξ_s are simple functions of the above geometric parameters, as determined by (2.1), and the wave-number parameter

$$c_1 = \frac{b_0}{\delta}\left[\left(\frac{a_0}{b_0}\right)^2 - 1\right]^{1/2}(1-i) \tag{4.1}$$

for prolate spheroids and

$$c_1 = \frac{a_0}{\delta}\left[\left(\frac{b_0}{a_0}\right)^2 - 1\right]^{1/2}(1-i) \tag{4.2}$$

for oblate spheroids. Numerical results are generated for spheroids made of good conducting materials with permeability that of free space $\mu = \mu_0$.

Figures $4.1 - 4.4$ give the absolute value of the magnetic vector potential normalized to $\mu_0 I_s$ on the surface of conducting prolate and oblate spheroids, respectively, as a function of η for different axial ratios a_0/b_0 and for various ratios of the penetration depth to the semi-minor axis. A small sample of numerical data is given in Table 4.1. The induced electric field intensity is obtained directly from the vector potential using (3.14), for given frequency, and the current density inside the spheroid from $\boldsymbol{J} = \sigma\boldsymbol{E}$, for specified frequency and conductivity. In figures $4.5 - 4.8$, the power loss normalized to $I_s^2/(\sigma\delta)$ is presented as a function of the ratio d_s/b_s for different axial ratios and for various δ/b_0 for prolate spheroids and various δ/a_0 for oblate spheroids. Similarly, figures $4.9- 4.12$, present data for the force normalized to $\mu_0 I_s^2$ acting upon conducting prolate and oblate spheroids, respectively, as a function of d_s/b_s. The normalized force gives directly the actual force for a given current carried

by the inducing turn, while the actual Joule losses are obtained from the normalized values by also specifying the product $\sigma\delta$,$\sigma\delta = (2\sigma/(\omega\mu_0))^{1/2}$. A sample of numerical data for normalized power loss and force is presented in Tables 4.2 and 4.3.

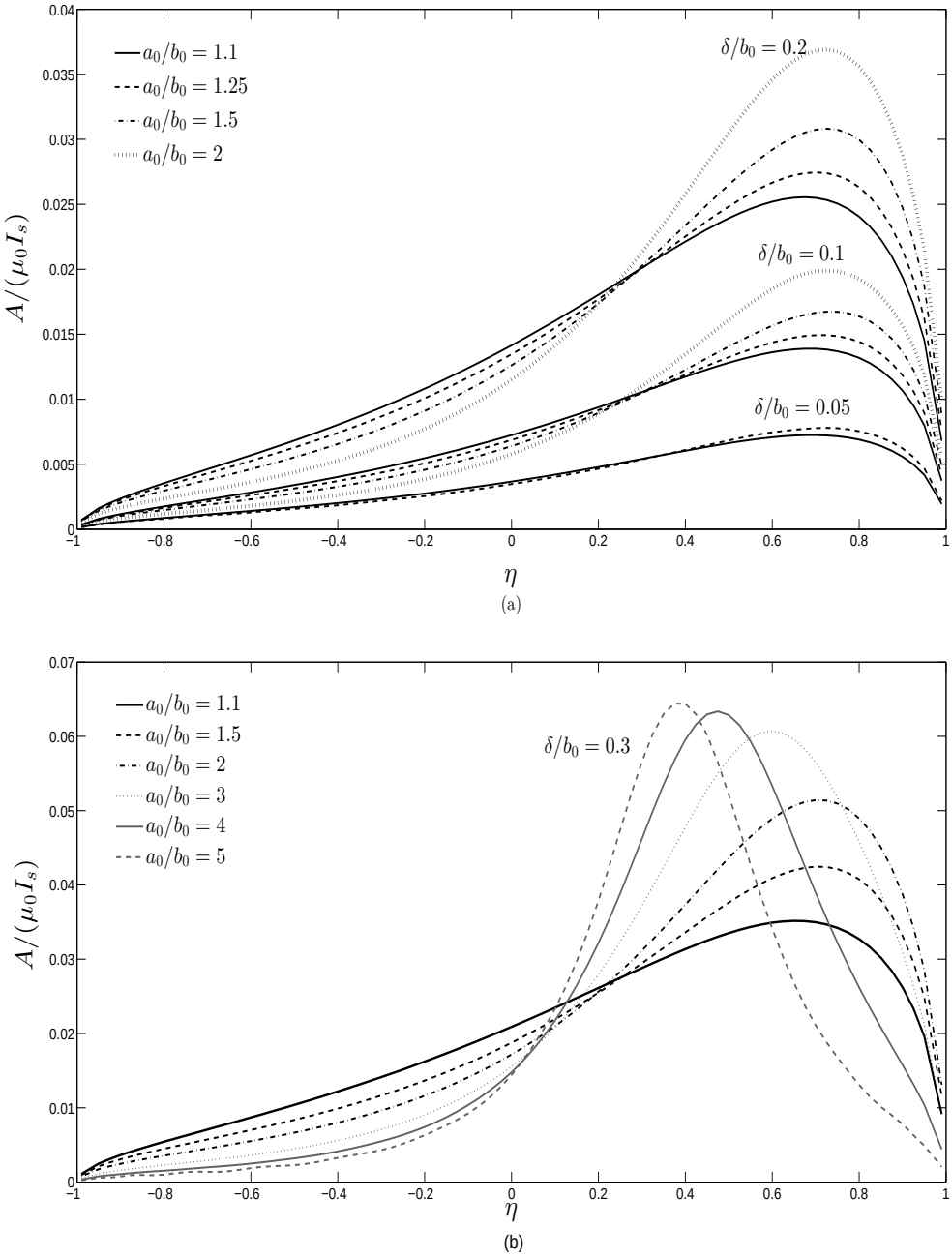

Figure 4.1: Normalized magnetic vector potential on the surface of conducting prolate spheroids as a function of η for the system shown in Fig. 3.1, with $b_0/b_s = 0.5$, $d_s/b_s = 1$, for different axial ratios a_0/b_0 and various ratios (a) $\delta/b_0 = 0.05, 0.1, 0.2$ and (b) $\delta/b_0 = 0.3$.

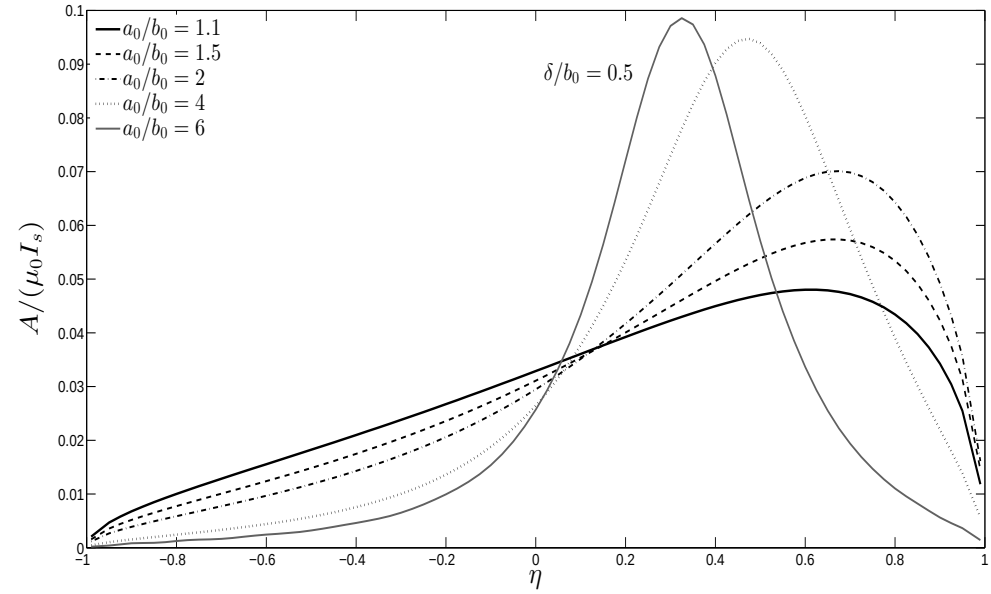

(c)

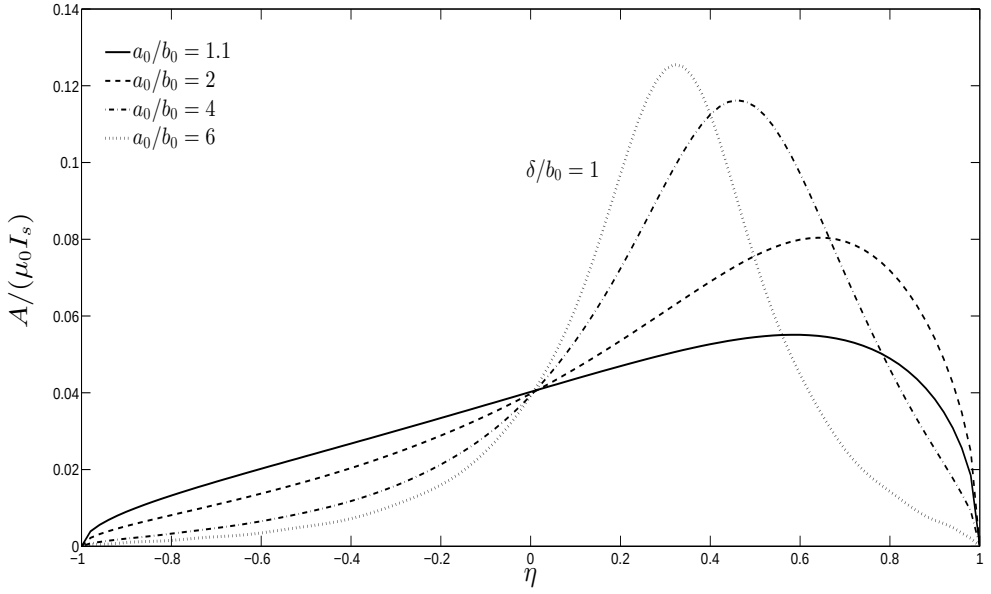

(d)

Figure 4.2: Normalized magnetic vector potential on the surface of conducting prolate spheroids as a function of η, with $b_0/b_s = 0.5$, $d_s/b_s = 1$, for different axial ratios a_0/b_0 and various ratios (a) $\delta/b_0 = 0.5$, and (b) $\delta/b_0 = 1$.

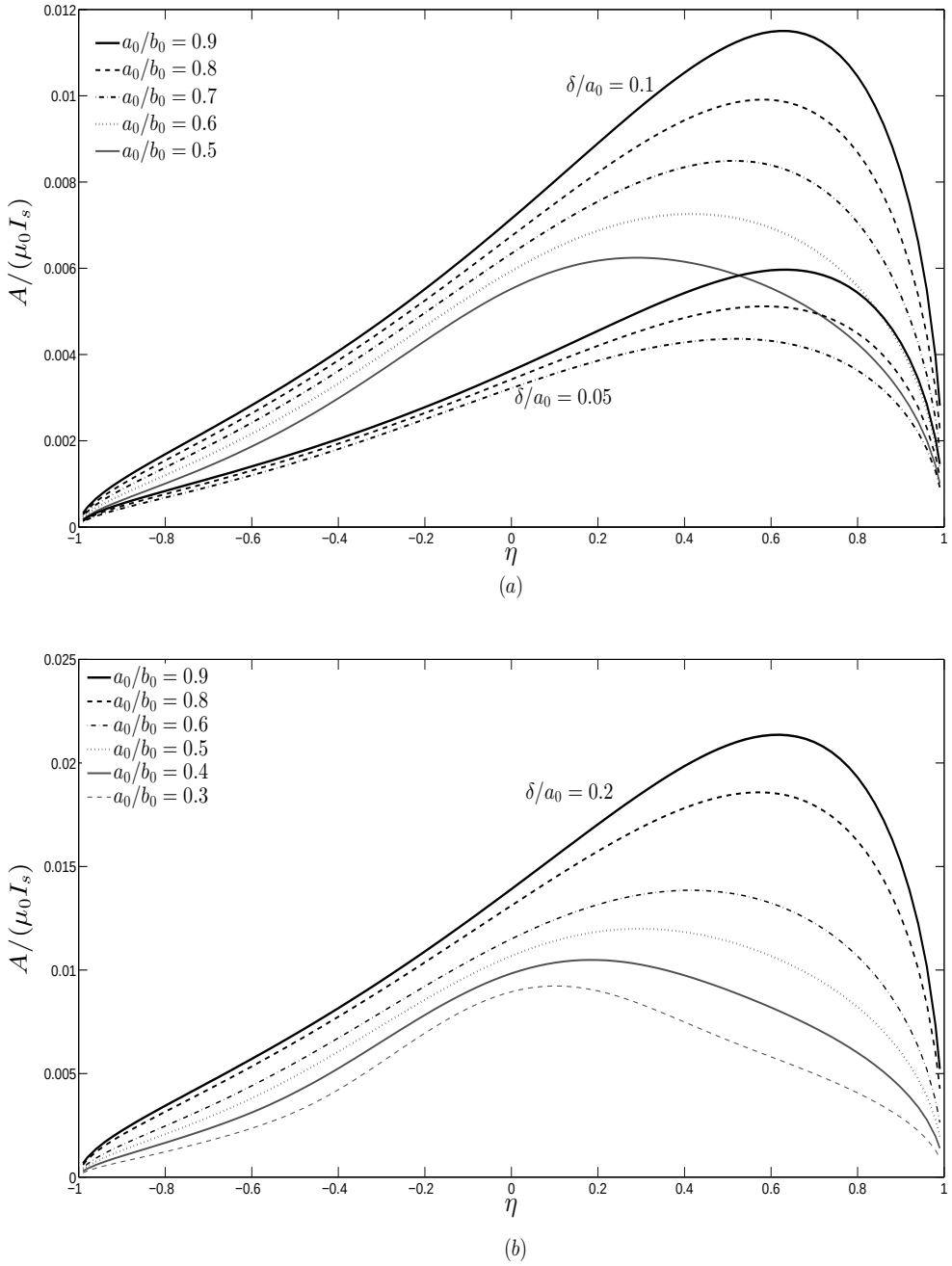

Figure 4.3: Normalized magnetic vector potential on the surface of conducting oblate spheroids as a function of η, with $b_0/b_s = 0.5$, $d_s/b_s = 1$, for different axial ratios a_0/b_0 and various ratios (a) $\delta/a_0 = 0.05, 0.1$ and (b)$\delta/a_0 = 0.2$.

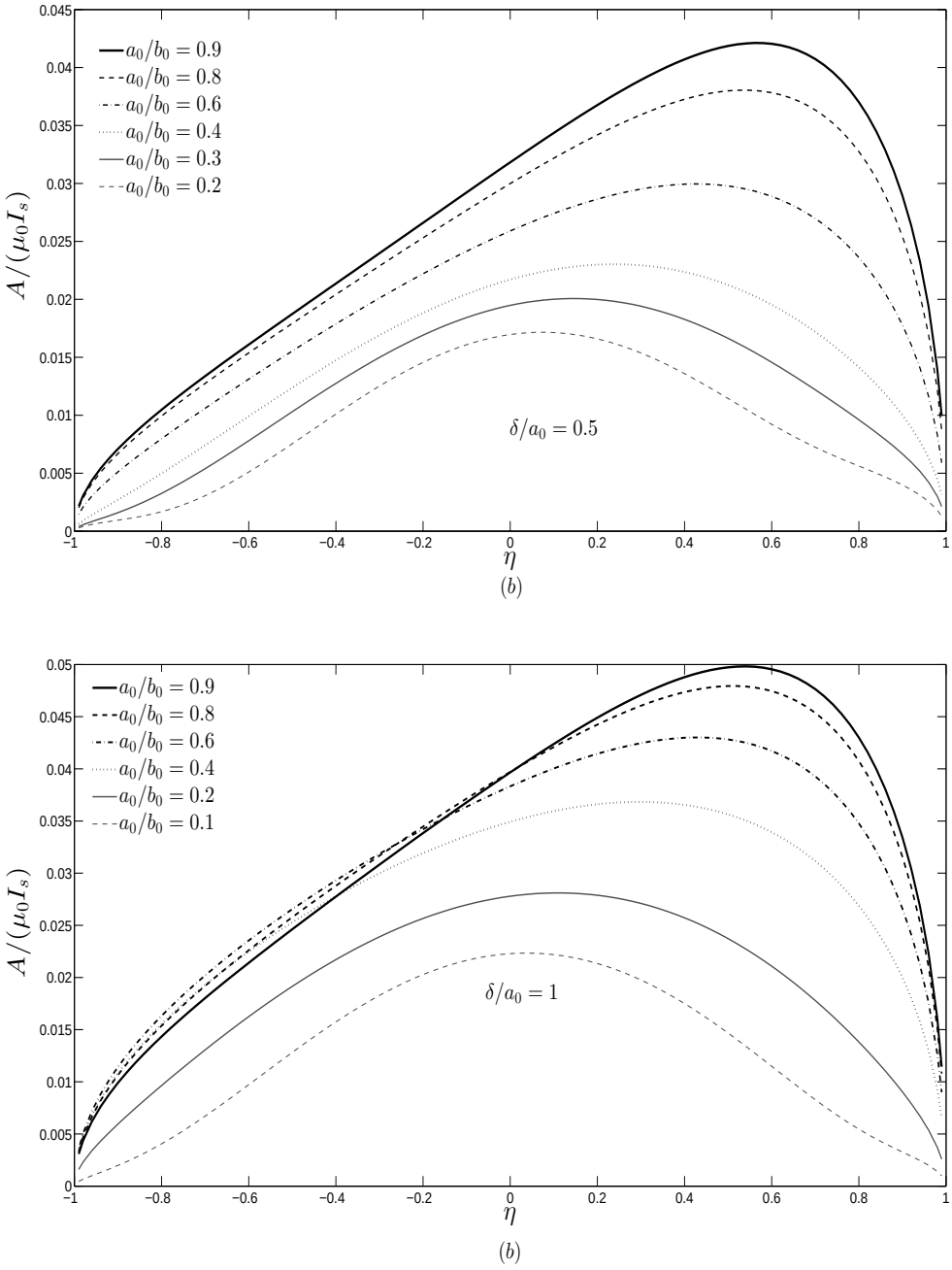

Figure 4.4: Normalized magnetic vector potential on the surface of conducting oblate spheroids as a function of η, with $b_0/b_s = 0.5$, $d_s/b_s = 1$, for different axial ratios a_0/b_0 and various ratios (a) $\delta/a_0 = 0.5$ and (b)$\delta/a_0 = 1$.

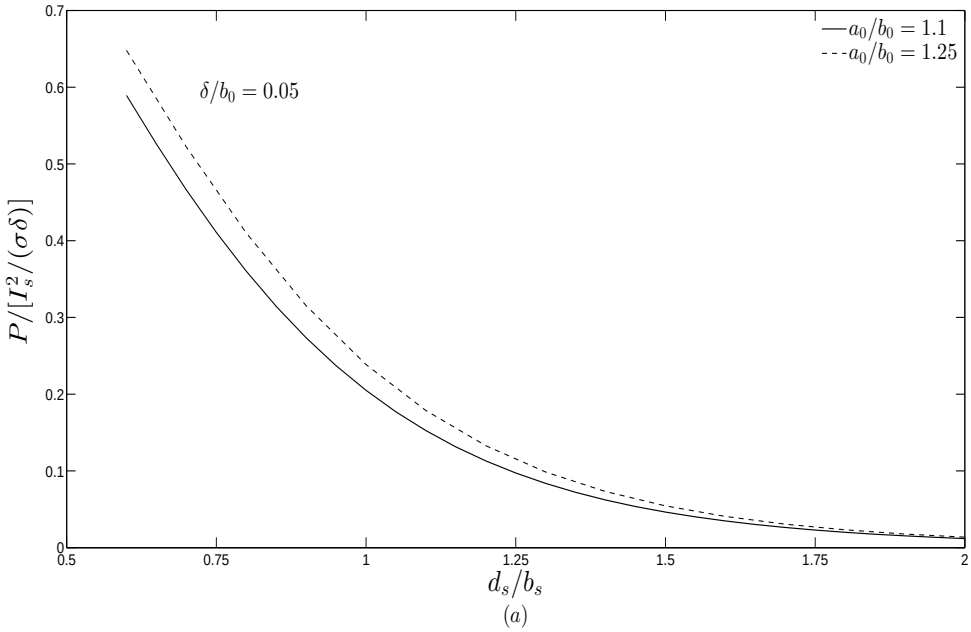

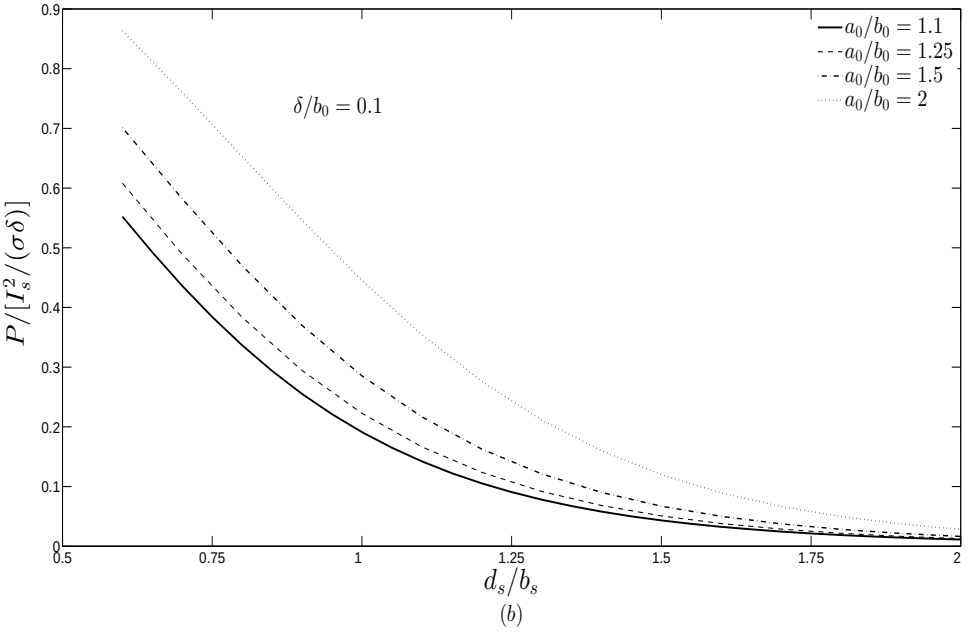

Figure 4.5: Normalized power loss in conducting prolate spheroids as a function of d_s/b_s for the system shown in Fig. 3.1, with $b_0/b_s = 0.5$, for different axial ratios a_0/b_0 and various ratios (a) $\delta/b_0 = 0.05$ and (b)$\delta/b_0 = 0.1$.

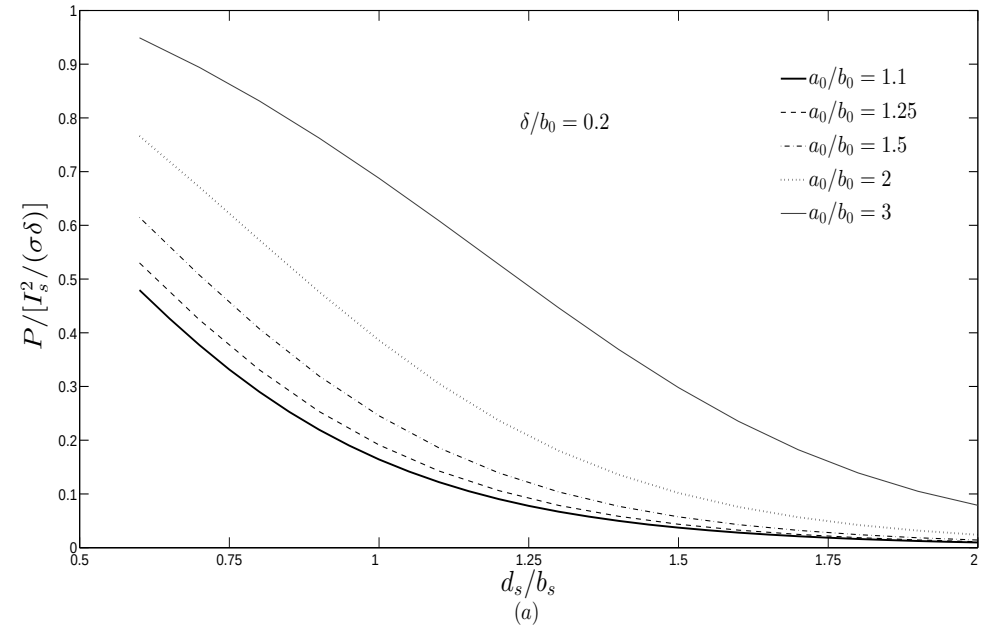

Figure 4.6: Normalized power loss in conducting prolate spheroids as a function of d_s/b_s, with $b_0/b_s = 0.5$, for different axial ratios a_0/b_0 and various ratios (a) $\delta/b_0 = 0.2$ and (b)$\delta/b_0 = 1$.

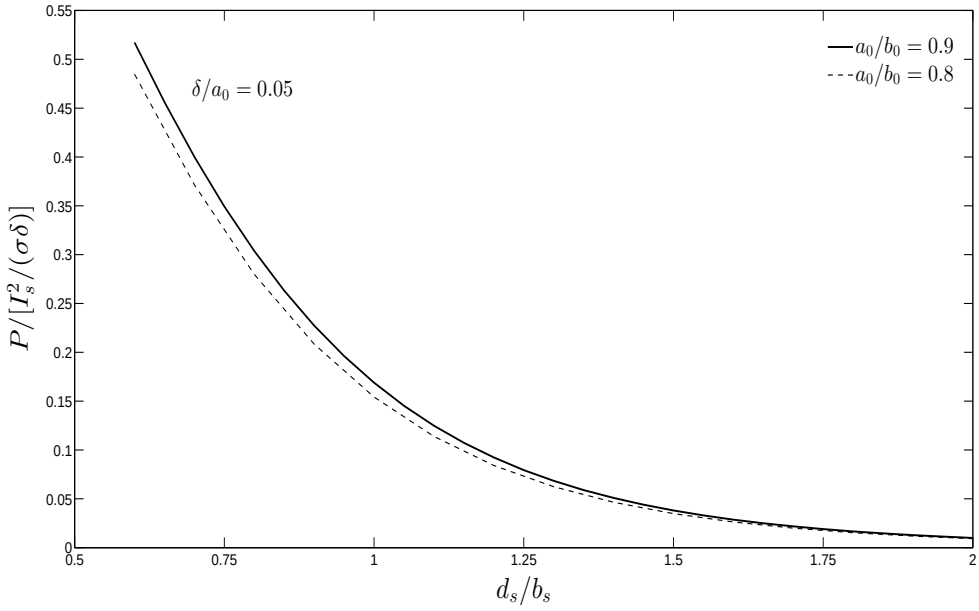

(a)

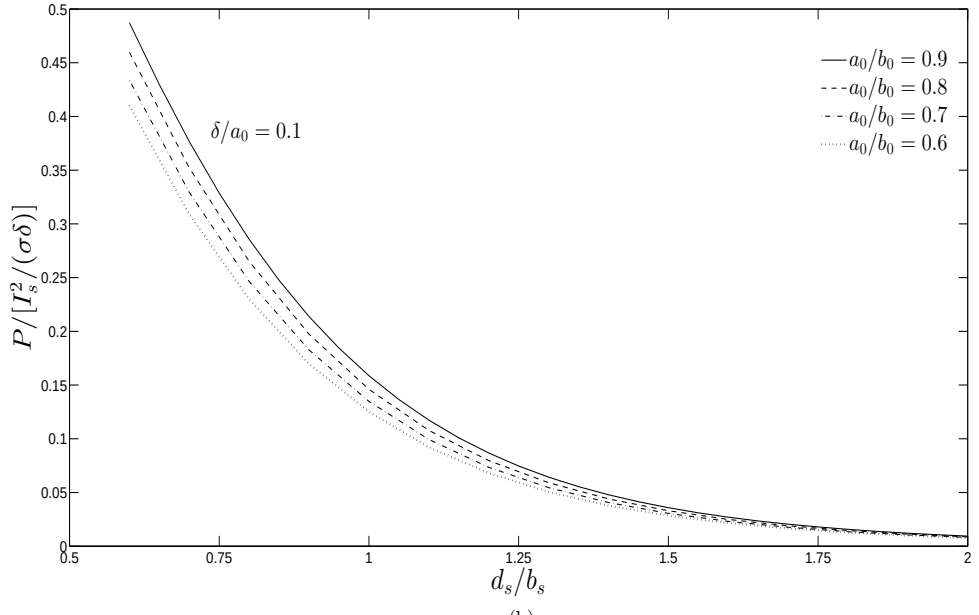

(b)

Figure 4.7: Normalized power loss in conducting oblate spheroids as a function of d_s/b_s, with $b_0/b_s = 0.5$, for different axial ratios a_0/b_0 and various ratios (a) $\delta/a_0 = 0.05$ and (b)$\delta/a_0 = 0.1$.

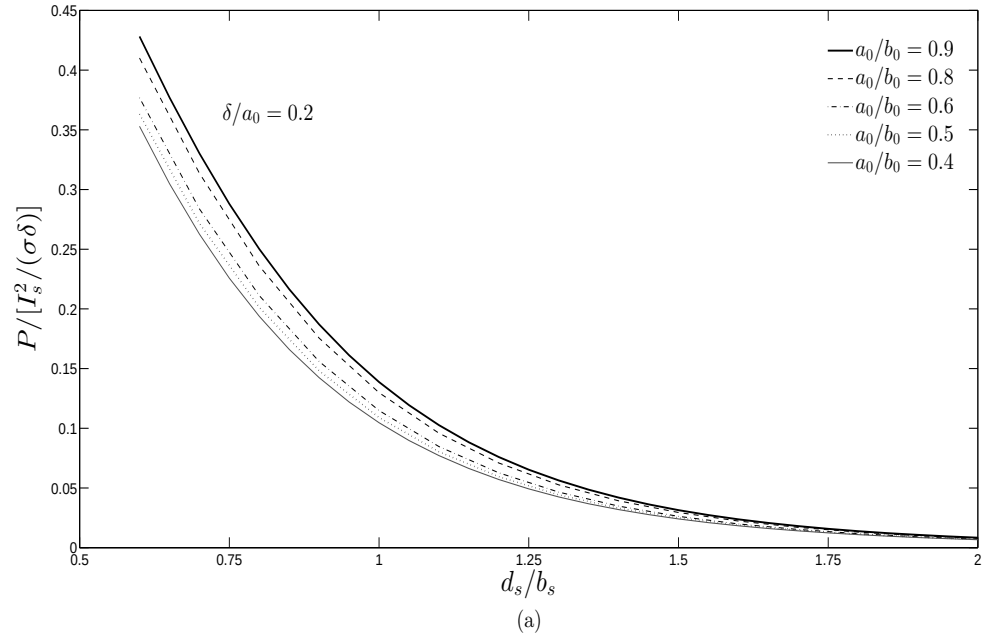

(a)

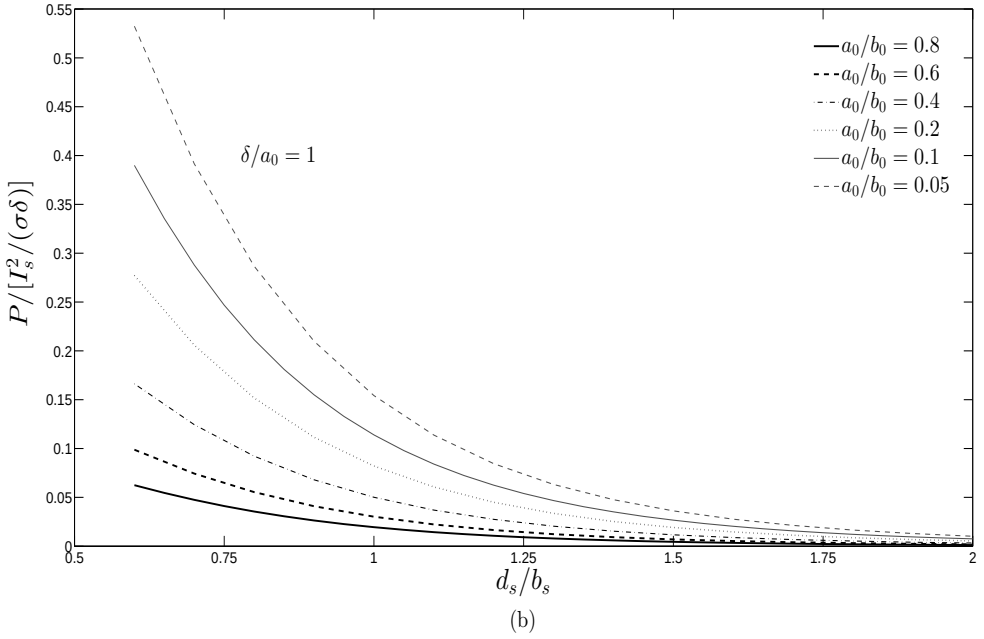

(b)

Figure 4.8: Normalized power loss in conducting oblate spheroids as a function of d_s/b_s, with $b_0/b_s = 0.5$, for different axial ratios a_0/b_0 and various ratios (a) $\delta/a_0 = 0.2$ and (b)$\delta/a_0 = 1$.

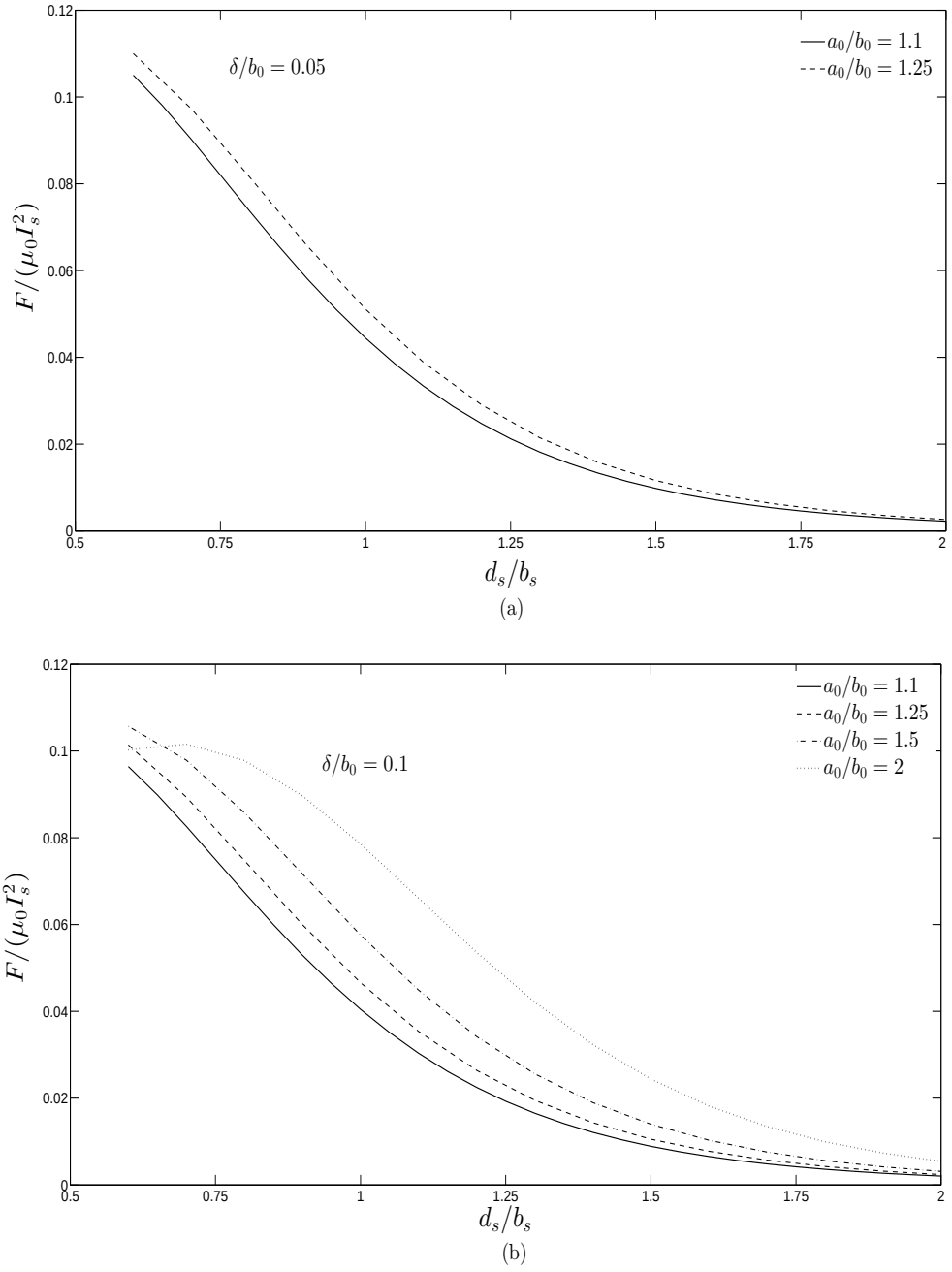

Figure 4.9: Normalized force acting on conducting prolate spheroids as a function of d_s/b_s for the system shown in Fig. 3.1, with $b_0/b_s = 0.5$, for different axial ratios a_0/b_0 and various ratios (a) $\delta/b_0 = 0.05$ and (b)$\delta/b_0 = 0.1$.

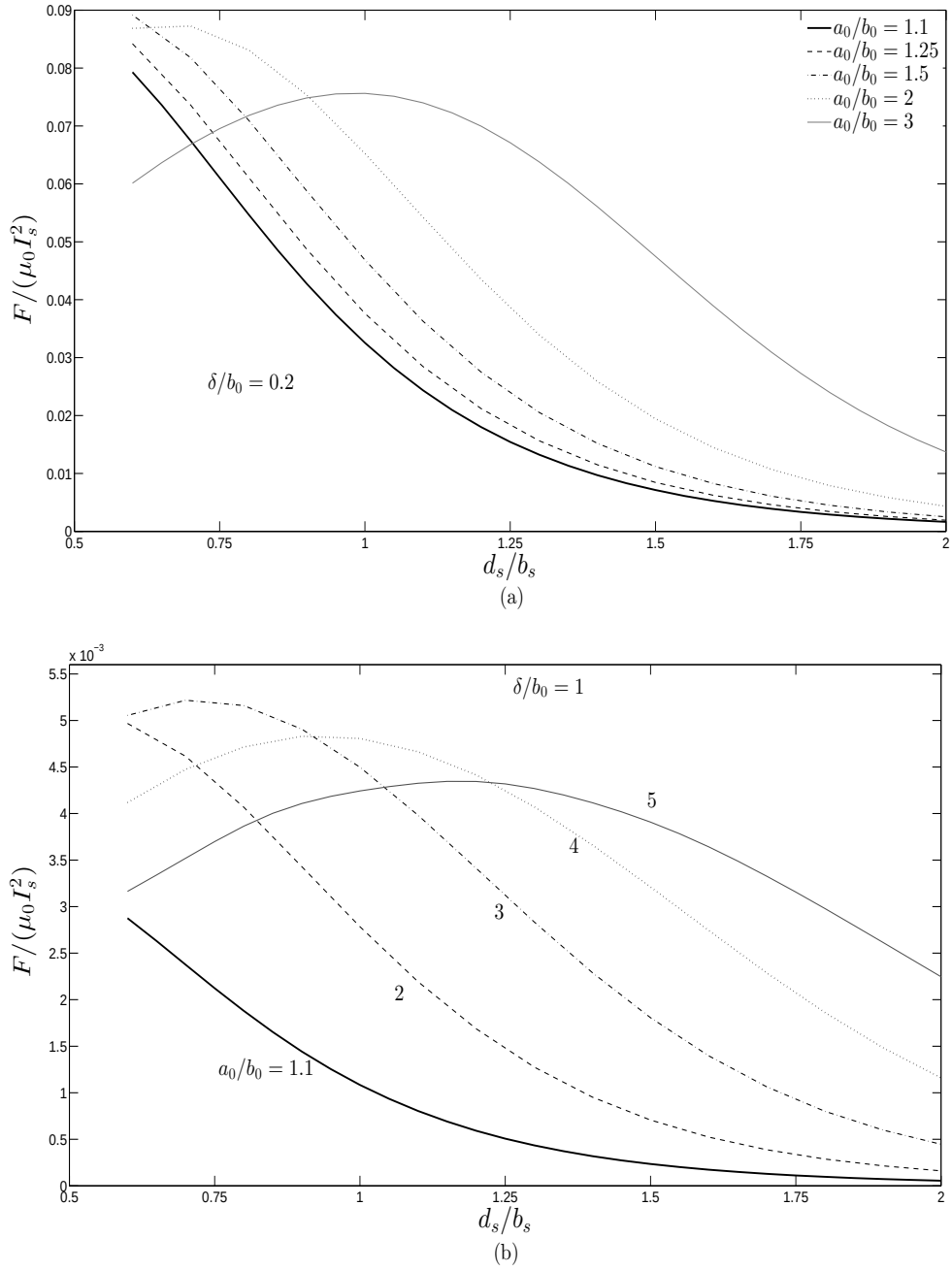

Figure 4.10: Normalized force acting on conducting prolate spheroids as a function of d_s/b_s, with $b_0/b_s = 0.5$, for different axial ratios a_0/b_0 and various ratios (a) $\delta/b_0 = 0.2$ and (b)$\delta/b_0 = 1$.

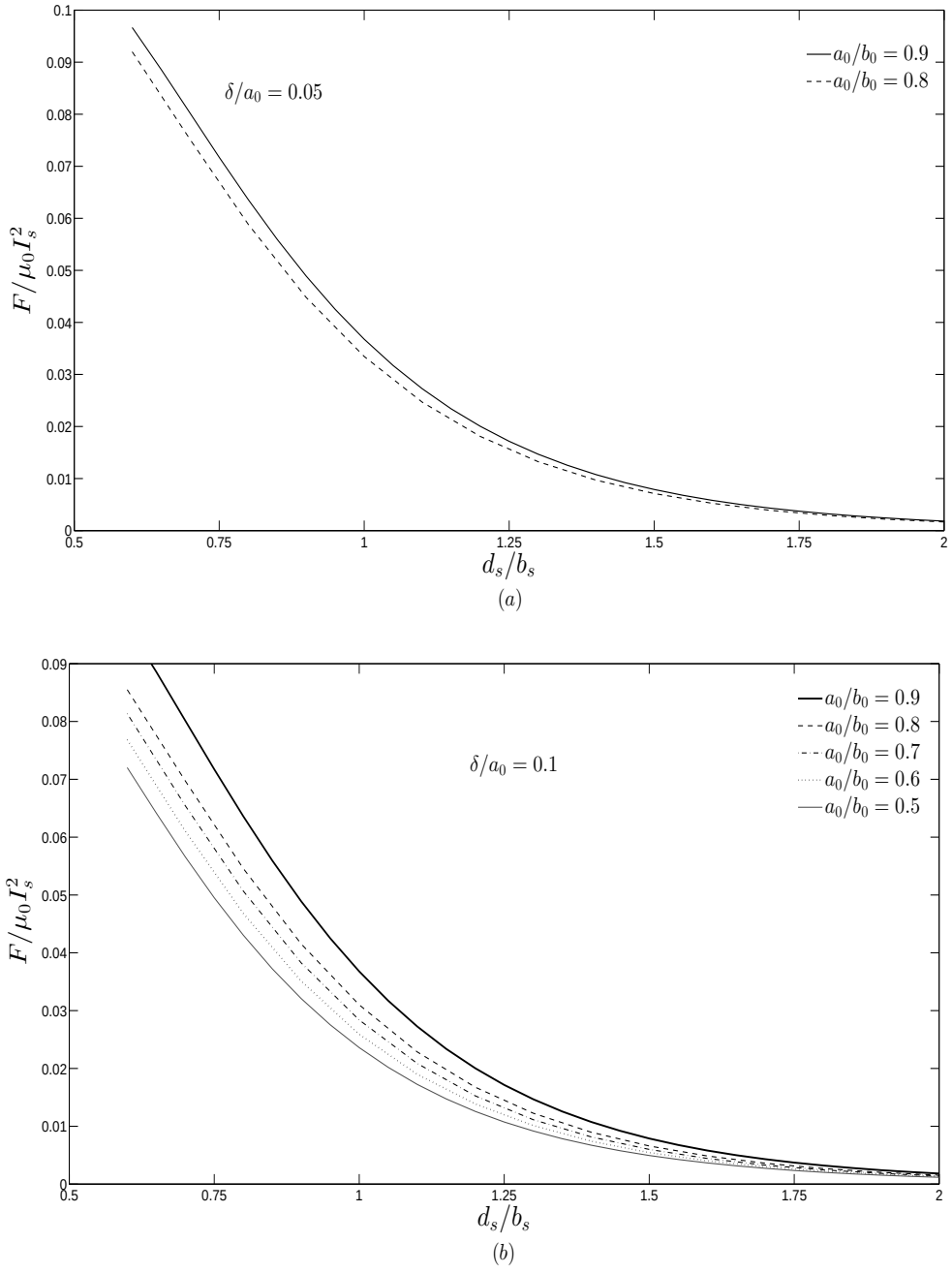

Figure 4.11: Normalized force acting on conducting oblate spheroids as a function of d_s/b_s, with $b_0/b_s = 0.5$, for different axial ratios a_0/b_0 and various ratios (a) $\delta/a_0 = 0.05$ and (b)$\delta/a_0 = 0.1$.

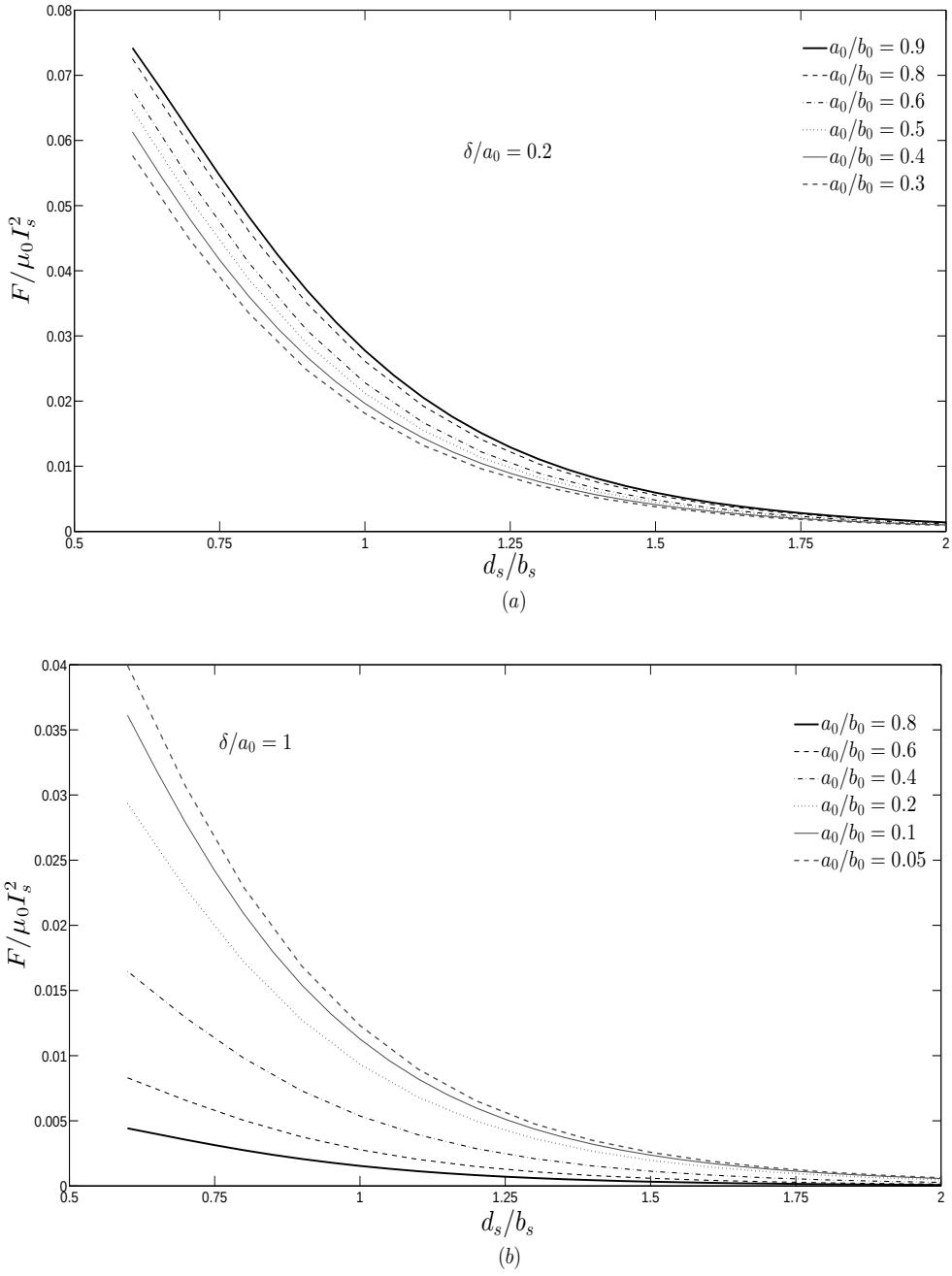

Figure 4.12: Normalized force acting on conducting oblate spheroids as a function of d_s/b_s, with $b_0/b_s = 0.5$, for different axial ratios a_0/b_0 and various ratios (a) $\delta/a_0 = 0.2$ and (b)$\delta/a_0 = 1$.

Table 4.1: Normalized Magnetic Vector Potential at Selected Points on the Surface of Conducting Spheroids with $b_0/b_s = 0.5$ and $d_s/b_s = 1$

Prolate spheroids						
δ/b_0	a_0/b_0 \ η	-0.9	-0.5	0.0	0.5	0.9
0.05	1.25	0.0005633	0.0015766	0.0034770	0.0068379	0.0062167
0.1	1.5	0.0010263	0.0027590	0.0064002	0.0140583	0.0136306
0.2	2.0	0.0016760	0.0043831	0.0114997	0.0305018	0.0287510
0.3	3.0	0.0016002	0.0044745	0.0155542	0.0570034	0.0308915
0.5	4.0	0.0015500	0.0057458	0.0264512	0.0938854	0.0219708
1.0	6.0	0.0009897	0.0051669	0.0392121	0.0745456	0.0067505
Oblate spheroids						
δ/a_0	a_0/b_0 \ η	-0.9	-0.5	0.0	0.5	0.9
0.05	0.8	0.0004888	0.0016113	0.0034243	0.0050547	0.0034707
0.1	0.6	0.0007527	0.0027202	0.0059351	0.0071963	0.0041633
0.2	0.5	0.0012898	0.0048695	0.0106791	0.0113927	0.0060279
0.5	0.4	0.0027068	0.0123805	0.0217067	0.0212369	0.0100062
1.0	0.2	0.0059499	0.0191490	0.0277921	0.0237231	0.0090349

Table 4.2: Normalized Power Loss in Conducting Spheroids with $b_0/b_s = 0.5$ for Different Values of d_s/b_s

Prolate spheroids						
δ/b_0	a_0/b_0 \ d_s/b_s	0.6	0.8	1.0	1.2	1.5
0.05	1.25	0.6480701	0.4099063	0.2386154	0.1328362	0.0544311
0.1	1.5	0.7011636	0.4696525	0.2854729	0.1627191	0.0670400
0.2	2.0	0.7662006	0.5728000	0.3858056	0.2366034	0.1017401
1.0	4.0	0.1671048	0.1455919	0.1208233	0.0948514	0.0585148
Oblate spheroids						
δ/a_0	a_0/b_0 \ d_s/b_s	0.6	0.8	1.0	1.2	1.5
0.05	0.8	0.4848963	0.2798169	0.1542241	0.0841390	0.0348434
0.1	0.6	0.4100920	0.2298146	0.1250292	0.0681218	0.0284730
0.2	0.4	0.3529920	0.1937294	0.1046251	0.0570780	0.0240819
1.0	0.2	0.2771922	0.1517754	0.0821522	0.0450399	0.0191746

Table 4.3: Normalized Force Acting on Conducting Spheroids with $b_0/b_s = 0.5$ for Different Values of d_s/b_s

Prolate spheroids						
δ/b_0	a_0/b_0 \ d_s/b_s	0.6	0.8	1.0	1.2	1.5
0.05	1.25	0.1099964	0.0815893	0.0510964	0.0290381	0.0116095
0.1	1.5	0.1056778	0.0857434	0.0575952	0.0341785	0.0139945
0.2	2.0	0.0868566	0.0831135	0.0652525	0.0435189	0.0194350
1.0	4.0	0.0041175	0.0047154	0.0048069	0.0044142	0.0032110
Oblate spheroids						
δ/a_0	a_0/b_0 \ d_s/b_s	0.6	0.8	1.0	1.2	1.5
0.05	0.8	0.0919979	0.0588474	0.0334537	0.0180929	0.0071143
0.1	0.6	0.0768384	0.0468238	0.0259157	0.0138642	0.0054518
0.2	0.4	0.0613165	0.0361042	0.0196398	0.0104441	0.0041149
1.0	0.2	0.0293615	0.0171937	0.0093369	0.0049698	0.0019652

For some cases, for instance of systems of prolate spheroids with various geometric parameters, the number of terms in the truncation of the field expressions (N) to achieve a desired accuracy in the power loss are shown in figures 4.13 and 4.14. This analysis is useful to identify the minimum number of terms required in the truncation of the field expressions to obtain, a certain accuracy for the power losses.

Figure 4.15 shows the comparison between the numerical results generated for the normalized power losses and forces in conducting prolate and oblate spheroids of axial ratio $a_0/b_0 \approx 1$ with the exact solution for a conducting sphere [32],[62] as a function of d_s/b_s, with $b_0/b_s = 0.5$, and various ratios of δ/r_0. The results are in good agreement.

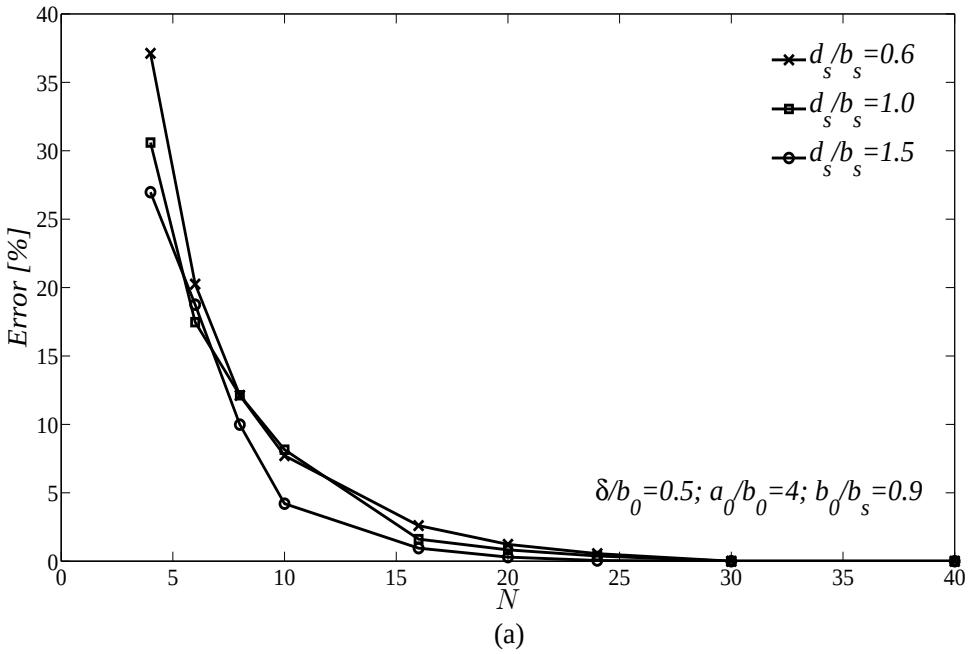

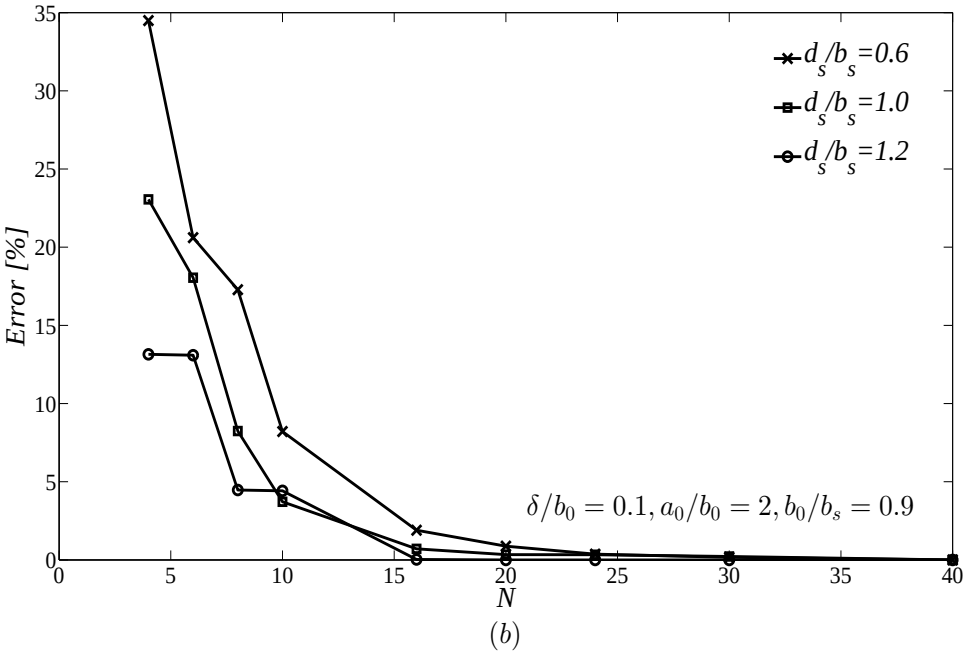

Figure 4.13: Truncation error as a function of the number of terms (N) retained in the field expressions to achieve a desired accuracy in power loss generated in conducting prolate spheroids for different ratios of d_s/b_s, with $b_0/b_s = 0.9$ and various ratios: (a) $\delta/b_0 = 0.5$, $a_0/b_0 = 4$, and (b)$\delta/b_0 = 0.1$, $a_0/b_0 = 2$.

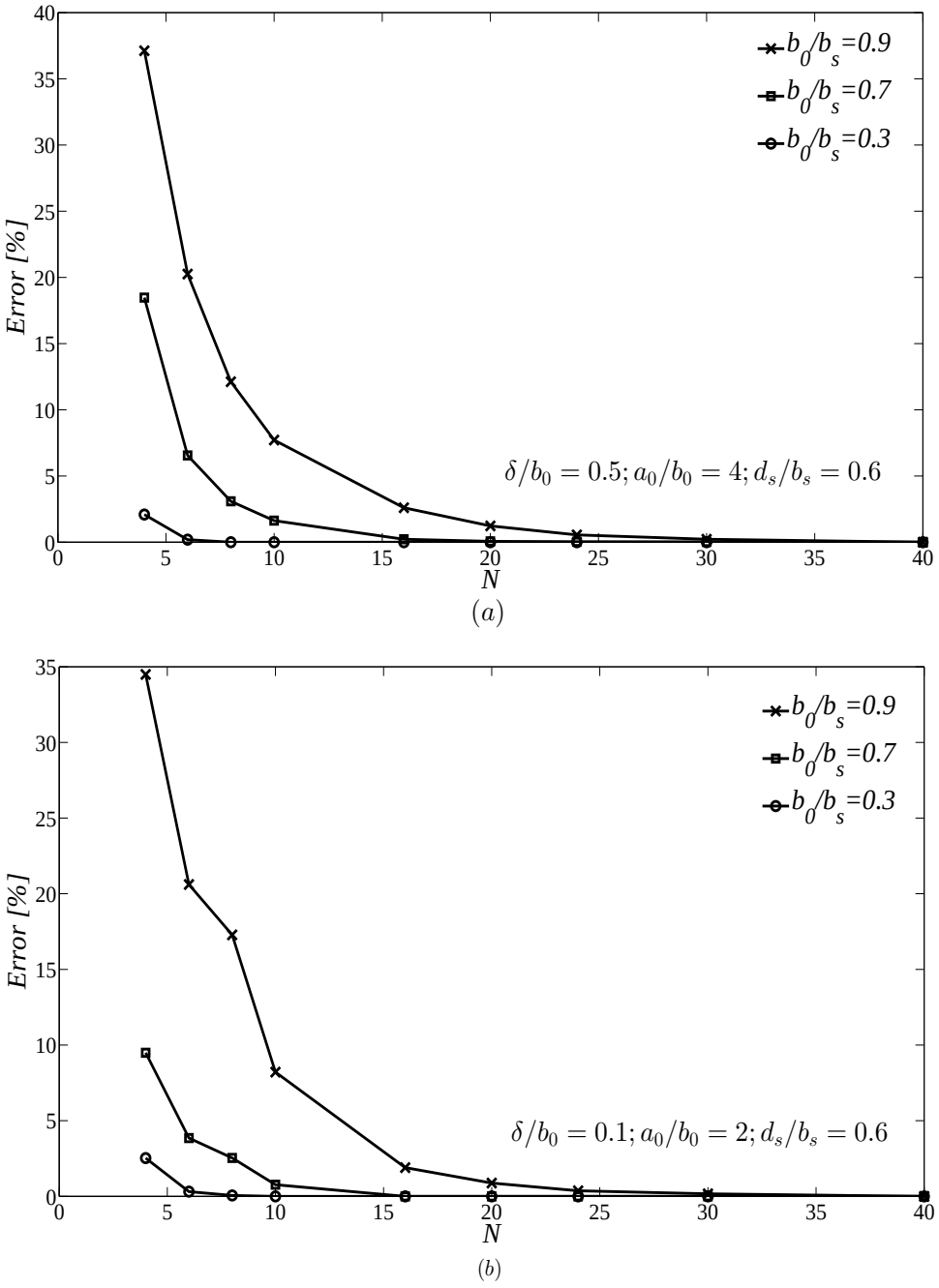

Figure 4.14: Truncation error as a function of the number of terms (N) retained in the field expressions to achieve a desired accuracy in power loss generated in conducting prolate spheroids for different ratios of b_0/b_s, with $d_s/b_s = 0.6$ and various ratios: (a) $\delta/b_0 = 0.5$, $a_0/b_0 = 4$, and (b)$\delta/b_0 = 0.1$, $a_0/b_0 = 2$.

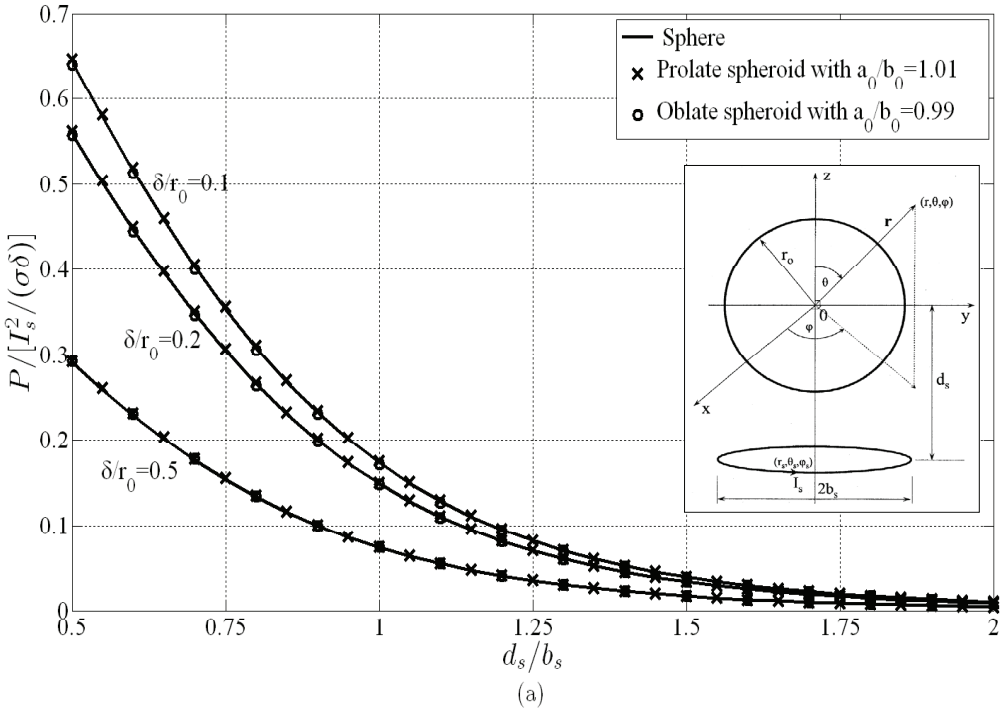

Figure 4.15: Comparison of normalized (a) power loss (b) force in conducting sphere approximated by conducting prolate and oblate spheroids with axial ratio $a_0/b_0 \approx 1$ with the exact solution for conducting sphere as a function of d_s/b_s, with $b_0/b_s = 0.5$, and various ratios of δ/r_0.

4.2 Concluding Remarks

The numerical results generated in this chapter have at least a 4−digit accuracy for the field quantities on the surface of the conducting spheroids, a 6−digit accuracy for the losses in the spheroids and an 8−digit accuracy for the forces exerted upon spheroids. The normalized values presented are the same for systems of various geometric sizes characterized by the same values of the dimensionless parameters $a_0/b_0, b_0/b_s, d_s/b_s$ and δ/a_0 or δ/b_0. Results are given for current-carrying turns located at various distances with respect to the spheroid mid-section, for spheroid axial ratios from 8 to 0.05 and for ratios of the penetration depth to the spheroid semi-minor axis from 1 to 0.05, i.e. for the range from weak skin effect to pronounced skin effect. To obtain the same accuracy for values of a_0/b_0 and δ/b_0 (or δ/a_0) which give a spheroidal wave-number parameter in (4.1) or (4.2) larger than $|c_1| \cong 30$, one has to increase the computational precision [51] in order to include more terms in the expressions used to calculate the spheroidal functions involved and more unknowns in the truncated systems (3.29) and (3.30), in order to compute sufficiently accurately their inverses.

Thus, the results given constitute a large set of benchmark data made available for an accurate evaluation of the performance of approximate numerical methods developed for the analysis of induced fields in the presence of solid conductors immersed in nonuniform quasistationary fields of various frequencies. On the other hand, the accurate numerical results presented for small depths of penetration of the electromagnetic field in the conducting material will allow the range of validity to be determined for simpler models developed to analyze real world objects, such as the perfect conductor model, the surface impedance model and the curvature-corrected surface impedance model.

Chapter 5

Evaluation of the Accuracy of Surface Impedance Models

5.1 Impedance Boundary Conditions

Schelkunoff (1934) first introduced the concept of surface impedance in electromagnetics for the analysis of coaxial transmission lines and cylindrical shields [63]. On the other hand the concept of skin depth was first introduced by Lord Rayleigh in 1886 for the propagation of plane waves from free space into a good conductor [64]. For a homogeneous conducting body, Rytov (1940) showed that the tangential components of the electric field intensity on the surface can be expressed as a series of powers of the depth of penetration of the electromagnetic field, with coefficients that involve the tangential component of the magnetic field intensity and their tangential derivatives [17]. Leontovich (1948) presented a simple form of the boundary condition for highly conducting bodies, which relates the electric field intensity $\boldsymbol{E}$ and the magnetic field intensity $\boldsymbol{H}$ at each point on the conductor surface [17] as

$$\boldsymbol{n} \times \boldsymbol{E} = Z_s \boldsymbol{n} \times (\boldsymbol{n} \times \boldsymbol{H}) \tag{5.1}$$

where $\boldsymbol{n}$ is the outwardly directed unit vector normal to the surface and Z_s is the surface impedance. Equation (5.1) represents the Leontovich surface impedance boundary condition (SIBC). Chapter-1 of [15], gives a detailed description about the three different approaches (Leontovich, Mitzner, and Rytov) to the development of various surface impedance boundary condition models and discussed the historical background. For a good conductor, of conductivity σ and permeability μ, the surface impedance in (5.1) is taken to be

$$Z_s = R_s(1+i) \tag{5.2}$$

where $i \equiv \sqrt{-1}$ and R_s is the surface resistance,

$$R_s = \frac{1}{\sigma\delta} \tag{5.3}$$

with δ denoting the skin depth,

$$\delta = \sqrt{\frac{2}{\omega\mu\sigma}} \tag{5.4}$$

and ω being the angular frequency. The relation (5.1) is applicable at the points on the conductor surface where δ is much smaller than the local radii of curvature.

For the perfect electric conductor model $Z_s = 0$ and the electric and the magnetic field intensities on the conductor surface satisfy the conditions

$$\begin{aligned} \boldsymbol{n} \times \boldsymbol{E} &= 0 \\ \boldsymbol{n} \cdot \boldsymbol{H} &= 0. \end{aligned} \tag{5.5}$$

In appendix-B, approximate analytical expressions are derived for the quasi-stationary field quantities by using the PEC and the SIBC models for a conducting spheroid placed in an external non-uniform magnetic field produced by a coaxial circular turn

carrying currents sinusoidal with time [46], [62].

5.2 Numerical Results

The expressions given in Appendix C were used for numerical computations of field quantities derived using both the PEC and the SIBC models of the prolate spheroids. For oblate spheroids, the expressions for the field quantities, as well as for losses and forces, can directly be determined from the expressions in the case of prolate spheroids by the transformations [49] $c \to -ic$ and $\xi \to i\xi$, $\xi_0 \to i\xi_0$, $\xi_s \to i\xi_s$.

As explained in Chapter 4.1, the numerical values of P_n^1 for all arguments and Q_n^1 with a real argument less than one have been computed using the recurrence formulas for the associated Legendre functions [58]. For Q_n^1 with a real argument greater than one, the algorithm in [59] has been used and, for complex arguments, the subroutine in [60]is used. The infinite series in the expressions of the field quantities are rapidly convergent for all the cases considered in this paper and numerical values have been computed by retaining the first $N = 25$ terms in the respective series. This number of terms was determined in each case by comparing the results with those obtained when retaining the first 35 terms in the series. The relative contribution to the absolute value of the field quantities of the additional ten terms was always smaller than 10^{-5}. This yields an accuracy of the results with respect to those from the exact analytical solution as shown in figures $5.1 - 5.18$ and in Tables I and II. The integrand of (B.12) has no singularities, but since it has more and more oscillations as n and m increase, the integrals in (B.12) were evaluated highly accurately by using the adaptive Gauss-Lobbatto quadrature, where the endpoints of the integration interval are also included among the quadrature nodes.

The tangential component of the magnetic field intensity on the conductor surface,

the Joule losses in and the forces acting upon conducting spheroids are expressed in terms of the dimensionless geometric parameters $a_0/b_0, b_0/b_s, d_s/b_s$ (see Fig. 3.1) and the ratio of the depth of penetration δ to the semi-minor axis of the spheroid. ξ_0, η_s, ξ_s are simple functions of these geometric parameters and can be determined from the relations

$$\begin{aligned} a_0 &= c\xi_0 \ , \qquad & b_0 &= c(\xi_0^2 - 1)^{1/2} \\ d_s &= c\eta_s\xi_s \ , \qquad & b_s &= c[(1-\eta_s^2)(\xi_s^2 - 1)]^{1/2}. \end{aligned} \tag{5.6}$$

The numerical results presented in this paper are calculated for conducting spheroids of permeability equal to that of free space.

Results computed using the PEC and the SIBC models are compared with the exact ones obtained as shown in Chapter-3 for a range of spheroids for which the wave-number parameter $|kc| < 30$, where $k^2 \equiv -i\omega\mu\sigma$. The latter have at least a $4-$digit accuracy for the absolute values of the field quantities, a $6-$ digit accuracy for the losses and an $8-$digit accuracy for the forces [46]. Numerical results for the real and imaginary parts of the normalized tangential magnetic field intensity on the surface of conducting prolate and oblate spheroids as functions of η are given, respectively, in Figs. 4.1 and 4.2 for various ratios of the depth of penetration to the semi-minor axis (δ/b_0 for prolate spheroids and δ/a_0 for oblate spheroids) and for different axial ratios a_0/b_0. In Figs. 3 and 4, numerical data for the power loss normalized to $I_s^2/(\sigma\delta)$ are plotted against the ratio d_s/b_s for different axial ratios and for various ratios of the depth of penetration to the semi-minor axis. Similarly, comparative computed results for the force acting upon the spheroids are shown in Figs. 5 and 6.

The effect of the nonuniformity of the inducing magnetic field on the accuracy of the field quantities, power losses and forces calculated by using the impedance bound-

ary condition models is evaluated by varying the parameters d_s/b_s and b_0/b_s in the case of prolate spheroids and a_0/b_s in the case of oblate spheroids. The maximum percentage errors of the results computed for the tangential component of the magnetic field intensity ($-0.99 \leq \eta \leq +0.99$), for power losses and for forces when using the PEC and the SIBC models are given in Table 5.1 for different ratios $\delta/b_0, a_0/b_0$ and b_0/b_s, in the case of prolate spheroids, and in Table 5.2 for different ratios $\delta/b_0, a_0/b_0$ and a_0/b_s, in the case of oblate spheroids. The analytical expression of the Rytov expansion relating the tangential field intensities at the smooth surface of an arbitrarily shaped conductor can be used to estimate the errors associated with various surface impedance models. For the PEC and the SIBC models these errors are of the order of magnitude of δ/D, for $\delta/D < 0.06$, and $(\delta/D)^2$, for $\delta/D < 0.25$, respectively, where D is the least of the smallest radius of curvature at the point considered on the conductor surface and the smallest distance to the field source [16]. For a good conductor, the absolute value of the relative difference between the surface impedance in the SIBC model and that in the first order curvature correction model of Rytov-Mitzner is given by $(\sqrt{2}/4)\delta/D_0$, where $1/D_0 = |1/d_1 - 1/d_2|$ and d_1 and d_2 are the local principal curvature radii. This is a good estimation of the relative error in surface impedance for convex sections of the conductor surface wherever δ is sufficiently small with respect to D_0 such that $(\delta/D_0)^3$ is negligible. It should be noticed that when d_1 and d_2 are approximately equal, then the first order correction is vanishing. For such points on the conductor surface, for instance for points at or in the vicinity of the poles of the spheroids considered in this paper, the errors for the SIBC model are of the order of magnitude of $(\delta/D)^3$ and are to be determined with respect to the results obtained by applying the Rytov second order curvature correction model.

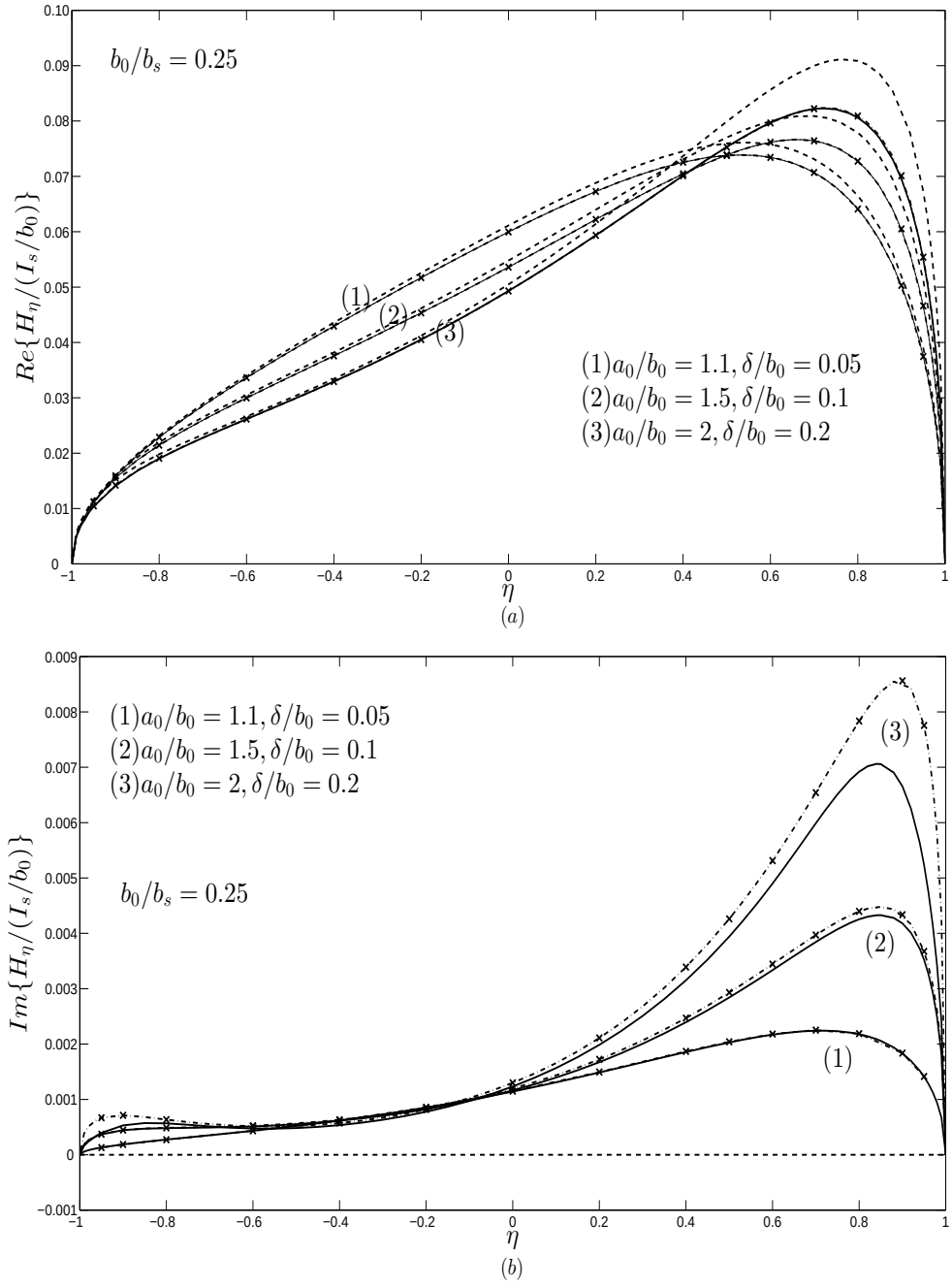

Figure 5.1: (a) Real and (b) imaginary parts of the normalized magnetic field intensity tangential to the surface of conducting prolate spheroids as a function of η , for $d_s/b_s = 1$, $b_0/b_s = 0.25$ and different ratios a_0/b_0 and δ/b_0 : ——— Exact solution; ·– ×· — SIBC; − − − PEC.

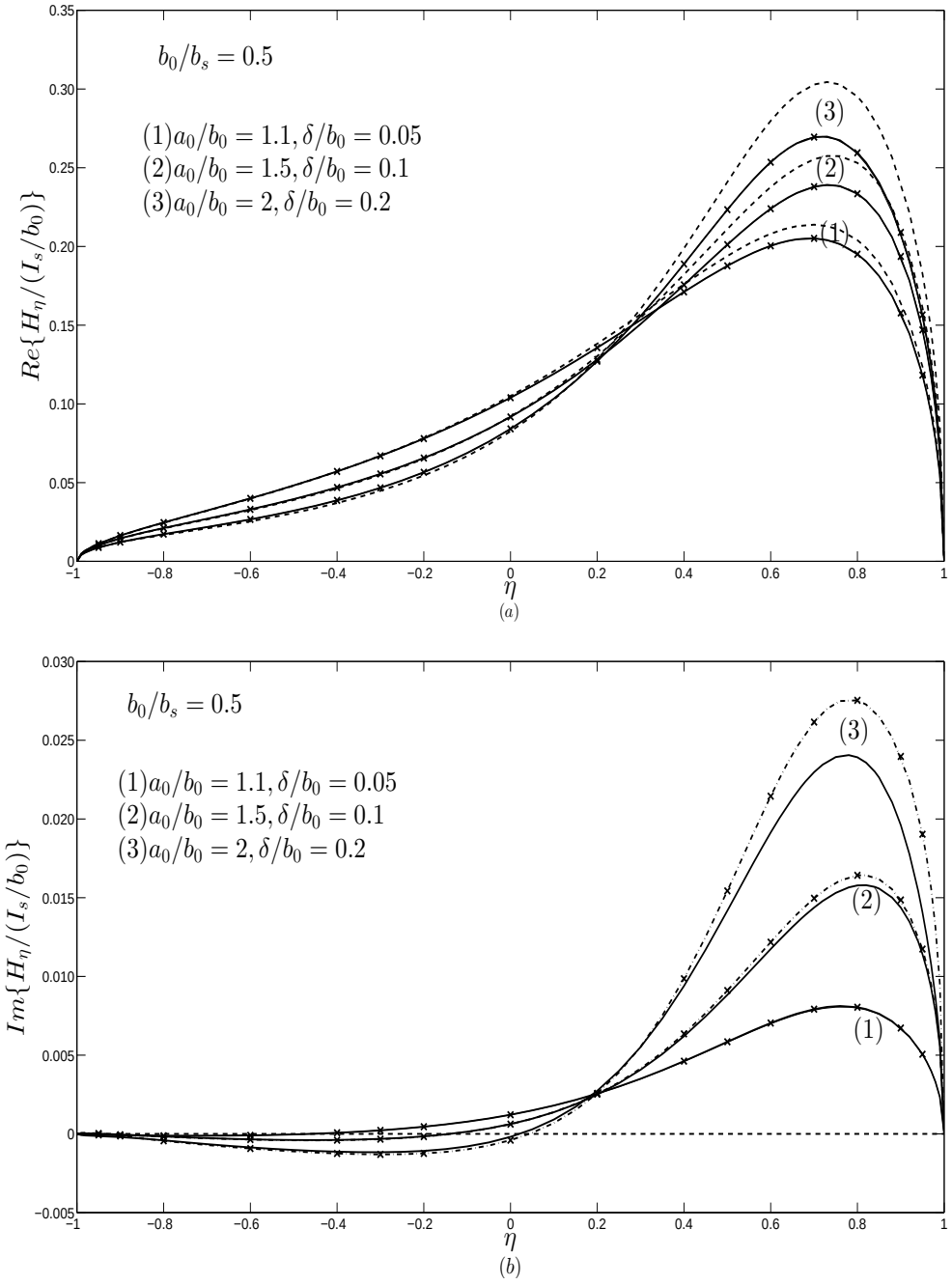

Figure 5.2: (a) Real and (b) imaginary parts of the normalized magnetic field intensity tangential to the surface of conducting prolate spheroids as a function of η , for $d_s/b_s = 1$, $b_0/b_s = 0.5$ and different ratios a_0/b_0 and δ/b_0 : ——— Exact solution; $\cdot$— $\times\cdot$ — SIBC; $- - -$ PEC.

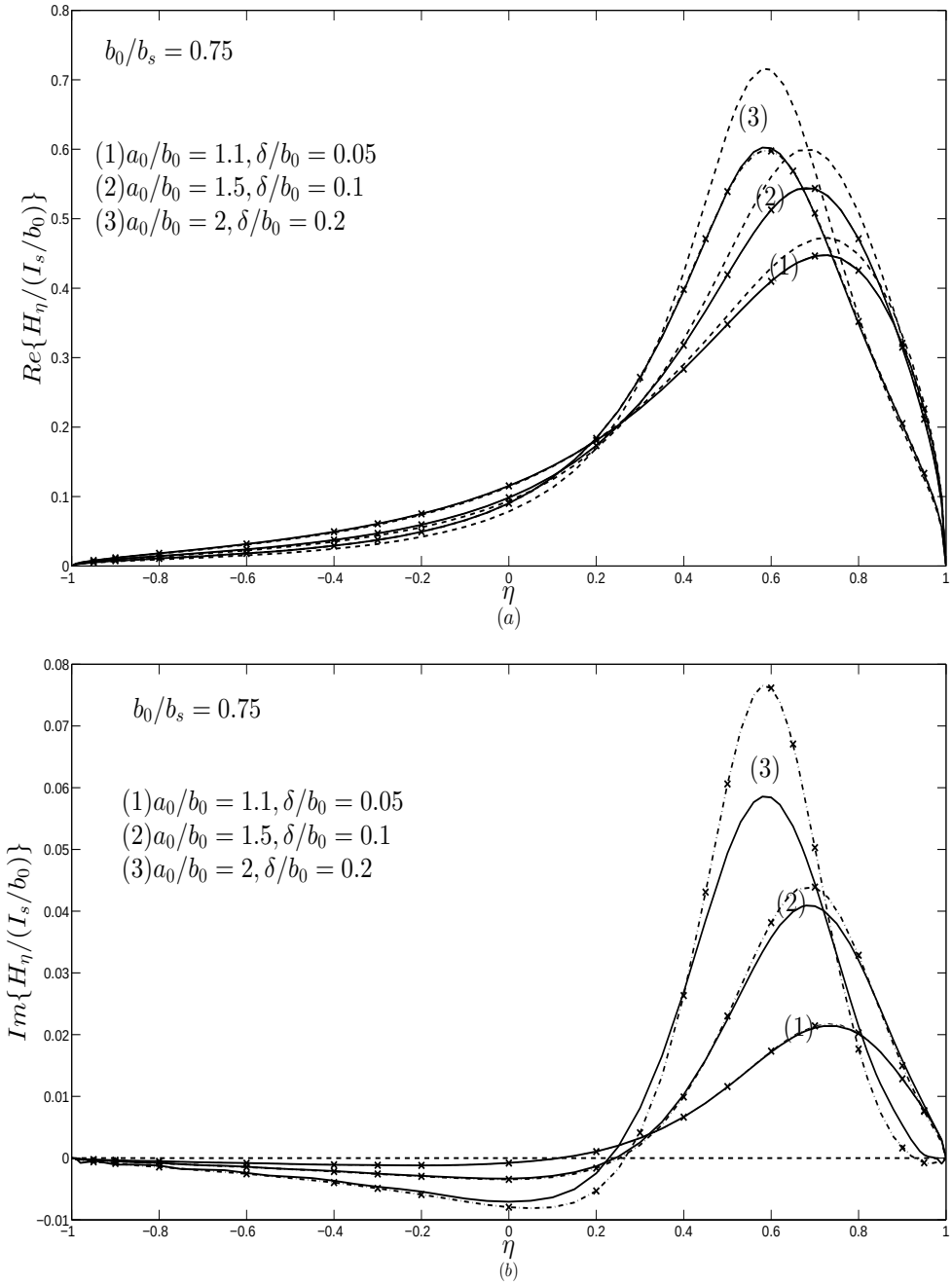

Figure 5.3: (a) Real and (b) imaginary parts of the normalized magnetic field intensity tangential to the surface of conducting prolate spheroids as a function of η , for $d_s/b_s = 1$, $b_0/b_s = 0.75$ and different ratios a_0/b_0 and δ/b_0 : ——— Exact solution; ·– ×· — SIBC; − − − PEC.

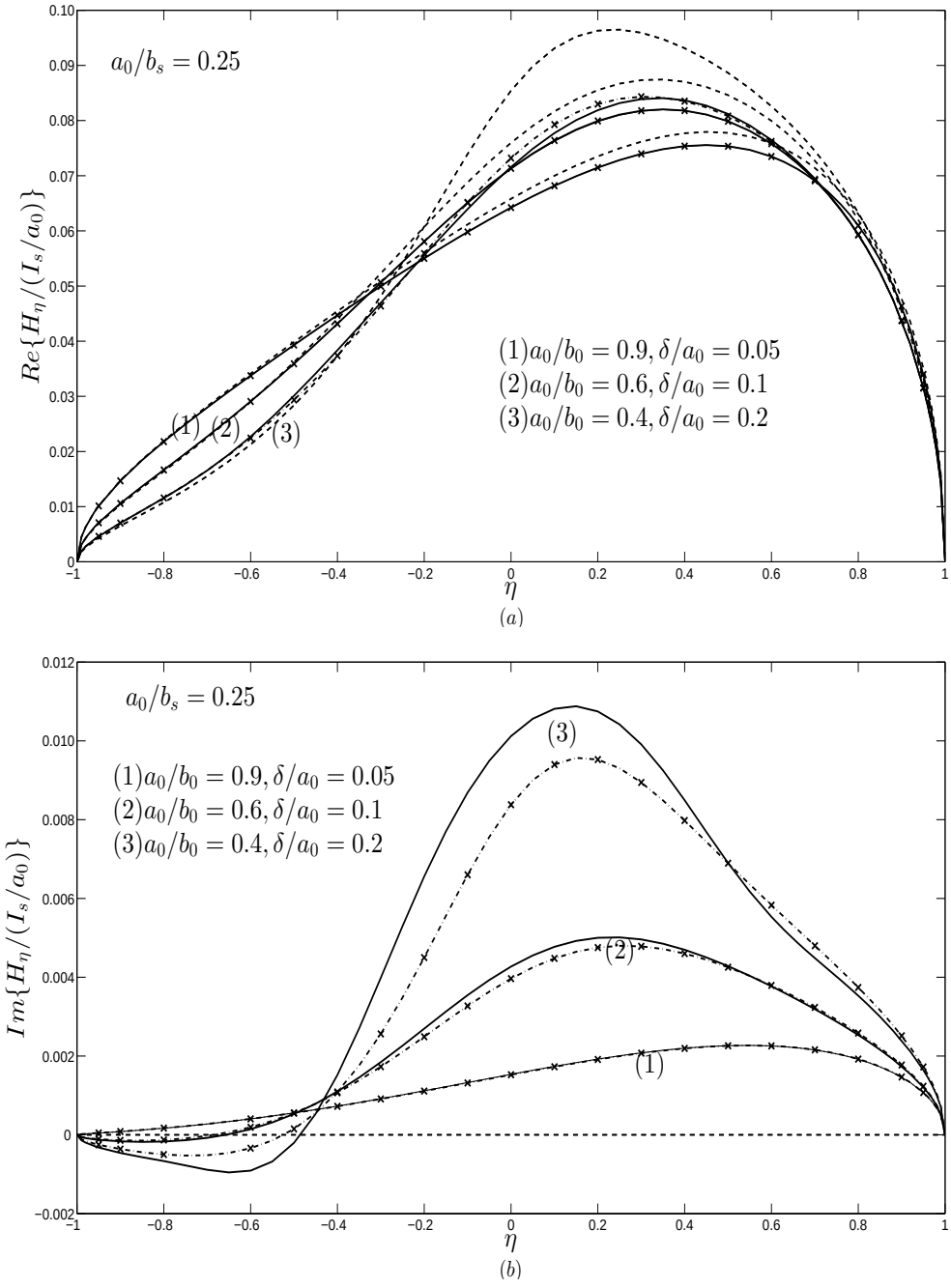

Figure 5.4: (a) Real and (b) imaginary parts of the normalized magnetic field intensity tangential to the surface of conducting oblate spheroids as a function of η , for $d_s/b_s = 1$, $a_0/b_s = 0.25$ and different ratios a_0/b_0 and δ/a_0 : ——— Exact solution; $\cdot - \times \cdot$ — SIBC; $- - -$ PEC.

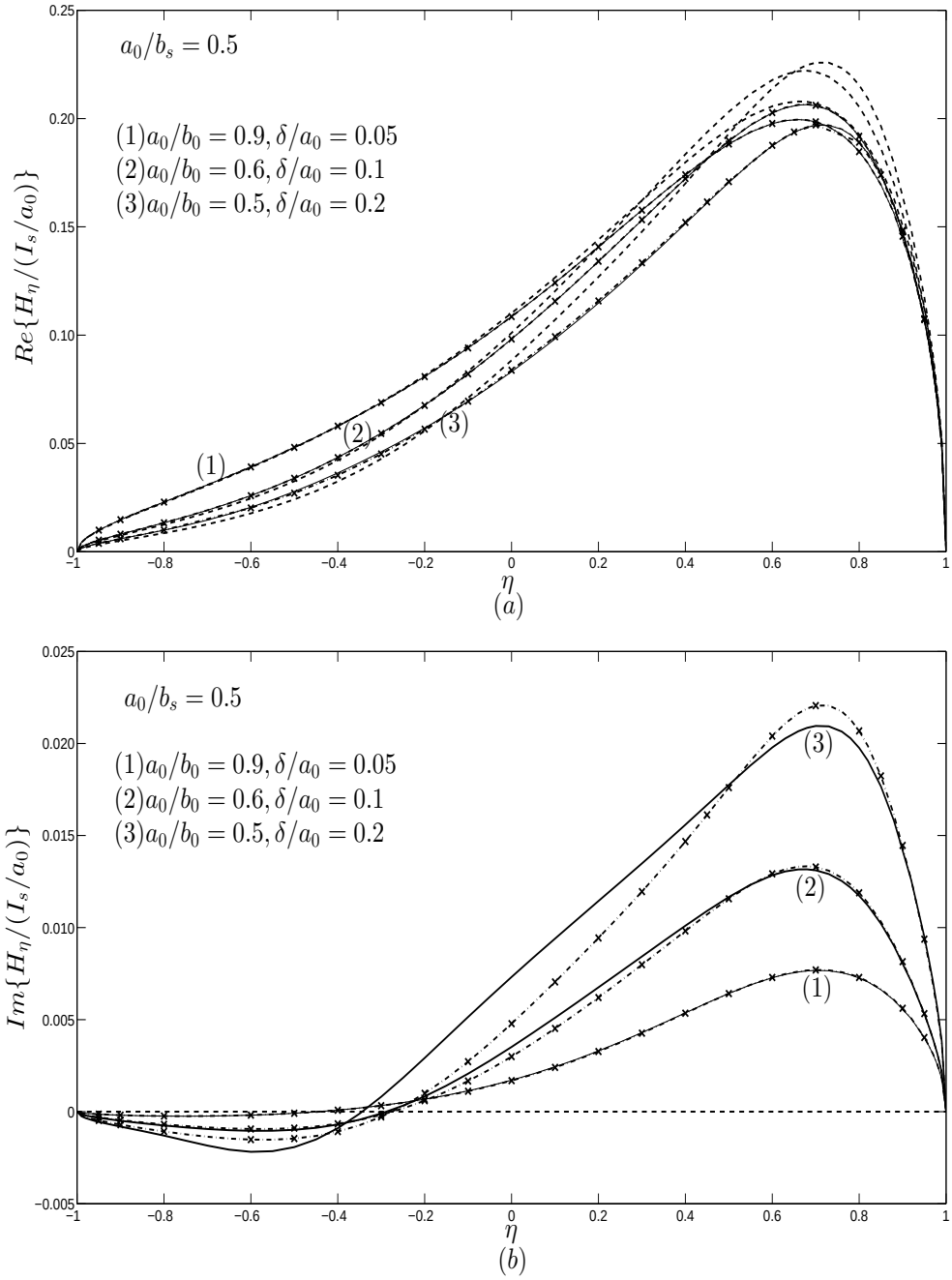

Figure 5.5: (a) Real and (b) imaginary parts of the normalized magnetic field intensity tangential to the surface of conducting oblate spheroids as a function of η , for $d_s/b_s = 1$, $a_0/b_s = 0.5$ and different ratios a_0/b_0 and δ/a_0 : ——— Exact solution; $\cdot - \times \cdot$ — SIBC; $- - -$ PEC.

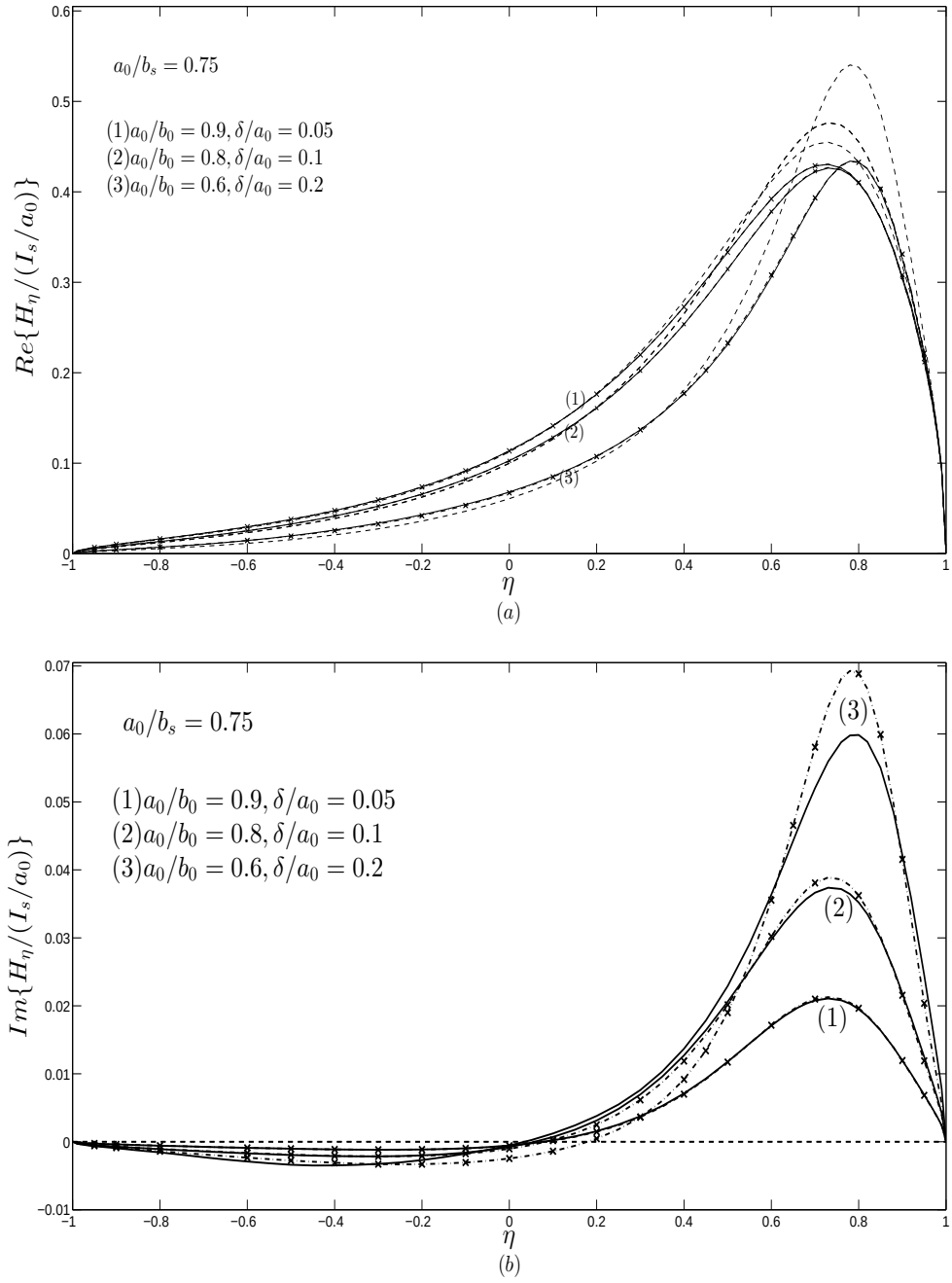

Figure 5.6: (a) Real and (b) imaginary parts of the normalized magnetic field intensity tangential to the surface of conducting oblate spheroids as a function of η , for $d_s/b_s = 1$, $a_0/b_s = 0.25$ and different ratios a_0/b_0 and δ/a_0 : ——— Exact solution; $\cdot - \times \cdot$ — SIBC; $- - -$ PEC.

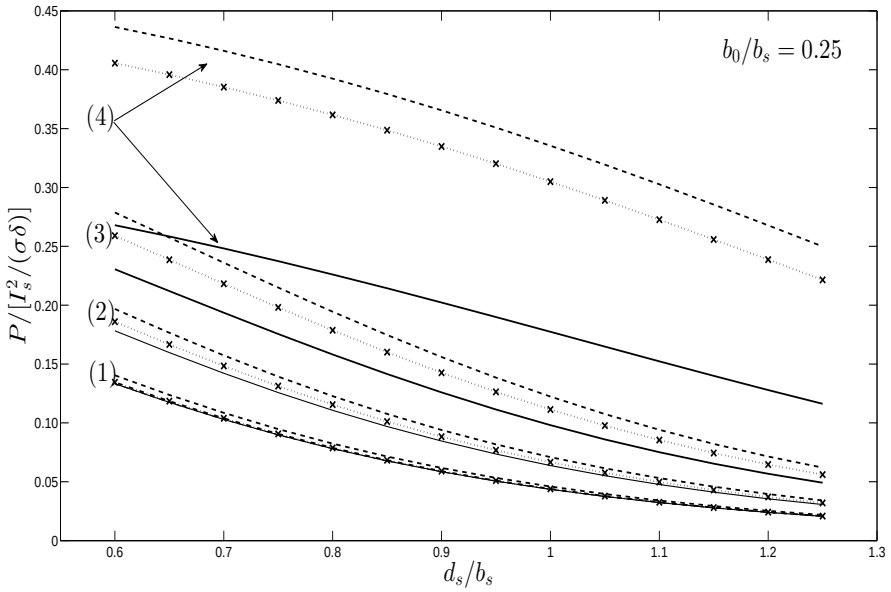

Figure 5.7: Normalized power loss for prolate spheroids with $b_0/b_s = 0.25$: and (1) $a_0/b_0 = 1.25$, $\delta/b_0 = 0.05$; (2) $a_0/b_0 = 2$, $\delta/b_0 = 0.1$; (3) $a_0/b_0 = 3$, $\delta/b_0 = 0.2$; (4) $a_0/b_0 = 6$, $\delta/b_0 = 0.5$; ——— Exact solution; $\cdot - \times \cdot$ — SIBC; $- - -$ PEC.

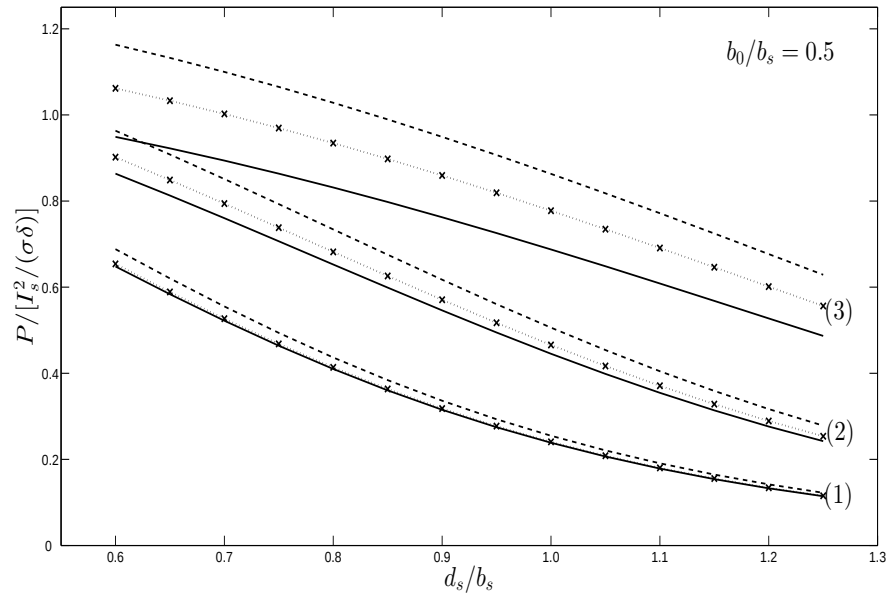

Figure 5.8: Normalized power loss for prolate spheroids with $b_0/b_s = 0.5$: and (1) $a_0/b_0 = 1.25$, $\delta/b_0 = 0.05$; (2) $a_0/b_0 = 2$, $\delta/b_0 = 0.1$; (3) $a_0/b_0 = 3$, $\delta/b_0 = 0.2$; ——— Exact solution; $\cdot - \times \cdot$ — SIBC; $- - -$ PEC.

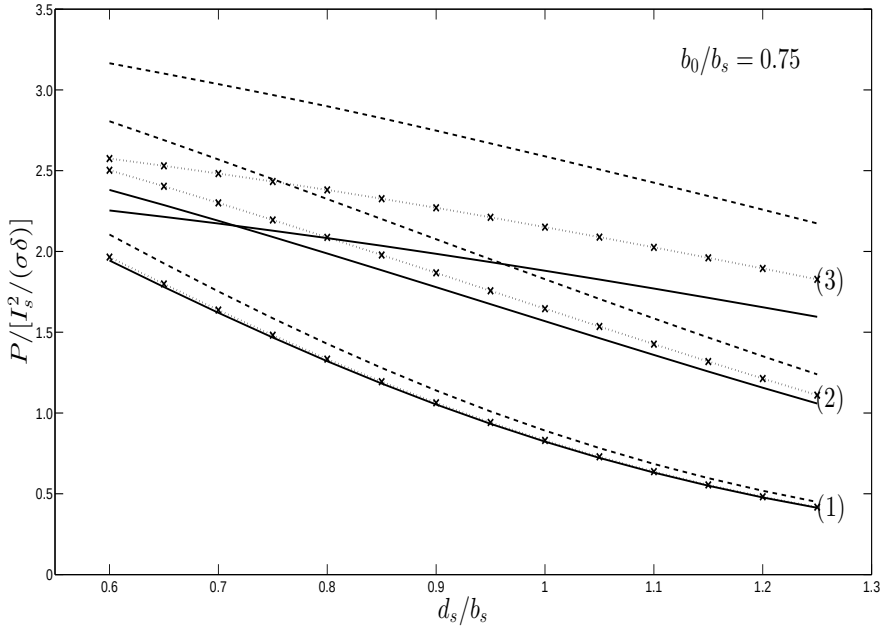

Figure 5.9: Normalized power loss for prolate spheroids with $b_0/b_s = 0.75$: and (1) $a_0/b_0 = 1.25$, $\delta/b_0 = 0.05$; (2) $a_0/b_0 = 2$, $\delta/b_0 = 0.1$; (3) $a_0/b_0 = 3$, $\delta/b_0 = 0.2$; ——— Exact solution; $\cdot - \times \cdot$ — SIBC; $- - -$ PEC.

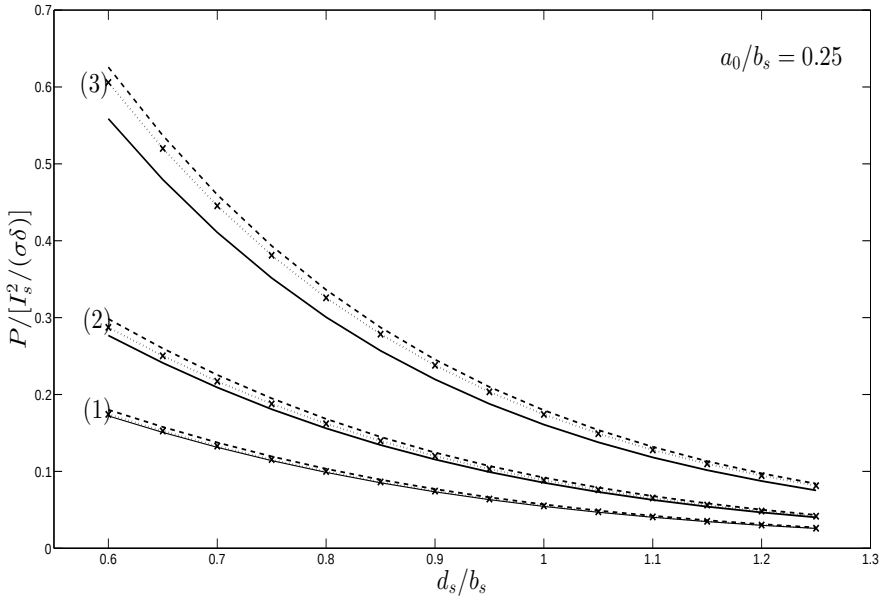

Figure 5.10: Normalized power loss for oblate spheroids with $a_0/b_s = 0.25$: and (1) $a_0/b_0 = 0.8$, $\delta/a_0 = 0.05$; (2) $a_0/b_0 = 0.6$, $\delta/a_0 = 0.1$; (3) $a_0/b_0 = 0.4$, $\delta/a_0 = 0.2$; ——— Exact solution; $\cdot - \times \cdot$ — SIBC; $- - -$ PEC.

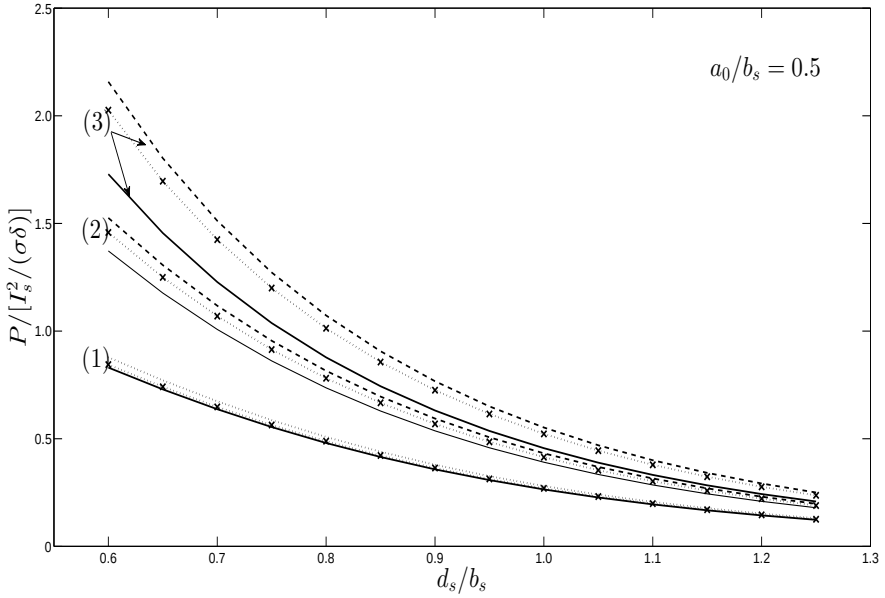

Figure 5.11: Normalized power loss for oblate spheroids with $a_0/b_s = 0.5$: and (1) $a_0/b_0 = 0.8$, $\delta/a_0 = 0.05$; (2) $a_0/b_0 = 0.6$, $\delta/a_0 = 0.1$; (3) $a_0/b_0 = 0.5$, $\delta/a_0 = 0.2$; ——— Exact solution; $\cdot - \times \cdot$ — SIBC; $- - -$ PEC.

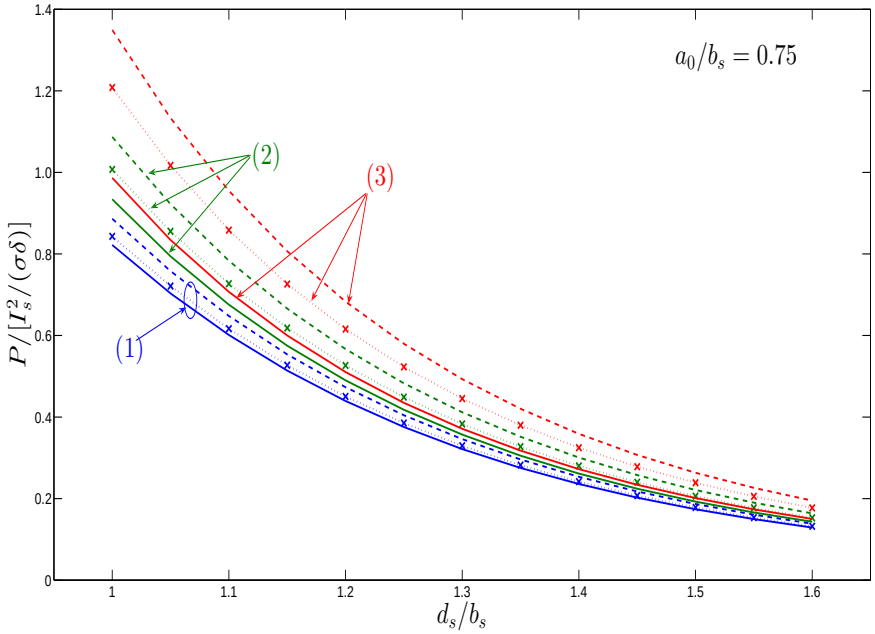

Figure 5.12: Normalized power loss for oblate spheroids with $a_0/b_s = 0.75$: and (1) $a_0/b_0 = 0.8$, $\delta/a_0 = 0.05$; (2) $a_0/b_0 = 0.7$, $\delta/a_0 = 0.1$; (3) $a_0/b_0 = 0.6$, $\delta/a_0 = 0.2$; ——— Exact solution; $\cdot - \times \cdot$ — SIBC; $- - -$ PEC.

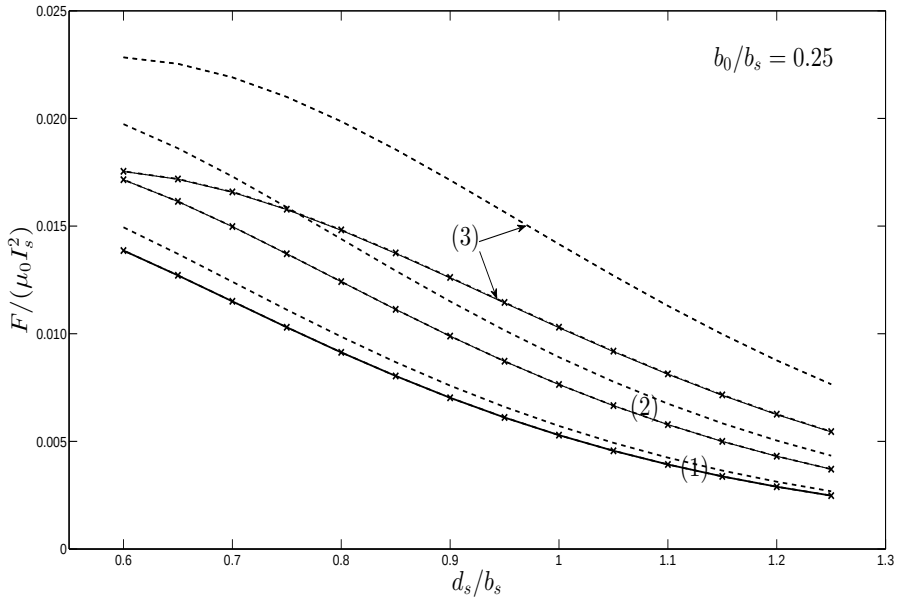

Figure 5.13: Normalized force for prolate spheroids with $b_0/b_s = 0.25$: (1) $a_0/b_0 = 1.25$, $\delta/b_0 = 0.05$; (2) $a_0/b_0 = 2$, $\delta/b_0 = 0.1$; (3) $a_0/b_0 = 3$, $\delta/b_0 = 0.2$; ——— Exact solution; $\cdot - \times \cdot$ — SIBC; $- - -$ PEC.

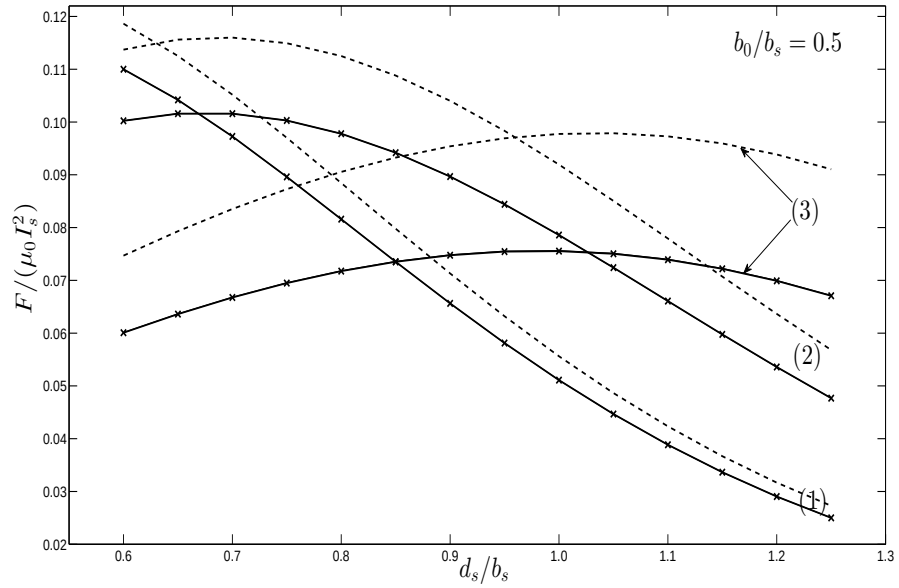

Figure 5.14: Normalized force for prolate spheroids with $b_0/b_s = 0.5$: (1) $a_0/b_0 = 1.25$, $\delta/b_0 = 0.05$; (2) $a_0/b_0 = 2$, $\delta/b_0 = 0.1$; (3) $a_0/b_0 = 3$, $\delta/b_0 = 0.2$; ——— Exact solution; $\cdot - \times \cdot$ — SIBC; $- - -$ PEC.

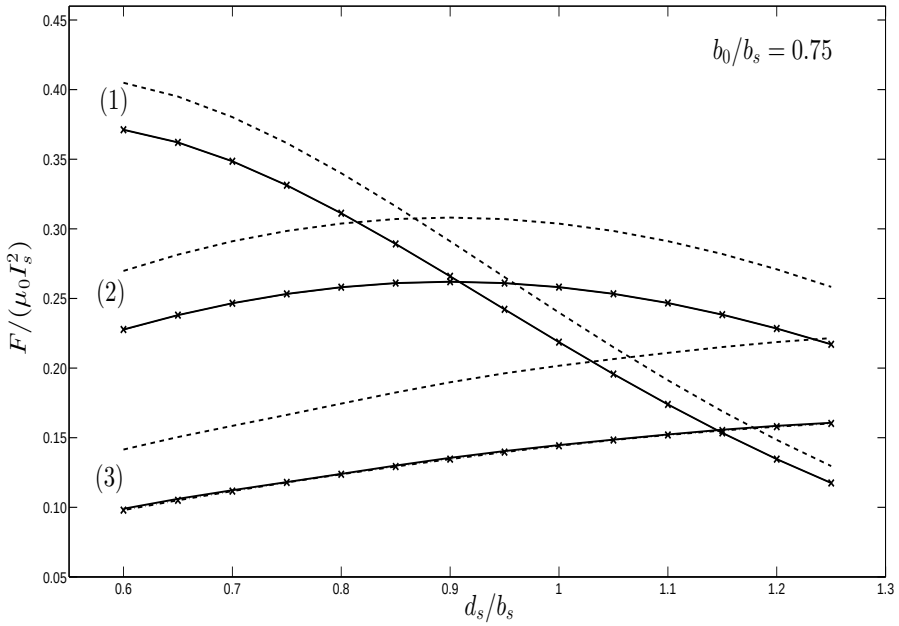

Figure 5.15: Normalized force for prolate spheroids with $b_0/b_s = 0.75$: (1) $a_0/b_0 = 1.25$, $\delta/b_0 = 0.05$; (2) $a_0/b_0 = 2$, $\delta/b_0 = 0.1$; (3) $a_0/b_0 = 3$, $\delta/b_0 = 0.2$; ——— Exact solution; $\cdot - \times \cdot$ — SIBC; $- - -$ PEC.

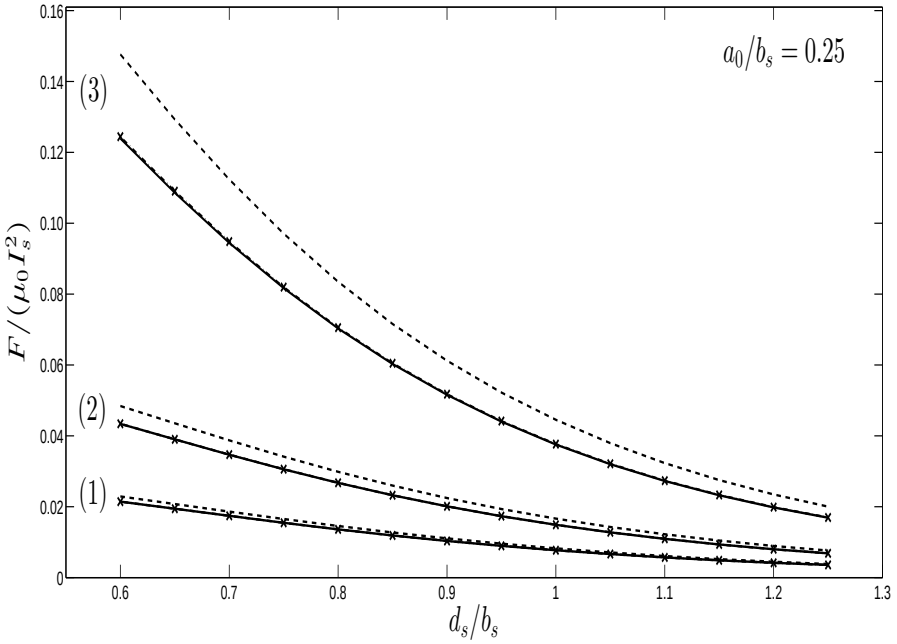

Figure 5.16: Normalized force for oblate spheroids with $a_0/b_s = 0.25$: and (1) $a_0/b_0 = 0.8$, $\delta/a_0 = 0.05$; (2) $a_0/b_0 = 0.6$, $\delta/a_0 = 0.1$; (3) $a_0/b_0 = 0.4$, $\delta/a_0 = 0.2$; ——— Exact solution; $\cdot - \times \cdot$ — SIBC; $- - -$ PEC.

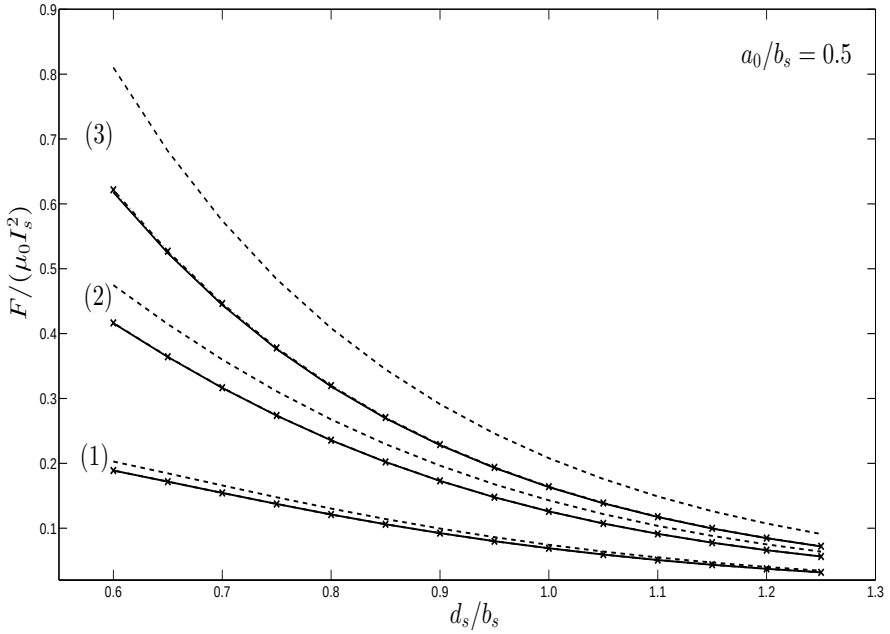

Figure 5.17: Normalized force for oblate spheroids with $a_0/b_s = 0.5$: and (1) $a_0/b_0 = 0.8$, $\delta/a_0 = 0.05$; (2) $a_0/b_0 = 0.6$, $\delta/a_0 = 0.1$; (3) $a_0/b_0 = 0.5$, $\delta/a_0 = 0.2$; ——— Exact solution; $\cdot - \times \cdot$ — SIBC; $- - -$ PEC.

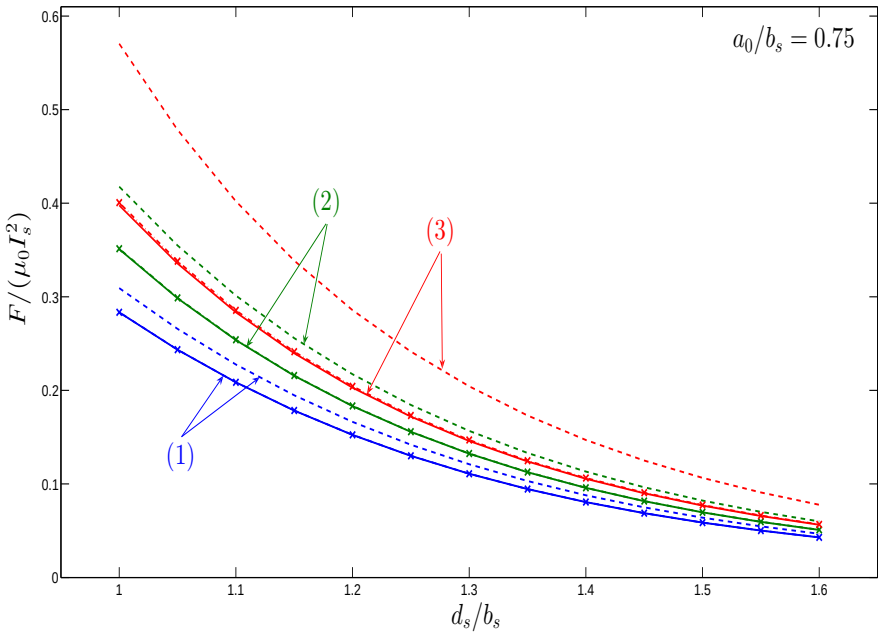

Figure 5.18: Normalized force for oblate spheroids with $a_0/b_s = 0.75$: and (1) $a_0/b_0 = 0.8$, $\delta/a_0 = 0.05$; (2) $a_0/b_0 = 0.7$, $\delta/a_0 = 0.1$; (3) $a_0/b_0 = 0.6$, $\delta/a_0 = 0.2$; ——— Exact solution; $\cdot - \times \cdot$ — SIBC; $- - -$ PEC.

Table 5.1: Relative Errors for the PEC and SIBC Models of Conducting Prolate Spheroids

Maximum Percentage Error in Tangential Magnetic Field Intensity ($-0.99 \leq \eta \leq 0.99$)							
δ/b_0	a_0/b_0	$b_0/b_s = 0.25$		$b_0/b_s = 0.5$		$b_0/b_s = 0.75$	
		PEC	SIBC	PEC	SIBC	PEC	SIBC
0.05	1.25	5.106	1.297	4.497	2.750	5.676	1.523
0.1	2	11.526	2.537	8.846	5.315	9.156	4.562
0.2	3	23.858	6.892	24.554	10.145	27.274	16.636
Maximum Percentage Error in Power Loss							
δ/b_0	a_0/b_0	$b_0/b_s = 0.25$		$b_0/b_s = 0.5$		$b_0/b_s = 0.75$	
		PEC	SIBC	PEC	SIBC	PEC	SIBC
0.05	1.25	5.535	0.907	6.882	0.930	8.638	1.083
0.1	2	11.355	4.408	14.851	4.675	17.846	5.120
0.2	3	26.006	13.959	29.203	14.299	40.439	14.533
Maximum Percentage Error in Force							
δ/b_0	a_0/b_0	$b_0/b_s = 0.25$		$b_0/b_s = 0.5$		$b_0/b_s = 0.75$	
		PEC	SIBC	PEC	SIBC	PEC	SIBC
0.05	1.25	8.129	0.008	9.135	0.013	10.377	0.020
0.1	2	16.999	0.041	19.217	0.052	19.013	0.084
0.2	3	40.717	0.274	35.669	0.128	42.999	0.996

Table 5.2: Relative Errors for the PEC and SIBC Models of Conducting Oblate Spheroids

Maximum Percentage Error in Tangential Magnetic Field Intensity ($-0.99 \leq \eta \leq 0.99$)									
δ/a_0	$a_0/b_s = 0.25$			$a_0/b_s = 0.5$			$a_0/b_s = 0.75$		
	a_0/b_0	PEC	SIBC	a_0/b_0	PEC	SIBC	a_0/b_0	PEC	SIBC
0.05	0.8	3.177	0.751	0.8	4.286	1.182	0.8	7.108	3.195
0.1	0.6	7.310	2.333	0.6	19.664	4.837	0.7	18.356	6.787
0.2	0.4	19.501	6.398	0.5	23.221	9.676	0.6	26.243	15.678
Maximum Percentage Error in Power Loss									
δ/a_0	$a_0/b_s = 0.25$			$a_0/b_s = 0.5$			$a_0/b_s = 0.75$		
	a_0/b_0	PEC	SIBC	a_0/b_0	PEC	SIBC	a_0/b_0	PEC	SIBC
0.05	0.8	4.753	1.253	0.8	5.907	1.768	0.8	7.842	2.588
0.1	0.6	7.845	3.889	0.6	11.190	6.250	0.7	16.338	7.830
0.2	0.4	12.026	8.451	0.5	24.829	17.180	0.6	36.782	22.470
Maximum Percentage Error in Force									
δ/a_0	$a_0/b_s = 0.25$			$a_0/b_s = 0.5$			$a_0/b_s = 0.75$		
	a_0/b_0	PEC	SIBC	a_0/b_0	PEC	SIBC	a_0/b_0	PEC	SIBC
0.05	0.8	6.972	0.009	0.8	7.764	0.014	0.8	9.146	0.023
0.1	0.6	11.739	0.065	0.6	14.107	0.115	0.7	19.042	0.154
0.2	0.4	19.181	0.420	0.5	31.154	0.625	0.6	43.438	0.732

5.3 Concluding Remarks

The performance of two surface impedance models for axisymmetric eddy-current problems is investigated by employing prolate and oblate conducting spheroids of various axial ratios placed in nonuniform inducing magnetic fields. Analytical expressions are derived for the magnetic vector potential, the field quantities, Joule losses and forces for spheroids in the proximity of current-carrying coaxial turns based on the PEC and the SIBC models. Using these expressions, numerical results have been generated for the magnetic field intensity tangential to the conductor surface, Joule losses and forces, and compared with those obtained by imposing the exact boundary conditions. The normalized numerical results presented are the same for systems of various geometric sizes characterized by the same values of the dimensionless parameters a_0/b_0, $d_s/b_s, b_0/b_s$ or a_0/b_s, and δ/b_0 or δ/a_0. This presentation of numerical data in a normalized form in terms of dimensionless parameters is most adequate from a practical point of view since the data provided can directly be employed for systems of any dimensions, material conductivities and inducing currents, corresponding to the same non-dimensional parameters.

From the numerical results presented in figures $5.1 - 5.6$, one can see that, for very small depths of penetration of the electromagnetic field, both the PEC and the SIBC models can be employed to accurately compute the amplitude of the field quantities, but the SIBC model also provides accurate values of their phases, while the PEC model does not give any information about the phase. A formula has been used for the estimation of the erros associated with the SIBC model as compared to the higher order Rytov-Mitzner model. The applicability of the PEC and the SIBC models to the determination of the power losses can be evaluated from figures $5.7 - 5.12$ for the geometric and physical parameters considered. As seen in Tables 5.1 and 5.2, only

for depths of penetration of about or less than 1/20 of the semi-minor axis of the spheroids, the SIBC model can be used to calculate the respective power losses with errors of 0.9 to 2.6%, while now the PEC model introduces errors of up to 8.7%. As shown in figures 5.13 − 5.18, and in Tables 5.1 and 5.2, the calculation of the forces on both the prolate and oblate conducting spheroids can be performed sufficiently accurately by employing the SIBC model for a large range of geometric shapes, field nonuniformities and frequencies, i.e. with errors less than 1% for skin depths of up to 1/5 of their semi-minor axis. The applicability of the PEC model is restrained to very small skin depths compared to the smallest local radius of curvature. The study presented in this paper can be extended to investigate the range of validity of higher order impedance boundary conditions [17], [18], [16],[31] for the solution of eddy-current problems.

Chapter 6

Conclusions and Future Work

6.1 General Conclusions

Exact analytical expressions are derived for the quasistationary field quantities due to circular turns carrying current in the presence of conducting prolate and oblate spheroids. These expressions are used to generate numerical results of specified accuracy for the field quantities inside and outside the spheroids, as well as for the Joule losses inside them and the forces acting upon them. Selected results are presented in a normalized form for extended ranges of the spheroid axial ratio, the ratio of the depth of penetration to the semi-minor axis and the position of the inducing turns relative to the spheroids. These benchmarked numerical results are useful as reference data to investigate the accuracy of the numerical methods as well as the impedance boundary condition models developed to solve complex quasistationary field problems related to real world conductors in the presence of nonuniform external magnetic fields.

The range of validity of the perfect electric conductor and the Leontovich surface impedance boundary condition model for the analysis of axisymmetric eddy-current problems is thoroughly investigated. Using these models, approximate expressions

are derived for the magnetic vector potential, field quantities, Joule losses and forces for conducting spheroids placed in external nonuniform magnetic fields produced by coaxial circular turns carrying currents varying sinusoidally with time. Numerical results have been generated for the magnetic field intensity at the conductor surface, power losses and forces, for both prolate and oblate spheroidally shaped conducting objects were compared with the numerical results from the analytical expressions derived by applying the exact boundary conditions. This comparison is useful in identifying the range of applicability of these simpler impedance boundary condition models. The simplest perfect electric conductor model can only be employed when the depth of penetration of electromagnetic fields is much smaller than the smallest local radius of curvature of the conducting object. On the other hand the numerical results obtained using the Leontovich surface impedance boundary condition model for conducting prolate and oblate spheroids of various axial ratios are in good agreement with the exact results for skin depths of about 1/5 of the semi-minor axis when calculating electromagnetic forces and for skin depths less than 1/20 of the semi-minor axis when calculating Joule losses.

6.2 Contributions

The main contributions of the work presented in this thesis are as follows.

- New benchmark exact analytical solutions were derived for quasistationary field quantities both inside and outside of a conducting spheroid placed in a non-uniform external field produced by circular turns carrying current.

- These expressions were used to generate numerical results of specified accuracy for field quantities, Joule losses and forces acting upon them. The results constitute reference data for comprehensive comparison of the accuracy of ap-

proximate numerical methods or impedance boundary condition models used for real-world conducting objects in the presence of non-uniform external fields.

- The range of validity of the PEC and the SIBC models were investigated in terms of frequency and field non-uniformity for the analysis of axisymmetric eddy-current problems. It is shown that for small depth of penetrations both PEC and SIBC models can be employed to accurately compute the amplitude of fields but SIBC also provides accurate values for the phase.

These contributions have led to the publication of two international journal papers [14],[46] and two conference proceedings papers [47],[48].

6.3 Suggestions for Future Research

In the present research work, exact analytical expressions are derived for the quasistationary electromagnetic fields produced by conducting spheroids in the presence of coaxial circular turns carrying current varying sinusoidal with time. Due to the axial symmetry of the system, the field quantities are independent of φ, which substantially reduces the complexity of the problem. It is also important to solve the quasi-stationary field problem for a conducting spheroid in the presence of an arbitrarily oriented inducing turn, as well as for a system of arbitrarily oriented conducting spheroids in the presence of an inducing turn which are useful in many applications such as in geophysics and in detecting subsurface metallic targets.

To be able to impose the boundary conditions at the conductor surface in a quasistationary field problem with a conducting spheroid in the proximity of an arbitrarily oriented inducing turn, it is necessary that the field produced by a circular turn (which can easily be expressed in the coordinate system attached to that turn) be expressed in terms of the coordinate system attached to the spheroid. This can be

done by applying the appropriate rotational-translational addition theorems for the scalar spheroidal functions. In [65], the translational addition theorems were developed for spherical scalar wave functions whereas the translation addition theorems for spherical vector wave functions were given in [66] and [67]. A general addition theorem for spheroidal wave functions is presented in [68] where the expansion of a spheroidal wave function in one coordinate system (say A_1) to other system (A_2) was obtained by expanding the spheroidal wave functions in terms of spherical wave functions. Translational addition theorems for spheroidal scalar and vector wave functions were derived in [69] and in [70] rotational-translational addition theorems are derived for the scalar spheroidal wave functions. Rotational-translational addition theorems for scalar and vector spheroidal wave functions are also presented in [71], [72], [73] for solving the problem of electromagnetic wave scattering by a system of arbitrarily oriented dielectric spheroids.

Addition theorem for the Laplacian solution in oblate spheroidal harmonics is presented in [74] for a special case of translation of coordinate origins along the z-axis. Recently general translational addition theorems for scalar Laplacian fields were derived in spherical coordinates [75]. In this case the translational addition theorems for spherical scalar wave functions derived in [65],[66], [67] were particularized in the limiting case of a vanishing wave number, $k \to 0$. These theorems are useful in deriving analytical expressions for the static and quasistationary field solutions in the presence of many body systems where the conventional methods such as separation of variables and method of images can not be employed.

Appendix A

Derivation of the Vector Potential Equations in Spheroidal Coordinates

A.1 Derivation of the Vector Laplacian Equations for Axisymmetric Problems

Let's consider the vector relation

$$\nabla \times \nabla \times \boldsymbol{A} = \nabla(\nabla \cdot \boldsymbol{A}) - \nabla^2 \boldsymbol{A}. \tag{A.1}$$

Suppose $\boldsymbol{A}$ satisfies the Coulomb gauge $\nabla \cdot \boldsymbol{A} = 0$. Thus

$$\nabla^2 \boldsymbol{A} = -\nabla \times \nabla \times \boldsymbol{A}. \tag{A.2}$$

Let v_1, v_2 and v_3 be a system of orthogonal curvilinear coordinates with the scale factors h_1, h_2 *and* h_3, respectively. In this coordinate system $\boldsymbol{A} = A_1\boldsymbol{u}_1 + A_2\boldsymbol{u}_2 + A_3\boldsymbol{u}_3$

and the curl($\boldsymbol{A}$) is given by

$$\nabla \times \boldsymbol{A} = \frac{1}{h_1 h_2 h_3} \begin{vmatrix} h_1 \boldsymbol{u}_1 & h_2 \boldsymbol{u}_2 & h_3 \boldsymbol{u}_3 \\ \partial/\partial v_1 & \partial/\partial v_2 & \partial/\partial v_3 \\ h_1 A_1 & h_2 A_2 & h_3 A_3 \end{vmatrix} \tag{A.3}$$

where $\boldsymbol{u}_i,\ i = 1, 2, 3$ are the unit vectors along the coordinate lines v_i and directed toward increasing v_i.

Equation (A.3) can be expanded as

$$\begin{aligned} \nabla \times \boldsymbol{A} = & \frac{1}{h_2 h_3} \left[\frac{\partial (h_3 A_3)}{\partial v_2} - \frac{\partial (h_2 A_2)}{\partial v_3} \right] \boldsymbol{u}_1 + \frac{1}{h_3 h_1} \left[\frac{\partial (h_1 A_1)}{\partial v_3} - \frac{\partial (h_3 A_3)}{\partial v_1} \right] \boldsymbol{u}_2 \\ & + \frac{1}{h_1 h_2} \left[\frac{\partial (h_2 A_2)}{\partial v_1} - \frac{\partial (h_1 A_1)}{\partial v_3} \right] \boldsymbol{u}_3. \end{aligned} \tag{A.4}$$

Due to axisymmetry, $\boldsymbol{A}$ has only a φ-component, which is independent of φ, thus in prolate spheroidal coordinates (A.4) can be simplified into the form

$$\nabla \times \boldsymbol{A} = \frac{1}{c(\xi^2 - \eta^2)^{1/2}} \frac{\partial}{\partial \xi} \left[(\xi^2 - 1)^{1/2} A \right] \boldsymbol{u}_\eta - \frac{1}{c(\xi^2 - \eta^2)^{1/2}} \frac{\partial}{\partial \eta} \left[(1 - \eta^2)^{1/2} A \right] \boldsymbol{u}_\xi. \tag{A.5}$$

Similarly, taking the curl in (A.5) yields

$$\nabla \times \nabla \times \boldsymbol{A} = \frac{1}{c^2(\xi^2 - \eta^2)} \left\{ (1-\eta^2)^{1/2} \frac{\partial^2}{\partial \eta^2} \left[(1 - \eta^2)^{1/2} A \right] + (\xi^2 - 1)^{1/2} \frac{\partial^2}{\partial \xi^2} \left[(\xi^2 - 1)^{1/2} A \right] \right\} \boldsymbol{u}_\varphi. \tag{A.6}$$

The solution for the vector Laplacian $\nabla^2 \boldsymbol{A}'_{out} = 0$ in (3.2) , is obtained from (A.2) and (A.6) in the form

$$\frac{1}{c^2(\xi^2 - \eta^2)} \left\{ (1 - \eta^2)^{1/2} \frac{\partial^2}{\partial \eta^2} \left[(1 - \eta^2)^{1/2} A'_{out} \right] + (\xi^2 - 1)^{1/2} \frac{\partial^2}{\partial \xi^2} \left[(\xi^2 - 1)^{1/2} A'_{out} \right] \right\} = 0. \tag{A.7}$$

The corresponding equation in oblate spheroidal coordinates can be obtained by the transformation $\xi \to i\xi$ and $c \to -ic$.

$$\frac{1}{c^2(\xi^2+\eta^2)}\left\{(1-\eta^2)^{1/2}\frac{\partial^2}{\partial\eta^2}\left[(1-\eta^2)^{1/2}A'_{out}\right]+(\xi^2+1)^{1/2}\frac{\partial^2}{\partial\xi^2}\left[(\xi^2+1)^{1/2}A'_{out}\right]\right\}=0. \tag{A.8}$$

A.1.1 Magnetic Vector Potential Due to Induced Currents

Equation (A.7) and (A.8) can be solved by using the method of separation of variables. for the prolate spheroid case let us assume that the solution of (A.7) can be expressed in the form

$$A'_{out}(\eta,\xi)=L(\eta)M(\xi). \tag{A.9}$$

Substituting (A.9) in (A.7) and dividing by $L(\eta)M(\xi)$, yields

$$\frac{1}{L(\eta)}\frac{d}{d\eta}\Big[(1-\eta^2)\frac{d}{d\eta}L(\eta)\Big]-\frac{1}{1-\eta^2}+\frac{1}{M(\xi)}\frac{d}{d\xi}\Big[(\xi^2-1)\frac{d}{d\xi}M(\xi)\Big]+\frac{1}{1-\xi^2}=0. \tag{A.10}$$

Taking the separation constant in the form $n(n+1)$ with n being an integer gives

$$\frac{1}{L(\eta)}\frac{d}{d\eta}\Big[(1-\eta^2)\frac{d}{d\eta}L(\eta)\Big]-\frac{1}{1-\eta^2}=-n(n+1) \tag{A.11}$$

$$\frac{d}{d\eta}\Big[(1-\eta^2)\frac{d}{d\eta}L(\eta)\Big]+\Big[n(n+1)-\frac{1}{1-\eta^2}\Big]L(\eta)=0. \tag{A.12}$$

Equation (A.12) is in the form of (C.1) in appendix-C and its solution can be expressed in terms of associated Legendre functions of the first kind P_n^1 and the second kind Q_n^1 in the form

$$L(\eta) = \alpha_n P_n^1(\eta) + \beta_n Q_n^1(\eta) \tag{A.13}$$

Similarly we have,

$$M(\xi) = \alpha'_n P_n^1(\xi) + \beta'_n Q_n^1(\xi) \tag{A.14}$$

$\alpha_n, \alpha'_n, \beta_n$ and β'_n are constants of integration. Due to the fact that $1 \leq \xi \leq \infty$ and $-1 \leq \eta \leq +1$ in case of a prolate spheroid, and by considering the properties of associated Legendre functions as given in (C.8) in appendix-C, the solution for (A.7) is expressed in the form

$$A'_{out} = \sum_{n=1}^{\infty} C_n Q_n^1(\xi) P_n^1(\eta) \tag{A.15}$$

where C_n are constants to be determined.

A.2 Magnetic Vector Potential Produced by a Circular Turn Alone

The solution of (3.7) can be expressed as

$$\boldsymbol{A}''(\boldsymbol{r}) = \frac{\mu_0}{4\pi} \int \frac{\boldsymbol{J}(\boldsymbol{r}')}{|\boldsymbol{r} - \boldsymbol{r}'|} d\upsilon' \tag{A.16}$$

where $\boldsymbol{r}$ is the position vector of the observation point and $\boldsymbol{r}'$ is the position vector of the source point. The inverse distance $1/|\boldsymbol{r} - \boldsymbol{r}'|$ can be expanded in terms of prolate

spheroidal harmonics [33].

$$\begin{aligned}\frac{1}{|\boldsymbol{r}-\boldsymbol{r}'|} =& \frac{1}{c}\sum_{n=0}^{\infty}\sum_{m=0}^{\infty}(-1)^m(2-\delta_m)(2n+1)\left[\frac{(n-m)!}{(n+m)!}\right]^2 \\ & \cdot P_n^m(\xi_<)Q_n^m(\xi_>)P_n^m(\eta')P_n^m(\eta)cosm(\varphi-\varphi').\end{aligned} \tag{A.17}$$

The quantity δ_m has the value $\delta_m = 0$ for $m \neq 0$ and $\delta_m = 1$ for $m = 0$, whereas $\xi_<$ and $\xi_>$ are the smallest and greatest of ξ and ξ_s, respectively. The relationship between $\boldsymbol{A}''$ and $\boldsymbol{J}$ is also valid for their scalar components in rectangular coordinates, i.e.

$$\begin{aligned} J_x &= -J_\varphi sin\varphi' \qquad & A_x &= -A'' sin\varphi \\ J_y &= +J_\varphi cos\varphi' \qquad & A_y &= +A'' cos\varphi \\ J_z &= 0 \qquad & A_z &= 0. \end{aligned} \tag{A.18}$$

Due to the axial symmetry of the system, the magnitude of $\boldsymbol{A}''$ does not depend on φ. For convenience, let us consider the semi-plane which is defined by $\varphi = 0$. With $dv' = h_{\eta'}h_{\xi'}h_{\varphi'}d\xi'd\eta'd\varphi'$ and substituting (A.10) and (3.4) in (3.7), A'' can be expressed in the form

$$\begin{aligned} A'' =& \frac{\mu_0 I_s}{4\pi}\frac{[(1-\eta_s^2)(\xi_s^2-1)]^{1/2}}{(\xi_s^2-\eta_s^2)}\sum_{n=0}^{\infty}\sum_{m=0}^{\infty}(-1)^m(2-\delta_m)(2n+1)\left[\frac{(n-m)!}{(n+m)!}\right]^2 \\ & \cdot P_n^m(\eta)\int_v \delta(\eta'-\eta_s)\delta(\xi'-\xi_s)(\xi'^2-\eta'^2)P_n^m(\xi_<)Q_n^m(\xi_>) \\ & \cdot P_n^m(\eta')cos\varphi' cos(m\varphi')d\eta'd\xi'd\varphi'. \end{aligned} \tag{A.19}$$

Due to the fact that $\int_0^{2\pi} cos\varphi' cos(m\varphi')d\varphi' = 0$ except for $m = 1$ in (A.11), A'' can finally be expressed in the form

$$A'' = \frac{-\mu_0 I_s}{2}[(1-\eta_s^2)(\xi_s^2-1)]^{1/2}\sum_{n=1}^{\infty}\frac{2n+1}{[n(n+1)]^2}P_n^1(\xi_<)Q_n^1(\xi_>)P_n^1(\eta_s)P_n^1(\eta). \quad \text{(A.20)}$$

In the case of an oblate spheroid, the expressions for A'' can be deduced from (A.13) by using the transformation $\xi \to i\xi, c \to -ic$, in the form

$$A'' = \frac{-i\mu_0 i_s}{2}[(1-\eta_s^2)(\xi_s^2+1)]^{1/2}\sum_{n=1}^{\infty}\frac{2n+1}{[n(n+1)]^2}P_n^1(i\xi_<)Q_n^1(i\xi_>)P_n^1(\eta_s)P_n^1(\eta). \quad \text{(A.21)}$$

Appendix B

Analytical Solution for Quasi-Stationary Field Quantities by using Impedance Boundary Conditions

Consider a conducting prolate spheroid placed in an external magnetic field produced by a coaxial circular turn carrying a time-harmonic current I_s as shown in figure 3.1. The magnetic vector potential has only a φ-component and depends only on η and ξ. Its expression outside the spheroid is given in the form (3.9),

$$A = \sum_{n=1}^{\infty} C_n Q_n^1(\xi) P_n^1(\eta) - \frac{\mu_0}{2} I_s [(1-\eta_s^2)(\xi_s^2-1)]^{1/2} \cdot \sum_{n=1}^{\infty} \frac{2n+1}{[n(n+1)]^2} P_n^1(\xi_<) Q_n^1(\xi_>) P_n^1(\eta_s) P_n^1(\eta) \tag{B.1}$$

where μ_0 is the permeability of the medium outside the spheroid, P_n^1 and Q_n^1 are the associated Legendre functions of the first and second kinds, respectively, and C_n are constants of integration. η_s and ξ_s are the spheroidal coordinates of the points of the

circular turn, and $\xi_<$ and $\xi_>$ are the smallest and the largest of ξ and ξ_s, respectively.

The induced electric field intensity has only a $\varphi-$component and the magnetic filed intensity has only η and ξ components,

$$E_\varphi = -j\omega A \tag{B.2}$$

$$H_\eta = \frac{1}{\mu_0 c}\frac{1}{(\xi^2-\eta^2)^{1/2}}\frac{\partial}{\partial \xi}\left[(\xi^2-1)^{1/2}A\right] \tag{B.3}$$

$$H_\xi = -\frac{1}{\mu_0 c}\frac{1}{(\xi^2-\eta^2)^{1/2}}\frac{\partial}{\partial \eta}\left[(1-\eta^2)^{1/2}A\right]. \tag{B.4}$$

B.1 PEC Model

In this case, C_n is determined by imposing the condition in (5.5) that the tangential component of the electric field intensity at the conductor surface $\xi = \xi_0$ is zero. From (B.1) and (B.2) and imposing the boundary condition $E_\varphi\big|_{\xi=\xi_0} = 0$ yields

$$\begin{aligned} C_n = {} & \frac{\mu_0 I_s}{2}\left[(1-\eta_s^2)(\xi_s^2-1)\right]^{1/2} \\ & \cdot\frac{(2n+1)}{[n(n+1)]^2}\frac{P_n^1(\xi_0)}{Q_n^1(\xi_0)}Q_n^1(\xi_s)P_n^1(\eta_s). \end{aligned} \tag{B.5}$$

B.2 SIBC Model

The boundary condition in (5.1) can be expressed in terms of the tangential components of the electric and magnetic field intensities at the conductor surface in the form

$$-\frac{E_\varphi}{H_\eta}\bigg|_{\xi=\xi_0} = Z_s. \tag{B.6}$$

Substituting (B.2) and (B.3) into (B.6) gives

$$\sum_{n=1}^{\infty}\big(\lambda_n C_n - \chi_n I_s\big)P_n^1(\eta) = \sum_{n=1}^{\infty}\big(\alpha_n C_n - \beta_n I_s\big)\frac{P_n^1(\eta)}{\sqrt{\xi_0^2-\eta^2}} \tag{B.7}$$

where $\lambda_n, \chi_n, \alpha_n$, and β_n are independent of η,

$$\begin{aligned}
\lambda_n &= j\omega Q_n^1(\xi_0) \\
\chi_n &= \frac{j\omega\mu_0}{2}[(1-\eta_s^2)(\xi_s^2-1)]^{1/2}\frac{(2n+1)}{[n(n+1)]^2} \\
&\quad \cdot P_n^1(\xi_0)Q_n^1(\xi_s)P_n^1(\eta_s) \\
\alpha_n &= \frac{Z_s}{\mu_0 c}n(n+1)Q_n(\xi_0) \\
\beta_n &= \frac{Z_s}{2c}[(1-\eta_s^2)(\xi_s^2-1)]^{1/2}\frac{(2n+1)}{n(n+1)} \\
&\quad \cdot P_n(\xi_0)Q_n^1(\xi_s)P_n^1(\eta_s).
\end{aligned} \tag{B.8}$$

The right hand side of (B.7) is expressed as an infinite series in the form

$$\sum_{n=1}^{\infty}\big(\alpha_n C_n - \beta_n I_s\big)\frac{P_n^1(\eta)}{\sqrt{\xi_0^2-\eta^2}} = \sum_{n=1}^{\infty}\gamma_n P_n^1(\eta) \tag{B.9}$$

and, thus, (B.7) becomes

$$\sum_{n=1}^{\infty}\big(\lambda_n C_n - \chi_n I_s\big)P_n^1(\eta) = \sum_{n=1}^{\infty}\gamma_n P_n^1(\eta). \tag{B.10}$$

Multiplying both sides of (B.9) by $P_m^1(\eta)$, then integrating with respect to η and using the orthogonality property of the associated Legendre functions [58], we obtain

$$\gamma_m = \frac{2m+1}{2m(m+1)}\sum_{n=1}^{\infty}M_{nm}(\alpha_n C_n - \beta_n I_s) \tag{B.11}$$

with

$$M_{nm} = \int_{-1}^{+1}\frac{P_n^1(\eta)P_m^1(\eta)}{\sqrt{\xi_0^2-\eta^2}}d\eta. \tag{B.12}$$

Thus, from (B.10) we get

$$\lambda_m C_m - \chi_m I_s = \frac{2m+1}{2m(m+1)} \sum_{n=1}^{\infty} M_{nm}(\alpha_n C_n - \beta_n I_s). \tag{B.13}$$

Truncating the infinite series in (B.13) at $n = N$ gives a system of N linear equations in N unknowns for the constants D_n. In matrix form the solution of this system can be written as

$$\Big[\ \mathbf{C}\ \Big]_{N\times 1} = I_s \Big[\mathbf{G}\Big]^{-1}_{N\times N} \Big[\mathbf{D}\Big]_{N\times 1} \tag{B.14}$$

where the entries of $\mathbf{G}$ and $\mathbf{D}$ are, respectively,

$$g_{mn} = \begin{cases} \alpha_n M_{mn}(2m+1)/[2m(m+1)] & \text{for } n \neq m \\ \alpha_m M_{mm}(2m+1)/[2m(m+1)] - \lambda_m & \text{for } n = m \end{cases} \tag{B.15}$$

$$d_m = \frac{2m+1}{2m(m+1)} \sum_{n=1}^{\infty} M_{mn}\beta_n - \chi_m. \tag{B.16}$$

B.3 Power losses and forces due to induced currents

B.3.1 Power losses in spheroid

The time-average power loss due to the induced currents in the conducting spheroid can be determined from

$$P = \frac{1}{2} \iint_s R_s \left|H_\eta\right|^2_{\xi=\xi_0} ds \tag{B.17}$$

with the surface resistance given in (5.3). The tangential component of the magnetic field intensity at the surface of a prolate spheroid can be computed approximately

from (B.3), with (B.1) and (B.14), as

$$H_\eta\Big|_{\xi=\xi_0} = \frac{1}{\mu_0 c\sqrt{\xi_0^2-\eta^2}}\sum_{n=1}^{\infty}\Big\{C_n n(n+1)Q_n(\xi_0) - \frac{\mu_0 I_s}{2}[(1-\eta_s^2)(\xi_s^2-1)]^{1/2}\frac{(2n+1)}{n(n+1)} \cdot P_n(\xi_0)Q_n^1(\xi_s)P_n^1(\eta_s)\Big\}P_n^1(\eta). \tag{B.18}$$

When using the PEC model $H_\eta\Big|_{\xi=\xi_0}$ becomes [33]

$$H_\eta\Big|_{\xi=\xi_0} = \frac{I_s}{2c}\left[\frac{(1-\eta_s^2)(\xi_s^2-1)}{(\xi_0^2-\eta^2)(\xi_0^2-1)}\right]^{1/2} \cdot\sum_{n=1}^{\infty}\frac{2n+1}{n(n+1)}\frac{Q_n^1(\xi_s)}{Q_n^1(\xi_0)}P_n^1(\eta_s)P_n^1(\eta) \tag{B.19}$$

and the power loss in a conducting prolate spheroid in the presence of the current-carrying turn is obtained in the form

$$P = \frac{1}{2}\frac{\pi R_s I_s^2}{\sqrt{\xi_0^2-1}}(1-\eta_s^2)(\xi_s^2-1)\int_{-1}^{+1}\frac{1}{\sqrt{\xi_0^2-\eta^2}} \cdot\left[\sum_{n=1}^{\infty}\frac{2n+1}{n(n+1)}\frac{Q_n^1(\xi_s)}{Q_n^1(\xi_0)}P_n^1(\eta_s)P_n^1(\eta)\right]^2 d\eta \tag{B.20}$$

and for an oblate spheroid in the form

$$P = \frac{1}{2}\frac{\pi R_s I_s^2}{\sqrt{\xi_0^2+1}}(1-\eta_s^2)(\xi_s^2+1)\int_{-1}^{+1}\frac{1}{\sqrt{\xi_0^2+\eta^2}} \cdot\left[\sum_{n=1}^{\infty}\frac{2n+1}{n(n+1)}\frac{Q_n^1(i\xi_s)}{Q_n^1(i\xi_0)}P_n^1(\eta_s)P_n^1(\eta)\right]^2 d\eta. \tag{B.21}$$

.

B.3.2 Force exerted upon the spheroid

The resultant time-average force acting on the spheroid is equal in magnitude and opposite in direction to the force acting on the inducing turn. It is oriented along the negative $z-$axis and its magnitude can be expressed as [14]

$$\begin{aligned} F = \; & 2\pi I_s^2 \frac{\left[(1-\eta_s^2)(\xi_s^2-1)\right]^{1/2}}{(\xi_s^2-\eta_s^2)} \\ & \cdot \mathrm{Re} \sum_{n=1}^{\infty} C_n (n+1) \mathcal{K}_n(\eta_s, \xi_s) \end{aligned} \tag{B.22}$$

where

$$\mathcal{K}_n(\eta_s, \xi_s) \equiv \eta_s Q_{n-1}^1(\xi_s) P_n^1(\eta_s) - \xi_s Q_n^1(\xi_s) P_{n-1}^1(\eta_s). \tag{B.23}$$

The magnitude of the resultant time-average force acting on a perfectly conducting prolate spheroid can be expressed in the form [33]

$$\begin{aligned} F \; = \; & \frac{\pi \mu_0 I_s^2}{4} \frac{(1-\eta_s^2)(\xi_s^2-1)}{(\xi_s^2-\eta_s^2)} \sum_{n=1}^{\infty} \frac{2n+1}{n^2(n+1)} \\ & \cdot \frac{P_n^1(\xi_0)}{Q_n^1(\xi_0)} Q_n^1(\xi_s) P_n^1(\eta_s) \mathcal{K}_n(\eta_s, \xi_s). \end{aligned} \tag{B.24}$$

The resultant force acting on conducting oblate spheroids can be derived from the corresponding equations derived for conducting prolate spheroids by performing the transformation $\xi \to i\xi, c \to -ic$.

Appendix C

Legendre Functions

C.1 Associated Legendre Functions

The associated Legendre equation is [58]

$$\frac{d}{dZ}\left[(1-Z^2)\frac{dW(Z)}{dZ}\right]+\left[n(n+1)-\frac{m^2}{1-Z^2}\right]W(Z)=0 \tag{C.1}$$

and its solution can be written as

$$W(Z)=A_{nm}P_n^m(Z)+B_{nm}Q_n^m(Z) \tag{C.2}$$

where $P_n^m(Z)$ and $Q_n^m(Z)$ are called associated Legendre functions of the first and the second kind, respectively, and A_{nm} and B_{nm} are arbitrary constants.

For an unrestricted domain of the argument, the associated Legendre functions are defined by [50]

$$\begin{aligned} P_n^m(Z) &= (1-Z^2)^{\frac{1}{2}m}\frac{d^mP_n(Z)}{dZ^m} \\ Q_n^m(Z) &= (1-Z^2)^{\frac{1}{2}m}\frac{d^mQ_n(Z)}{dZ^m}. \end{aligned} \tag{C.3}$$

C.2 Some Useful Properties of Legendre Functions

$$\begin{aligned}
\frac{d}{d\eta}\left[(1-\eta^2)^{1/2}P_n^1(\eta)\right] &= n(n+1)P_n(\eta) \\
\frac{d}{d\xi}\left[(\xi^2-1)^{1/2}P_n^1(\xi)\right] &= n(n+1)P_n(\xi) \\
\frac{d}{d\xi}\left[(\xi^2-1)^{1/2}Q_n^1(\xi)\right] &= n(n+1)Q_n(\xi)
\end{aligned} \tag{C.4}$$

$$\begin{aligned}
(1-\eta^2)^{1/2}P_n(\eta) &= -\frac{1}{n}\left[\eta P_n^1(\eta) - P_{n-1}^1(\eta)\right] \\
(\xi^2-1)^{1/2}Q_n(\xi) &= -\frac{1}{n}\left[\xi Q_n^1(\xi) - Q_{n-1}^1(\xi)\right]
\end{aligned} \tag{C.5}$$

where P_n and Q_n are called Legendre functions of the first kind and the second kind, respectively. The Wronskian relationship is given by

$$P_n^m(Z)\frac{dQ_n^m(Z)}{dZ} - Q_n^m(Z)\frac{dP_n^m(Z)}{dZ} - = \frac{\Gamma(n+m+1)}{\Gamma(n-m+1)}\frac{1}{(1-Z^2)}. \tag{C.6}$$

C.3 Orthogonality property

$$\begin{aligned}
\int_{-1}^{+1} P_n^m(x)P_l^m(x)dx =& \frac{2}{2n+1}\frac{(n+m)!}{(n-m)!}\delta_{nl} \; for \; x \in [-1,+1] \\
n =& 0,1,2,3,..... \\
m =& 0,\pm 1,\pm 2,.....,\pm n \\
\delta_{nl} =& \begin{cases} 0 & \text{if } l \neq n, \\ 1 & \text{if } l = n. \end{cases}
\end{aligned} \tag{C.7}$$

where δ_{nl} is the Kronecker delta.

$$\begin{aligned}
P_n^1(\infty) \to \infty, \qquad & Q_n^1(\pm 1) \to \infty \\
P_n(-1) \to \infty, \quad & when \; n \neq integer.
\end{aligned} \tag{C.8}$$

C.4 Asymptotic Expansions of Associated Legendre Functions with Large Arguments

$$\begin{aligned} P_n^m(Z) &\underset{|Z|\to\infty}{\longrightarrow} \frac{(2n)!}{2^n n!(n-m)!} Z^n \\ Q_n^m(Z) &\underset{|Z|\to\infty}{\longrightarrow} -\frac{(n)!(n+m)!2^n}{(2n+1)!Z^{n+1}}. \end{aligned} \tag{C.9}$$

C.5 Recurrence Relations

For real or complex arguments

$$(n-m+1)P_{n+1}^m(Z) = (2n+1)ZP_n^m(Z) - (n+m)P_{n-1}^m(Z). \tag{C.10}$$

References

[1] J.R. Wait, "A conducting sphere in a time varying magnetic field", *Geophysics*, vol. 16, pp. 666–672, October 1951.

[2] J.R. Wait, "A conducting permeable sphere in the presence of a coil carrying an oscillating current", *Can. J. Phys*, vol. 31, pp. 670–678, 1953.

[3] J.R. Wait, "Some solutions for electromagnetic problems involving spheroidal, spherical and cylindrical bodies", *J. Res. Nat. Bur. Stand.*, vol. 64-B, pp. 15–32, September 1959.

[4] A. Tugulea and I.R. Ciric, "Electromagnetic field of current-carrying circular turns in the presence of conducting spherical shells", *St. Cerc. Energ. Electr*, vol. 18, pp. 355–379, 1968.

[5] I.R. Ciric, "New model for the computation of quasi-stationary fields due to arbitrary distributions of magnetic dipoles", *IEEE Trans. Magn.*, vol. 36, pp. 1990–1995, July 2000.

[6] I.R. Ciric, "General expressions of the vector potential for axisymmetric quasistationary magnetic fields", *St. Cerc. Energ. Electr*, vol. 20, pp. 591–613, 1970.

[7] I.R. Ciric, "New models for current distributions and scalar potential formulations of magnetic field problems", *J. App. Phys*, vol. 61, pp. 2709–2717, April 1987.

[8] T.P. Theodoulidis, N.N Kantartzis, T.D. Tsiboukis, and E.E. Kriezis, "Analytical and numerical solution of the eddy current problem in spherical coordinates based on the second order vector potential formulation", *IEEE Trans. Magn.*, vol. 33, pp. 2461–2472, July 1997.

[9] I. J. Won, Dean A. Keiswetter, and Thomas H. Bell, "Electromagnetic induction spectroscopy for clearing landmines", *IEEE Trans. Geosci. Remote Sensing*, vol. 39, pp. 703–709, April 2001.

[10] H. Braunisch, C.O. Ao, K. O'Neill, and J.A. Kong, "Magnetoquasistatic response of conducting and permeable prolate spheroid under axial excitation", *IEEE Trans. Geosci. Remote Sensing*, vol. 39, pp. 2689–2701, April 2001.

[11] C.O. Ao, H. Braunisch, K. O'Neill, and J.A. Kong, "Quasi-magnetostatic solution for a conducting and permeable spheroid with arbitrary excitation", *IEEE Trans. Geosci. Remote Sensing*, vol. 40, pp. 887–897, April 2002.

[12] B.E. Barrowes, K. O'Neill, T.M. Grzegorczyk, X. Chen, and J.A. Kong, "Broadband analytical magnetoquasistatic electromagnetic induction solution for a conducting and permeable spheroid", *IEEE Trans. Geosci. Remote Sensing*, vol. 42, pp. 2479–2489, April 2004.

[13] T.M. Grzegorczyk, B Zhang, J.A. Kong, B.E. Barrowes, and K. O'Neill, "Electromagnetic induction from highly permeable and conductive ellipsoids under arbitrary excitation: application to the detection of unexploded ordanances", *IEEE Trans. Geosci. Remote Sensing*, vol. 46, pp. 1164–1176, April 2008.

[14] K.A.S.N. Jayasekera and I.R. Ciric, "Benchmark computations of the fields, losses and forces for conducting spheroids in the proximity of current-carrying turns", *IEEE Trans. Magn.*, vol. 42, pp. 1802–1811, July 2006.

[15] S.V. Yuferev and N. Ida, *Surface impedance boundary conditions: A comprehensive approach*, ICRC Press, Taylor and Francis Group, LLC, 2010.

[16] S. Yuferev and N. Ida, "Selection of surface impedance boundary conditions for a given problem", *IEEE Trans. Magn.*, vol. 35, pp. 1486–1489, May 1999.

[17] T.B. Senior and J.L. Volakis, *Approximate boundary conditions in electromagnetics*, IEE electromagnetic waves series 41, The Institution of Electrical Engineers, London, United Kingdom, 1995.

[18] K.M. Mitzner, "An integral equation approach to scatering from a body of finite conductivity", *Radio Science*, vol. 2, pp. 1459–1470, Dec. 1967.

[19] G. S. Smith, "On the skin effect approximation", *Am. J. Phys.*, vol. 58(10), pp. 996–1002, March 1990.

[20] Z. Godzinski, "The surface impedance and the structure of radio waves over real earth", *Proc. IEEE.*, vol. 108C, pp. 362–373, March 1961.

[21] D. Wang, "Limits of validity of the impedance boundary condition on penetrable surfaces", *IEEE Trans. Antennas Propagat.*, vol. 35, pp. 453–457, April 1997.

[22] A. Sebak and L. Shafai, "Electromagnetic scattering by spheroidal objects with impedance boundary conditions at axial incidance", *Radio. Sci.*, vol. 23, pp. 1048–1060, 1988.

[23] T.H. Fawzi, M.T. Ahmed, and P.E. Burke, "On the use of the impedance boundary conditions in eddy current problems", *IEEE Trans. Magn.*, vol. 21, pp. 1835–1840, Sept. 1985.

[24] S. Subramaniam and S.R.H. Hoole, "The impedance boundary condition in the boundary element-vector potential formulation", *IEEE Trans. Magn.*, vol. 24, pp. 2503–2505, Nov. 1988.

[25] K. Ishibashi, "Eddy current analysis by boundary element method utilizing impedance boundary condition", *IEEE Trans. Magn.*, vol. 31, pp. 1500–1503, May 1995.

[26] E.M. Deeley, "Surface impedance near edges and corners in three-dimensional media", *IEEE Trans. Magn.*, vol. 26, pp. 712–714, March 1990.

[27] S. Yuferev, L. Proekt, and N. Ida, "Surface impedance boundary conditions near corners and edges: rigorous consideration", *IEEE Trans. Magn.*, vol. 37, pp. 3465–4368, Sept. 2001.

[28] L. D. Rienzo, S. Yuferev, and N. Ida, "Calculation of energy related quantities of conductors using surface impedance concept", *IEEE Trans. Magn.*, vol. 44, pp. 1322–1325, June 2008.

[29] A. Viljanen, A. Pulkkinen, O. Amm, R. Pirjola, T. Korja, and BEAR Working Group, "Fast computation of the geoelectric field using the method of elementary current systems and planar earth models", *Annales Geophysicae*, vol. 22, pp. 101–113, 2004.

[30] D.H. Boteler, L. Trichtchenko, R. Pirjola, J. Parmelee, S. Souksaly, A. Foss, and L. Marti, "Real-time simulation of geomagnetically induced currents", in *Electromagnetic Compatibility and Electromagnetic Ecology, 2007 7th International Symposium on*, Saint-Petersburg, 2007, pp. 261 –264.

[31] W.T. Shaw and A.J. Dougan, "Curvature corrected impedance boundary conditions in an arbitrary basis", *IEEE Trans. Antennas Propagat*, vol. 43, pp. 1699–1705, May 2005.

[32] K. A. S. N. Jayasekera and I. R. Ciric, "On the limits of validity of the impedance boundary conditions for the analysis of induced currents in solid conductors", in *Proc. Int. Symp. Antenna Technology and Applied Electromagnetics (ANTEM)*, Ottawa, ON, Canada, 2004, pp. 501–504.

[33] I.R. Ciric, "Electromagnetic levitation in axially symmetric systems", *Rev. Roum. Sci. Electotech. et Energ.*, vol. 15, pp. 35–73, 1970.

[34] H.C. Jayatilaka and I. R. Ciric, "Performance of surface impedance integral equations for quasi-stationary field analysis in axisymmetric systems", *IEEE Trans. Magn.*, vol. 40, pp. 1350–1353, March 2004.

[35] J. A. Stratton, *Electromagnetic Theory*, McGraw-Hill Book Company, Inc, pp. 225, 438, 1941.

[36] W. R. Smythe, *Satic and Dynamic Electricity, Third Edition*, McGraw-Hill Book Company, Inc, pp. 368, 1968.

[37] V. Rudnev, D. Loveless, R. Cook, and M. Black, *Handbook of Induction Heating*, Marcel Dekker, New York, 2003.

[38] H.F. Storm, "Induction heating of long cylindrical chargers", *AIEE Transactions*, vol. 46, pp. 369–377, June 1946.

[39] A. Gagnoud and I. Leclercq, "Electromagnetic modelling of induction melting devices in cold crucible", *IEEE Trans. Magn.*, vol. 24, pp. 573–574, Jan. 1988.

[40] N.J. Siakavellas, "Two simple models for analytical calculation of eddy currents in thin conducting plates", *IEEE Trans. Magn.*, vol. 33, pp. 2245–2257, May 1997.

[41] V. Kelha, R. Peltonen, J. Pukki, J. Heino, R. Ilmoniemi, and A. Penttinen, "Design, construction, and performance of a large-volume magnetic shield", *IEEE Trans. Magn.*, vol. 18, pp. 260–270, Jan. 1982.

[42] K.V. Namjoshi, J.D. Lavers, and P.P. Biringer, "Eddy current power loss in structural steel due to cables carrying current in a perpendicular direction", *IEEE Trans. Magn.*, vol. 30, pp. 85–91, Jan. 1994.

[43] O. Bíró and K. Preis, "On the use of magnetic vector potential in the finite element analysis of three-dimensional eddy currents", *IEEE Trans. Magn.*, vol. 25, pp. 3145–3159, July 1989.

[44] I.D. Mayergoyz and G. Bedrosian, "Iterative solution of 3-d eddy current problems", *IEEE Transactions on Power Systems*, vol. 15, pp. 804–810, May 2000.

[45] Y. Kato and S. Iwamoto, "Computation of three-dimensional unbounded eddy current problems using asymptotic boundary conditions", *IEEE Trans. Magn.*, vol. 31, pp. 1348–1351, May 1995.

[46] K.A.S.N. Jayasekera and I.R. Ciric, "Evaluation of surface impedance models for axisymmetric eddy-current fields", *IEEE Trans. Magn.*, vol. 43, pp. 1991–2000, May 2007.

[47] K. A. S. N. Jayasekera and I. R. Ciric, "Exact analytical solution for the losses in and forces on an induced conducting spheroid", in *Proc. Int. Symp. Antenna Technology and Applied Electromagnetics (ANTEM)*, Saint Malo, France, 2005.

[48] K. A. S. N. Jayasekera and I. R. Ciric, "Performance of the impedance boundary conditions for eddy-current problems", in *IEEE Conference on electromagnetic field computations (IEEE CEFC2006)*, Miami, Florida, USA, 2006.

[49] C. Flammer, *Spheroidal Wave Functions*, Stanford: Stanford Univ. Press, 1957.

[50] S. Zhang and J. Jin, *Computation of Special functions*, New York: Wiley, 1996.

[51] P.E. Falloon, P.C. Abbott, and J.B. Wang, "Theory and computation of spheroidal wavefunctions", *J. Phys. A: Math. Gen.*, vol. 36, pp. 5477–5495, May 2003.

[52] P.E. Falloon, *Theory and computation of spheroidal harmonics with general arguments*, M.Sc. Thesis, The University of Western Australia, 2001.

[53] J.A. Stratton, P.M. Morse, L.J. Chu, and R.A. Hutner, *Elliptic cylinder and spheroidal wave functions*, John Wiley and Sons, Inc, New York, 1941.

[54] A.L.V. Buren and J.E. Boisvert, "Imporoved calculation of prolate spheroidal radial functions of the second kind and their first derivatives", *Quart. Appl. Math.*, vol. LXII, pp. 493–507, Sept. 2004.

[55] C.J. Bouwkamp, "On spheroidal wave functions of order zero", *J. Math. Phys.*, vol. 26, pp. 79, 1947.

[56] D.B. Hodge, "Eigenvalues and eigenfunctions of the spheroidal wave equation", *J. Math. Phys.*, vol. 11, pp. 2308–2312, Aug. 1970.

[57] G. Blanch, "On the computation of mathieu functions", *J. Math. Phys.*, vol. 25, pp. 1–20, 1946.

[58] M. Abramowitz and I.A. Stegun, *Handbook of Mathematical Functions with Formulas, Graphs, and Mathematical Tables*, National Bureau of Standards, Applied Mathematics Series, 55. Washington, D.C., pp. 331-353, 1964.

[59] W. Gautshi, *Algorithm 259, Legendre functions for arguments larger than one*, Cambridge University Press, 2000.

[60] B.E. Barrowes, *MATLAB routines for computation of special functions*, Available at http://ceta.mit.edu/comp_spec_func/.

[61] B.E. Barrowes, *Electromagnetic scattering and induction models for spheroidal geometries*, PhD thesis, Massachusetts Institute of Technology, 2004.

[62] K.A.S.N. Jayasekera, *Performance analysis of the impedance boundary conditions for axisymmetric eddy current problems*, M.Sc. Thesis, The University of Manitoba, 2004.

[63] S.A. Schelkunoff, "The electromagnetic theory of coaxial transmission lines and cylindrical shields", *The Bell Syst. Tech. J.*, vol. 13, pp. 532–579, 1934.

[64] Lord Rayleigh, "On the self inductance and resistance of straight conductors", *Philos. Mag.*, vol. 21, pp. 381–394, 1886.

[65] B. Friedman and J. Russek, "Addition theorems for spherical waves", *Quart. Appl. Math.*, vol. 12, pp. 13–23, 1954.

[66] S. Stein, "Addition theorems for spherical wave functions", *Quart. Appl. Math.*, vol. 19, pp. 15–24, 1961.

[67] O.R. Cruzan, "Translational addition theorems for spherical vector wave functions", *Quart. Appl. Math.*, vol. 20, pp. 33–40, 1962.

[68] B.J. King and A.L.Van Buren, "A general addition theore for spheroidal wave functions", *SIAM J. Math. Anal.*, vol. 4, pp. 149–160, Feb. 1973.

[69] B.P Sinha and R.H. Macphie, "Translational addition theorems for spheroidal scalar and vector wave functions", *Quart. Appl. Math.*, vol. 38, pp. 143–158, July 1980.

[70] R.H. Macphie, J. Dalmas, and R. Deleuil, "Rotational-translational addition theorems for scalar spheroidal wave functions", *Quart. Appl. Math.*, vol. 44, pp. 737–749, Jan. 1987.

[71] M.F.R Cooray, *Electromagnetic scattering by systems of arbitrarily oriented spheroids*, PhD thesis, University of Manitoba, 1990.

[72] M.F.R. Cooray and I.R. Ciric, "Rotational-ttranslational addition theorems for vector spheroidal wave functions", *COMPEL*, vol. 8, pp. 151–166, Sept. 1989.

[73] M.F.R. Cooray and I.R. Ciric, "Scattering of electromagnetic waves by a system of two dielectric spheroids of arbitrary orientation", *IEEE Trans. Antennas Propagat*, vol. 39, pp. 680–684, May 1991.

[74] R. Shail, "On addition theorems for spheroidal harmonics with some applications", *Mathematica*, vol. 14, pp. 132–141, 1967.

[75] S.C.K.M. Kotuwage, *Application of translational addition theorems to electric and magnetic field analysis in many-sphere systems*, M.Sc. Thesis, The University of Manitoba, 2011.